Preparation of Graphite from Bamboo (*Yashinia alpine)* and its Application for Fluoride Ion Removal in Water Treatment

Biniyam Alemayhu Kelkay

A Thesis Submitted to

The Department of Chemical Engineering

School of Mechanical Chemical and Materials Engineering

Presented in Partial Fulfillment of the Requirement for the Degree of Master's in Chemical Engineering (Process Engineering)

Office of Graduate Studies

Adama Science and Technology University

October 2021

Adama, Ethiopia

Preparation of Graphite from Bamboo (*Yashinia alpine)* and its Application for Fluoride ion Removal in Water Treatment

Biniyam Alemayhu Kelkay

Advisors

Dr. Tatek Temsgen

Dr. Melaku Tesfay

Dr. P. Selvakumar

A Thesis Submitted to

The Department of Chemical Engineering

School of Mechanical, Chemical and Materials Engineering

Presented in Partial Fulfillment of the Requirement for the Degree of Master's in Chemical Engineering Specialization in Process Engineering

Office of Graduate Studies

Adama Science and Technology University

October 2021

Adama, Ethiopia

Declaration

I hereby declare that this MSc Thesis is my original work and has not been presented for a degree in any other university, and all sources of material used for this thesis/ dissertation have been duly acknowledged.

Name: _____

Signature:_____

This MSc/ MA Thesis /PhD dissertation has been submitted for examination with my approval as thesis advisor/ dissertation Supervisor.

Name: _____

Signature:_____

Date of submission…

Recommendation

(This should be on separate page student thesis) I/we, the advisor(s) of this thesis, hereby certify that I/we have read the revised version of the thesis entitled "---------- ---------- ---------- ----------" prepared under my/our guidance by ---------- (name of student) submitted in partial fulfillment of the requirements for the degree of Mater's of Science in ----------. Therefore, I/we recommend the submission of revised version of the thesis to the department following the applicable procedures.

_____	_____	_____
Major Advisor	Signature	Date
_____	_____	_____
Co-advisor	Signature	Date
_____	_____	_____
Co-advisor	Signature	Date

Approval of Board of Examiners

I/we, the advisors of the thesis entitled "_____" and developed by (name of student)_____, hereby certify that the recommendation and suggestions made by the board of examiners are appropriately incorporated into the final version of the thesis.

Major Advisor	Signature	Date
Co-advisor	Signature	Date
Co-advisor	Signature	Date

We, the undersigned, members of the Board of Examiners of the final open defense by _____ have read and evaluated his/her thesis entitled "_____" and examined the candidate. This is, therefore, to certify that the thesis has been accepted in partial fulfillment of the requirement of the Degree of ……..

Chairperson	Signature	Date
Internal Examiner	Signature	Date
Nigus Gabbiye Habtu(PhD)		19/11/2021
External Examiner	Signature	Date
Department Head	Signature	Date
School Dean	Signature	Date
Office of Postraduate Studies Dean	Signature	Date

ACKNOWLEDGEMENT

I would like to thank first and foremost to almighty God. My special thanks goto the Department of Chemical Engineering for hosting me these past few years' study.

I would like to express my sincere gratitude towards my advisor, Dr.Tatek Temesgen and my Co-advisors Dr. Melaku Tesfay and Dr P.Selvakumar , for working under their guidance and being around them refreshing approach towards research has been eye-opening for me.

Most importantly, my heartfelt, sincere thanks should go to my beloved brother Abiyu Alemayhu, raising me to the heights that I am in at present with his love, courage, and support. My special gratitude and deep love go to the number one father ever, whose name is Alemayhu Kelkay, and to my beloved love Mahder Wubet for their mysterious love and kindness, my stories, I feel your smiles at heaven.I dedicate this thesis to them.

Finally, words are not enough; you have made this journey one for the books, and I thank you all for helping me add to my library again.

Abstract

People in several regions of the Rift Valley of Ethiopia are consuming much higherfluoride ion concentrations beyond WHO recommended level, which has resulted in both dental and skeletal fluorosis.Under this study,an average of the five selected boreholeswater samples (11.72mg/L) around Adama was taken to prepare synthetic fluoride water. Low cost and easily available lignocellulosic biomass, bamboo,was used as a precursor for graphite preparation and application on fluoride removal.Activated raw bamboo was calcined at different temperatures of {400 and 600°C} and biochar was activated using two different catalysts {Al and $FeCl_3.6H_2O$*}. Method of heat treatment was used for graphitization, andthe catalyst impregnated biochar was graphitized at different temperatures {800, 900 and 1000°C} and at different graphitization times {1.5, 2.5 and 3.5 hr} in muffle furnace.Those parameter effects were studied using XRD and FTIR instruments and X'pert Software. An obvious Graphite reflection peak was detected and confirmed by diffraction peaks at 26.65° and around 44°. Better graphitization with increasing temperature was confirmed using X'pert softwareand FTIR as graphite diffraction pattern and skeleton of graphite structure was formed. The experiments were conducted on batch adsorption test at conditions of adsorbent dosage {0.5, 1, 1.5 and 2 g}, particle size of {250-355, 355-500 and 500-7010µm} and contact time of {30, 60, 90 and 120 min}. The maximum adsorption efficiency (48.70%) was obtained at an adsorbent dose of 2g, the particle size of 250-355µm and 2hr contact time. In this research, fluoride removal on bamboo driven graphite samples {G-*$FeCl_3.6H_2O_{1000°C}$*and G-*$Al_{900°C}$*} was also studied. The residual fluoride concentration reduced from initial fluoride concentration 11.72 mg/L to {7.65 and 5.055 mg/L} after agitation for 2 hrs using*G-$FeCl_3.6H_2O_{1000°C}$ *and G-*$Al_{900°C}$*) respectively. Moreover, an alternative modification was done on the graphite sample (G-*$Al_{900°C}$*) to enhance its property by coating it with Aluminum Hydroxide and its fluoride removal efficiency enhanced (fluoride removal 95.63% after agitation for 2 hrs). The equilibrium data obtained in this study were closely fitted with the Langmuir isotherm for graphite (G-*$Al_{900°C}$*). The Freundlich isotherm model was the best description of fluoride adsorption by a modified graphite sample (mG-*$Al_{900°C}$*). Adsorption kinetics was also determined and the kinetic results obtained from those studies fitted well with the pseudo-second-order kinetic model.*

Keywords: *Bamboo, Graphite, Fluoride, Adsorption, Catalyst.*

Table of Contents

List of Figures and Illustrations

List of Tables

List of Acronyms and Abbreviations

UNESCO……...United Nations Educational, Scientific and Cultural Organization

OSHO……Oromo self-help organization

WHO…….World health organization

NPK……..Nitrogen (N), phosphorus (P) and potassium (K)

SLSI……. Sri Lanka Standards Institution

WSSA……Water Supply and Sewerage Authority

FTIR…….. Fourier transform infrared

XRD……...X-ray diffraction

SNNPRS……....South nation nationalities regional state

RB……..Raw bamboo

BC……..Biochar

ABC……...Activated biochar

CHAPTER ONE

1. INTRODUCTION

1.1. Backgrounds of the Study

Water is an essential resource for all living things on the globe [1]. The composition of freshwater is only 3% of the total water content on earth, in which only a small percentage (0.01%) is available for human use [2]. However, some of this freshwater is under serious stress or unfit for daily consumption due to geological factors, fast population growth, urbanization, and unsustainable water usage in industry and agriculture [3]. As water is an essential component of human survival, its quality and safety, particularly for drinking water, is a major concern. The situation in developing countries is becoming increasingly worrisome due to a lack of efficient management, a scarcity of professionals, and financial constraints [4]–[7]. The majority of health issues that arise in our bodies are primarily following the ingestion of contaminated water. Many water sources contain hazardous chemicals, making the water unfit for drinking or household usage. As a result, drinking contaminated water can lead to a variety of illnesses [8]. According to the UNESCO research, about 2.3 billion people worldwide are affected by water-related problems [3]. The chemical composition of water is one of the most significant things to keep track of in order to ensure that any community has access to clean drinking water. Chemical composition is primarily determined by water sources. Fluoride is one such contaminant, and while there are other chemical components that influence water quality, the issue of maintaining an optimal fluoride concentration is gaining traction in today's society. Excess fluoride in drinkable water is now having consequences in both developed and developing countries [4]–[7].

Ethiopia is one of the countries in the world where fluoride-rich drinking water is consumed by the many people's [9], [10]. The World Health Organization (WHO) has identified 28 countries that have high fluoride levels in their drinking water. Ethiopia, is among the countries that are severely affected [3]. Fluoride (F-) is a hazard for human health, according to the World Health Organization (WHO), if its concentration exceeds the allowed limit, which is 1.5 mg/L [11].

People in Ethiopia's Rift Valley, on the other hand, drink water with far higher fluoride ion concentrations than the permitted limit. As a result, many residents in the region are affected by dental and skeletal fluorosis because high fluoride water seems to be the only source of water [12]. The majorities of fluoride-affected people in the Ethiopian Rift Valley are poor and rely on underground water as a source of drinking water. As a result, treatment technologies such as discovering defluoridation methods and adsorbent materials with a high fluoride removal rate are crucial. Adsorption is considered to be the simplest and most cost-effective process when compared to other procedures. Adsorption is the adhesion of atoms, ions, and molecules to the surface of a material. As a result, on the adsorbent (material which adsorbs), an adsorbate layer (atoms to be adsorbed) formed. Adsorption is a surface phenomenon that occurs when the surface of a solid phase has imbalanced or residual stresses. These imbalanced residual forces tend to attract and hold molecular species that come into contact with the surface.

Synthetic graphite production has inspired a lot of attention in recent years, owing to the ever-increasing need. Due to its ubiquity, environmentally friendly nature, and low cost, biomass waste has recently been identified as a promising precursor for graphite synthesis [13]. It provides the advantages of being plentiful functionalities, inexpensive, and clean, with a high use potential[14]. The use of high carbon content feedstock is an important feature of graphite production. Activated alumina, bone char, raw bauxite, activated carbon, and natural clays, among others, have been discovered as defluoridation adsorbents in several investigations. Because there are numerous types of active sites on the surface of bio char, including ion exchange sites, it has been good adsorbent. Locally available, low-cost graphitic carbon derivatives from biomass are a promising adsorbent for treating contaminated water.Their large surface areas and exchange capacities could contribute to adsorption abilities [15].

1.2. Statement of the problem

Depending on the dosage and total amount consumed, fluoride in drinking water can be useful or harmful. Fluoride, when present within permissible limits of 1.0-1.5mg/L for calcification of dental enamel, is especially beneficial to young children under the age of eight. Fluoride (F-) is a hazard for human health, according to the World Health Organization (WHO), if its concentration exceeds the allowed limits, which were 1.5 mg/L. People in Ethiopia's Rift Valley, on the other hand, drink water with far higher fluoride ion concentrations than the permitted limit. As a result, many people in the regionwhere high fluoride water is the only water supply are affected by dental and Skelton problems. According toa study with Oromo Self-Help Organization (OSHO), excessive fluoride content was foundin groundwater samples that were taken from five boreholes in the Adama (Meja, Anano, Garba fila, Gura, and Serity) districts. The average fluoride concentration ion among those sites was 11.72 mg/L this beyond much higher than the permissible limit. The vast majorities of the people in the Ethiopian Rift Valley who are affected by fluoride groundwater pollution are poor and rely on groundwater resources as a source of drinking water. Attempts to overcome the problem have already been made in a variety of ways. Using an adsorbent defiloridation plant, the Oromo Self-Help Organization (OSHO) attempted to meet the clean water needs of around 94,000 people in the Mojo and surrounding zones.Despite all the efforts, fluorosis continues to have an impact on a vast number of communities. As a result, it's critical to devise corrective procedures, such as identifying defluoridation methods and alternative adsorbent materials with high fluoride removal rates. Graphite and its derivatives are currently utilized in a variety of industries. Despite graphite's excellent characteristics and the vast range of applications, the main source of concern is supply risk. Due to its high demand and limited supply from natural sources, graphite has been labeled as a "supply risk" commodity. Also,Graphite derived from natural coal and fossil fuels isa very expensive and detrimental effect on the environment. This study planned to prepare bamboo-driven graphite as it could be anexcellent option to fill the gap.

1.3. Objective

1.3.1. General objective

Preparation of graphite from bamboo (*Yashinia alpine*) and its application in water treatment to remove fluoride ions

1.3.2. Specific objectives

- Preparation of graphite and study the effect of graphitization parameters and characterization using XRD and FTIR
- Surface modification of bamboo driven graphite using aluminum hydroxide
- Adsorption test for fluoride ion removal using biochar, bamboo driven graphite and aluminum hydroxide modified graphite
- To study adsorption isotherm of fluoride ion removal
- To study adsorption kinetics of fluoride ion removal

1.5. The scope of the study

The major goal of this study was to prepare bamboo-driven modified graphiteand its application for defluoridation by applying activation and surface modification in a sequential manner. Batch experiments were used to explore the modification effects of graphite materials using aluminum hydroxide for the removal of fluoride ions from water using jar tests. The effects of contact time, dose, and particle size for biochar and activating catalyst type for graphitic carbon have been studied. Adsorbent characteristics of aluminum hydroxide modified graphite and bamboo char and graphite produced were evaluated to know the reason for the change of removal efficiency.

1.6. Significance of the study

Graphite is a relatively new material that has a wide range of applications, including adsorption owning to its distinct characteristics.The key concern about growth is supply risk issues due to the wide use of graphite.This research offers promise in terms of alternate resources for making graphite from biomass. This study can be utilized as supporting research for future studies on bamboo to graphite conversion,also gives additional information for the research in the area of lignocellulosic biomass for the applicationin water treatment and suggesting alternative adsorbent resources for fluoride ion removal. This study also aims to build aluminum hydroxide modified graphite for water defluoridation. The use of bamboo in the development of the improved defuloridation adsorbent is intended to increase community access to fluoride-free water. This is due to the fact that bamboos are cheap, abundant locally and have a limited purpose.

CHAPTER TWO

2. LITERATURE REVIEW

2.5. Environmental Occurrence and Geochemistry of Fluoride

2.5.1. Occurrence

Fluorine is the lightest of the halogens and the 13th most abundant naturally occurring element in the Earth's crust. It's present in almost all soils and rocks, plants and animals [16]. Fluoride is more common in the lithosphere than in the hydrosphere, atmosphere, or biosphere, because most fluoride in the lithosphere is bound in various minerals. In the hydrosphere, the concentration varies dramatically as well. Fluoride levels in saltwater are around 1.3 mg/l [17]. The main reason of releasing fluoride into water bodies are due to natural and anthropogenic factors.

2.5.1.1.Natural source

Fluoride is a naturally occurring ion that can be found in different levels in minerals, rocks, and volcanic areas. Fluoride has been mostly obtained by leaching from rocks and minerals [18], [19]. Fluoride concentrations are considerably greater in places rich in flurorite, fluoroappatite, and cryolite-rich rock, which are related to numerous geological interactions. The principal sources of fluoride minerals, which are found in nearly all rocks, are fluorospar and fluoroappatite [20].It can be found in sedimentary rocks as fluorspar and igneous rocks as cryolite. Water doesn't dissolve these fluoride minerals at all. As a result, fluorides will only be found in groundwater when conditions favor their dissolution which will deposited into bodies of water [21]. Volcanoes are the primary source of fluorine in the natural world [22]. The addition of fluoride by volcanic activities, strong water-rock interaction, and low calcium concentration are the main reasons for the high fluoride concentrations in ground water.

2.5.1.2.Anthropogenic Sources

Fluoride is released from various types of human-involved processes, industrial wastes [23] plastic factories, and glass manufacturing process, agricultural fertilizers and combustion of coal, brick and tile [24]. Usage of fertilizers as NPK, potash, superphosphate releases considerable amounts of fluoride into soil and water. Waste on those industry and others including aluminum, copper, and nickel production also release fluoride into the environment. Controlled addition of fluoride to dental products, food products, and pharmaceutical products also contributes to accumulation of fluoride in the environment.

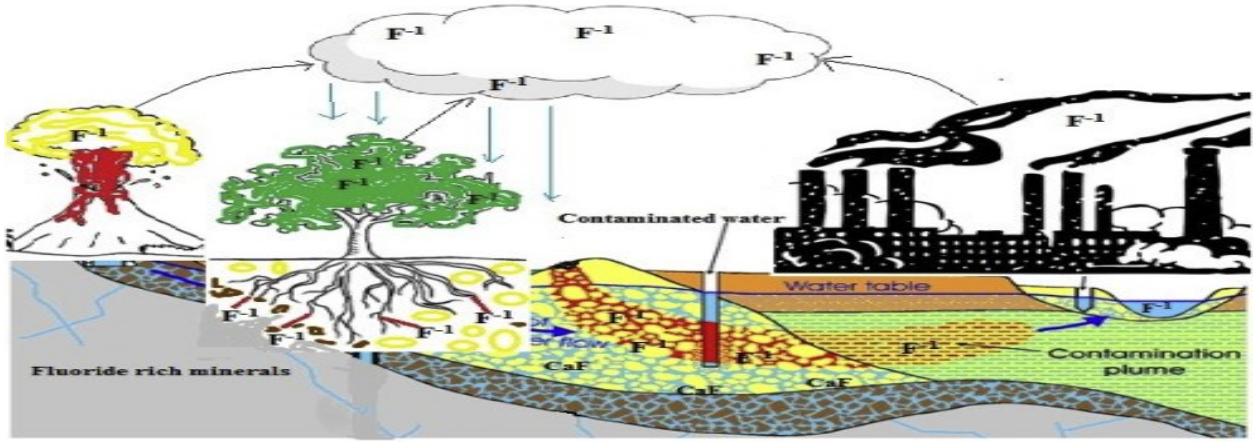

Figure 2. 1 Sources of fluoride in the environment [25].

2.5.2. Chemistry of Fluoride

2.5.2.1.Fluorine

Fluorine (F_2) is a pale, yellow-green, corrosive gas which almost cannot be found in natural environment in elemental form due to its high electro negativity and reactivity. Fluorine, having nine protons in its nucleus, is the most electronegative and reactive element in the periodic table. Fluoride (F^-) is a fluorine anion characterized by small radius, great tendency to behave as ligand and easiness to form a great number of different organic and inorganic compounds in soil, rocks, air, plants and animals [26], [27].

2.5.2.2.Geochemical reactions of fluorine

In groundwater, the natural concentration of fluoride depends on the geological, chemical and physical characteristics of the aquifer, the porosity and acidity of soil and rocks, temperature, action of other chemical elements and depth of the aquifer. The mobilization of fluoride from those into groundwater is dependent on the pH and time of contact with water through the bed of minerals. The possible chemical reactions that happen when water percolates over the bed of fluoride mineral are shown below [28], [29].

$CaF_2 + 2HCO_3 - \rightarrow CaCO_3 + 2F- + H_2CO_3$…….(2.1)

$CaF_2 + H_2CO_3 + 2OH- \rightarrow CaCO_3 + 2F- + H_2O$……...(2.2)

It is clear from the above mentioned geochemical reaction that fluoride ion is naturally released into the surface and ground water that leads to the increase in fluoride concentration in surface and underground water which are the main sources of drinking water in most of the countries including Ethiopia. In some of the calcite and lime containing regions, some amount of fluoride released by geochemical reaction express by equations 2.1 and 2.2 are converted into fluorite as:

$CaCO_3 + 2F- + H_2O \rightarrow CaF_2 + 2HCO_3 - + 2OH^-$……...(2.3)

The fluorspar or fluorite (CaF_2) formed according to the reaction express in equation (2.3) is slightly soluble in water. In groundwater, fluoride ions appear to stay intact or as aqua complexes due to the lower percentage of other cations such as aluminum and iron. Fluorine can replace hydrogen thus, there are so many organic compounds in many industries that contains fluoride ion [30].

2.6. Standard Levels of Fluoride

World health organization (WHO) recommends a fluoride concentration of 1.5 mg/l in drinking water maximum limit, with 1 mg/L being useful to humans in terms of reducing dental cavities [31], [32]. Fluoride has an important function in the normal mineralization of some (hard) tissues. Fluoride stabilizes the skeletal system at low concentrations by lowering the solubility of

apatite crystals and increasing the size of the crystals [33]. Fluoride has an important function in the normal mineralization of some (hard) tissues. Fluoride stabilizes the skeletal system at low concentrations by reducing the solubility of apatite crystals and increasing the size of the crystals [34]. According to SLSI, the highest ideal level of fluoride for drinking water is 0.6 mg/L, while the maximum permissible level is 1.5 mg/l [35]. High fluoride concentrations in the Ethiopian rift valley cause a variety of health hazards [36]. According to a study conducted in India, [37], The average fluoride levels in ground drinking water was lower than the Ethiopian rift valley average. The average fluoride concentration in Ethiopian rift valley ground drinking water is well over the WHO limit (1.5 mg/L) [37].

2.7. Fluoride toxicity and its adverse effect on human health

Humans have suffered from dental fluorosis for ages, but the cause of the condition was unknown until the nineteenth century. Fluoride and fluorosis were first linked in the early twentieth century, when brown stains appeared on certain people's teeth [38]. It was discovered that the amount of fluoride intake was directly related to the occurrence and severity of this type of mottled enamel [18], [39]. Fluoride has some physiological effects [40], [41] in terms of human health and well-being. Fluoride concentration in drinking water, continuous fluoride exposure, severe physical labor, inadequate nutrition, climatic conditions, and reduced renal function owing to disease are all factors that influence the development of fluorosis and hence the ideal F – levels [42].

2.7.1. Effect in dental health

Dental fluorosis is described as an enamel hypo mineralization characterized by greater surface and subsurface porosity than normal enamel as a result of excessive fluoride intake during enamel development [42]. Permanent teeth are the ones that are most impacted, and they lose their natural creamy white translucent appearance and become gritty, opaque, and chalky white. Dental fluorosis is a developmental disorder that worsens over time [43]. More than 60% of the population is impacted by dental fluorosis if they drink water containing more than 2 mg dm^{-3} fluoride, according to research [44]. The similar study by [45] predicted that consuming drinking water with more than 6 mg/l would cause dental fluorosis in 100 percent of the population [46].

Figure 2. 2 Dental fluoresis [47].

2.7.2. Skeletal fluorosis

Fluoride has been demonstrated to enhance bone growth in humans to a greater level. Skeletal fluorosis develops when humans are exposed to or consume water containing substantial amounts of fluoride or other fluoride compounds at high doses for an extended period of time. It occurs as a result of increased bone mass and density. The enlarged size of the vertebral bone, as well as the constriction of the spinal canal, causes paralysis. Neurological and auditory harm are the severe abnormalities caused by fluorosis.

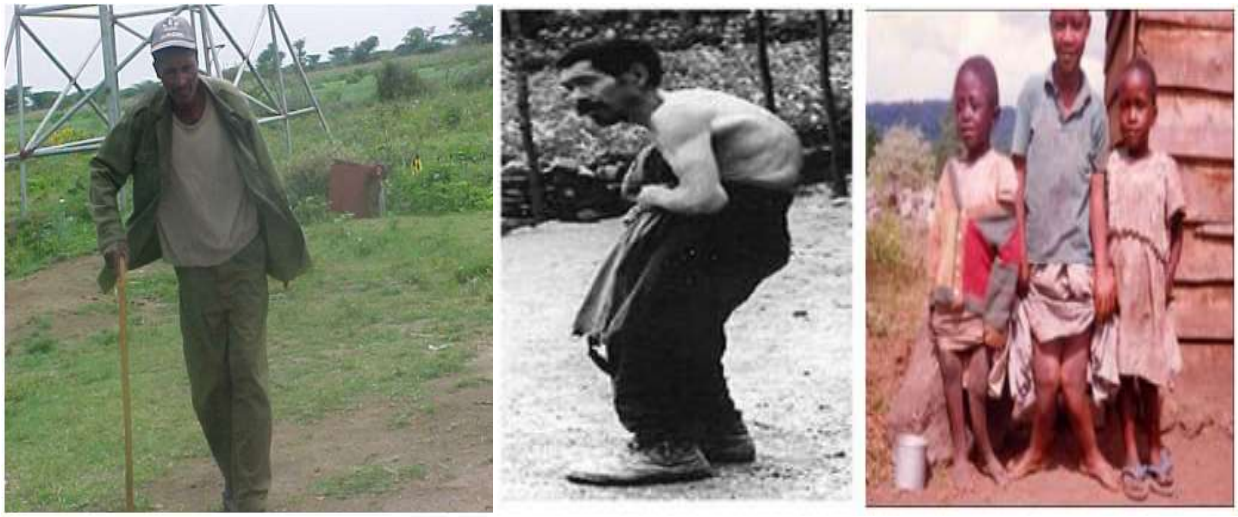

Figure 2. 3Severe cases of fluoresis [48][49].

2.7.3. Other human health effects

In addition to these health hazards, long-term exposure to high levels of fluoride has been linked to major health problems such as infertility in mammals. Studies have shown that increasing fluoride concentration in their diet or drinking water in fluoride-polluted areas reduces fertility power. Because bone tissue is the primary site of fluoride accumulation in the body, it may play a role in the development of bone cancer. A number of studies have suggested a relation between fluoride intake and the development of bone cancer [47], [48], [50], [51]. Fluoride accumulates in the brain of the fetus, causing harm to cells and neurotransmitters, according to research, and there is a link between fetal fluoride exposure and behavioral abnormalities in newborns. When fluoride concentrations exceed 2 mg/l in human bodies, the symptom of neurotoxicity is said to occur [52], [53]. Fluoride buildup in the body has an effect on health, particularly in calcifying tissues like the bones and pineal gland [54], [55].Fluoride levels in drinking water that are too high it will be a severe hazard for society.

2.8. Fluoresis impact in Ethiopia

The Ethiopian Water Supply and Sewerage Authority (WSSA) and several other organizations and individual researchers examined over 150 settlements and natural water sources for fluoride levels. The Rift Valley region of Ethiopia had the highest levels of fluoride concentrations of any section of the country. According to [56] Afar, Oromia, and the Southern Nations and Nationalities Regional States (SNNPRS) are among the regions with high fluoride levels in ground water.in another investigation fluoride concentrations in water provided from boreholes in the Rift Valley three settlements were observed between 1 and 33mg/l [57], Volcanoes, high temperatures, high subsurface carbon dioxide pressure, and low calcium content have all been linked to the Rift system's high fluoride content [12]. The prevalence of the problem of high fluoride groundwater (fluorosis) in the region can simply be deduced from the above investigations.

Table 2. 1:Water fluoride content in various areas of Ethiopian rift valley.

Sample sites	Fluoride (mg/l)
Gewane (town)	0.7-2.5
Abadir (farm)	4.0
Koka (town)	26
Alem tena (village)	9
Abernosa (village)	36
Jido (village)	33.6

Source [58].

Groundwater from five selected boreholes around Adama was analyzed for chemical components, according to [59]. Table 2.2 shows the fluoride content of groundwater from selected areas.

Table 2.2:Ground water fluoride content around Adama Town

No.	Site Name	Fluoride (mg/l)
1	Anano	13.76
2	Garba fila	10.93
3	Gura	9.09
4	Serity	12.55
5	Meja	8.29

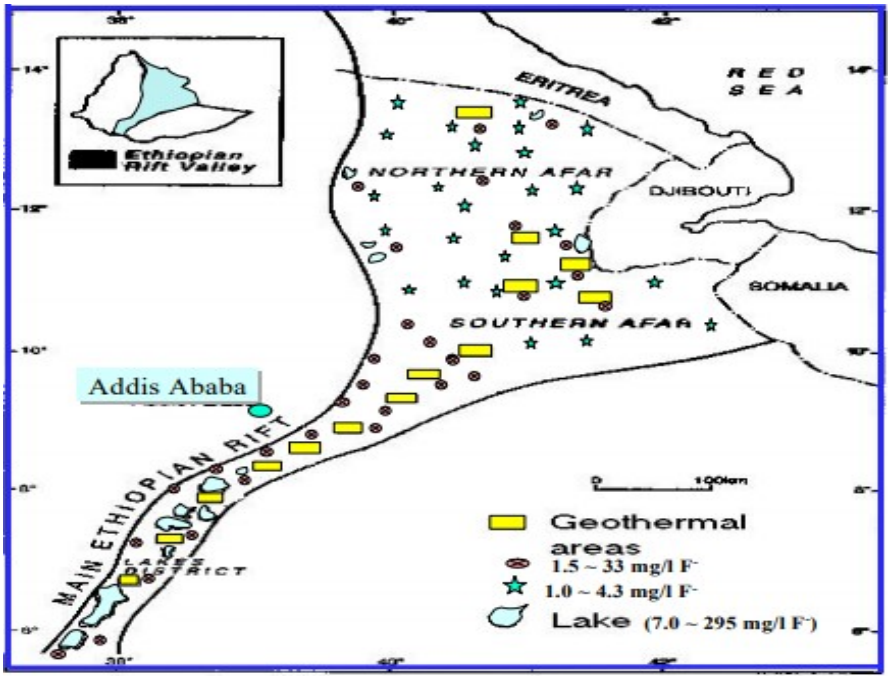

Figure 2.4 Map shows the Rift Valley of Ethiopia fluoride content in surface water and groundwater Source [58].

In Ethiopia's most comprehensive research of endemic fluorosis, 1,456 people from 14 communities in the central Rift Valley were studied. [68][57] In the groups studied, the prevalence of dental fluorosis ranged from 69% to 98 percent (mean 84%). The early retirement of 244 local workers, due to skeletal fluorosis demonstrates the disease's significant public health and economic consequences in Wonji-Shoa Farm State (and, presumably, other commercial agricultural and industrial sectors) [57][56] due to disability among 530 retired workers After complaints of discomfort in the joints and limitations in movement, another 300 workers were checked. 65 percent of them had skeletal fluorosis, with 30 of them having the severe debilitating kind, which is defined by complete physical disability [60]. Both dental and skeletal fluorosis is well known public health issues in Ethiopia, according to the studies above, in addition to the country's social and economic concerns. It is an incurable condition for which there is no medical cure.

2.9. Mitigation Options

Fluorosis prevention through a variety of methods is a challenging endeavor that necessitates ideal socioeconomic conditions in terms of knowledge, motivation, discipline, and technique[61]. The following are some of the probable fluorosis mitigation strategies in places where fluoride concentrations are over the allowed level:

- ✓ Provision of alternative source of water.
- ✓ Blending high fluoride water with low fluoride containing water.
- ✓ Provision of bottled water at least for growing young people.
- ✓ Treatment of water supply (defluoridation) at source and at the point of use.
- ✓ Transporting water from a distant source and harvesting rain water etc.

Transporting water from a long distance requires a significant initial investment, and providing bottled water is not economically viable in developing countries. As a result, for populations in underdeveloped countries like Ethiopia's Rift Valley Regions, where alternative water supplies are few, treatment is the only way to ensure safe drinking water. As a result, effective defluoridation technologies and adsorbent must be developed.

2.10. Defluoridation Techniques

Defluoridation is the process of eliminating fluoride ions from water. Treatment of excess fluoride concentrations by an appropriate method of eliminating fluoride from water is required to comply with the safe drinking water rule. Defluoridation of water at the point of use or source is required in drinking water with a high fluoride concentration to eliminate any unwanted effects. For the elimination of excess fluoride from water, a variety of treatment approaches have been invented. Among them Precipitation, adsorption, and membrane-based approaches are obvious categories based on the mechanism of fluoride removal. Adsorption is the most regularly used method for removing fluoride from drinking water among commonly used methods of defluoridation of water. Adsorption seems to be economical and user-friendly especially in the developing world where point of use treatment is recommended.

2.10.1. Adsorption methods

Adsorption is the process by which ions or molecules in one phase tend to condense and concentrate on the surface of another phase [62]. Fluoride is removed via adsorption processes due to physical, chemical, or ion exchange interactions with the adsorbent.

2.10.1.1. Surface Chemistry and Forces Involved in Adsorption

Adsorption is a mass transfer process in which adsorbate accumulates spontaneously on a solid surface (adsorbent or substrate) as opposed to the bulk phase. Adsorption is the ability of porous solids with large surfaces, such as activated carbon, to selectively hold and release chemicals on the solid's surface adsorption. Physical adsorption and chemical adsorption are two different types of adsorption. Physical adsorption is defined as adsorption in which the forces involved are intermolecular forces (Vander Waals forces) and in which the electronic orbital patterns of the species involved do not change significantly.Adsorption in which the forces involved are valence forces of the same kind is known as chemical adsorption.

2.10.2. Common Adsorbent

For fluoride adsorption as an adsorbent, a variety of materials have been attempted and investigated. The cost of the medium and operating costs, ease of operation, adsorption capacity, potential for reuse, number of useful cycles, and the possibility of regeneration are all factors to consider when choosing an appropriate sorbent. The following sections categorize some of the most often used adsorbents for fluoride uptake from water.

Natural materials as adsorbents: A variety of natural materials are capable of adsorbing fluoride ions. Several studies have discovered that clay and zeolite which are naturally found in various regions of the earth's surface, can be utilized to remove fluoride from water [47], [63].

Metal and metal oxide based adsorbent: Some metal ions, such as Ca, Al and Fe, have a strong affinity for fluoride, and their fluoride complexes are naturally stable. Different researchers have shown that calcium-based adsorbents (lime stone, modified lime stone), iron-based adsorbents

(granular ferric hydroxide), and mixed oxide and hydroxide are excellent fluoride adsorbents [64]–[66].

Alumina based adsorbents: Water defluoridation has been claimed to be successful using alumina, activated alumina, and certain modified alumina. After an impregnation reaction, both unmodified activated alumina and chemically modified activated alumina with certain earth metal ions were reported to have effective performance for fluoride ion removal from water [16], [67], [68].

Biosorbents for fluoride removal: Biomass materials are made up of a variety of polymer compounds containing multifunctional groups. As a result, they will be crucial materials for separation and purification research. The principal biomaterials investigated and indicated to be efficient adsorbents for fluoride removal from aqueous solution include chitosan and modified chitosan, algal biomass, and cellulose [69]–[72].

Waste materials as adsorbent for fluoride ion removal: There are many different sorts of waste materials that come from agricultural fields, industrial processes, and mining, and they all need to be managed in some way. According to previous studies, some industrial waste (H_2SO_4 processing waste, Al industry trash, fly ash, fertilizer industry waste, and agricultural waste (corn, coconut, rice straw) were also evaluated and proved to be effective in removing fluoride from water [61], [73].

Carbonaceous Materials*:* Diverse carbons from various species have been synthesized and employed as adsorbents for defluoridation investigations and other reasons in recent years. The raw elements required to make carbon are widely available. Any carbonaceous material with high carbon content (animal, plant, or mineral origin) can be easily converted to activated carbon (using both chemical or gas activation methods). Wood, charcoal, fruit pits, lignite, bone, and paper mill waste (lignin) are the most frequent raw materials used in the production of activated carbon [74]. Activated Carbon Most of the carbons prepared from different carbonaceous sources showed fluoride removal capacity after alum impregnation. High Fluoride removal capacities of various types of activated carbons had been reported. Alkali digested alum impregnated paddy husk carbon was an efficient defluoridating agent [75]. Carbon Activated After alum impregnation, the majority of carbons synthesized from various carbonaceous sources

demonstrated fluoride removal potential. Activated carbons of various sorts have been reported to have high fluoride removal capabilities [76]. Also porous carbon materials with a large surface area can be employed as a support matrix for metals/metal oxides, improving their adsorption characteristics. Graphene (G), graphene oxide (GO), and their composites are promising adsorbents that are beast candidate to remove pollutants from water due to their large surface areaand surface functional group [77].

2.11. Graphite and its derivatives application on adsorption

Graphite is another crystalline carbon form besides from diamond and fullerene. It is a naturally occurring mineral found in metamorphic rocks [78].Graphite is an anisotropic material that has strong electrical and thermal conductivity inside the layer (owing to in-plane metallic bonding) but poor conductivity between layers (due to weak van der Waals forces between the layer) [79]. Graphite is an attractive substance with a wide range of applications due to its metal and non-metal characteristics. Due to its high demand and limited supply from natural sources, graphite has been labeled as a "supply risk" commodity. Synthetic graphite will be a wonderful choice for closing the gap between supply and demand.Synthetic graphite production has attracted a lot of attention in recent years, owing to the ever-increasing need. Plants or plant-based material generated from nature that may be synthesized through biological photosynthesis are commonly referred to as biomass [80]. Due to its ubiquity, environmental safety, and low cost, biomass has recently been suggested as a potential precursor for graphite manufacturing [13]. It offers the advantages of being plentiful, inexpensive, and clean, with a high use potential [14].

Research has been carried out on potential application of biomass. Among the potential application discovered were biochar for soil amendment as biomass waste are rich with carbon super sorbent characteristic. In their study also reported that present of early development of crystalline structure through XRD data. This study relays on this concept which is, high carbon content and crystalline structure making biomass are suitable precursor for development of graphite.The use of high carbon content feedstock is an important feature of graphite production.The abundant availability of fast-growing lignocellulosic biomass makes it a fantastic alternative to food crops as a raw material. Lignocellulosic biomass is a fibrous, complex substance present in cell walls. Cellulose, hemicelluloses, and lignin are the three primary

structural units [81], [82]. Cellulose makes up 40-50 percent of lignocelluloses, while hemicelluloses make up 20-30 percent and lignin makes up 15-25 percent. The use of biomass in a sustainable and efficient manner will have a huge impact on the environment [83]. Among that lignocellulostic biomassbamboo is a renewable biomass resource because it is one of the fastest growing plants on the planet and have high amount of carbon content in its chemical structure.

2.12. Graphite from biomass

The chemical composition of carbon sources is one key aspect that affects the degree of graphitization. In order to achieve a high yield and high degree of graphitization, plant-based biomass with a high lignin percentage, low cellulose fraction, low oxygen, and high nitrogen content must be chosen[78].Graphite powder can be replaced with any hydrocarbon-rich agro-waste (cellulose 45-55 percent, hemicellulose 20-25 percent, and lignin 18-24 percent). In Scurlock et al research measured the cellulose, hemicelluloses, and lignin content of bamboo and found that it was 43.3 percent, 24.6 percent, and 26.2 percent, respectively. According to that study bamboo is a promising biomass due to having high carbon content and relatively fulfils composition requirements for better graphitization. It was believed that biomass waste is an ideal choice of raw material for graphite processing because the primary focus is the environment and cost. But most recently interesting findings become observed including this study.

2.12.1. Bamboo Resource in Ethiopia

Bamboos are enormous woody grasses that are members of the Poaceae family. Ethiopia has Africa's largest bamboo resources. Natural bamboo forests span around 1 million hectares in Ethiopia, accounting for about 7% of the global total and 67% of the African bamboo forest. which is covered in natural bamboo on an area of 850,000 hectares [84]. Kassahun [85] report that, there are highland and lowland bamboos.

Highland bamboo: The highland bamboo [86] Ethiopia's highlands in the south, south-west, central, and north-west are home to this plant.

Lowland Bamboo: Oxytenanthera Abyssinian is the Ethiopian botanical name for lowland bamboo. It is an Ethiopian native and unique to tropical Africa [87]. This species grows only in the Western part of Ethiopia.

Table 2.3 Component analysis of Bamboo in Ethiopia

Components Analysis	Y. alpine (highland bamboo)	O. abyssinica (lowland bamboo)
Moisture (%	3.92± 0.46	-
Ash (%)	3.77 ± 0.86	5.30
Lignin (%)	25.27 ± 1.52	22.47
Cellulose (%)	46.76 ± 1.09	52.06
Hemicellulose (%)	12.18 ± 1.01	16.90
Reference	[88]	[89]

Table 2. 4 Major highland bamboo areas in Ethiopia

No	Bamboo area	region	Plantation(hectare)	Natural Stand (h)
1	Mizan Teferi/Kulish	South	1850	1850
2	Agaro	Oromiya	1500	---
3	Gera	Oromiya	1250	36,000
4	Chencha/Arbamench	South	3250	2460
5	Wushewush/Bonga	South	1120	---
6	Masha	South	---	18652
7	Munesa/Shashemene	South/Oromiya	---	4183
8	Injibara	Amhara	2350	30

Sources:[90].

2.12.2. Biochar preparation Technologies

When biomass, such as wood, manure, or leaves, is heated in a closed container with little or no available air, biochar (BC) is produced. BC is created through the so-called thermal decomposition of organic material in the presence of a limited supply of oxygen (O2) and at a low temperature [91]. Biochar production methods and the growing interest in using biochar for diverse uses have resulted in a higher conversion of biomass to biochar. Thermochemical conversion is a common method for making biochar. Pyrolysis, hydrothermal carbonization, gasification, and torrefaction are examples of thermochemical conversion methods [92], [93]. For maximal biochar yield, the manufacturing technology must be suited for the biomass type, and process factors such as heating rate, temperature, residence time, and so on.

2.12.3.General Production Method of Graphite

In recent years, there has been a surge in interest in graphite, prompting studies into possible synthetic graphite alternatives. Chemical vapor deposition, thermo-chemical technique, microwave heating, and laser evaporation are some of the methods that can be utilized to manufacture carbon material with graphitic framework. One viable avenue to prepared carbon material is by thermal heating method[82].

2.12.3.1. Thermal heating method

The thermal heating method is a method of converting biomass into energy or a chemical product through the use of heat. The process of thermal heating results in the majority of carbon remaining and other elements being expelled. In fact, the majority of today's carbon products are made from carbon-rich organic precursors processed at high temperatures in an inert gas flow [80]. Heat treatment is frequently done at extremely high temperatures, up to 3000 degrees Celsius, and takes a long period [94]. Graphitization is usually done with the help of a transition metal or a derivative of it as a catalyst to help lower the heat treatment temperature. During heat treatment, a portion of the carbon precursor is heated to a specific temperature in an inert environment. Graphitization is usually done with the help of a transition metal or a derivative of

it as a catalyst to help lower the heat treatment temperature. During heat treatment, a portion of the carbon precursor is heated to a specific temperature in an inert environment. With the inclusion of a pre-treatment or activating agent, graphitization can be done at various temperatures, with various catalyst compositions, and with various carbon precursors [94]–[96]. The quality of graphite produced is totally determined by the production parameter chosen. The use of a logical range and the best possible conditions will aid in the production of better-quality synthetic graphite[97].

2.12.3.2. Effect of heat treatment temperature

Heat treatment is a key aspect of the graphitization process because it provides energy for the macromolecule rearrangement process [97].The temperature effect could be caused by catalyst nucleating and growing into larger nanoparticles as the heating temperature rises. When heated to a higher temperature, the catalyst particle immediately expands into a large particle with strong crystallinity and dispersion, allowing the creation of a shell-like graphitic nanostructure [98].

2.12.3.3. Effect of pre-carbonization

procedure prior to pyrolysis some researchers used biomass as a carbon source by impregnating it with a catalyst and then heat treating it directly, while others used carbonization at a lower temperature before heat treatment [95], [99], [100].Those that have undergone hydrothermal carbonization have a highly structured graphite structure, whereas samples that have not undergone hydrothermal carbonization have a largely amorphous phase. They claim that the simple pyrolysis process is not responsible for the production and stacking of graphite, but rather that it is a phase in a two-step process that leads to the formation of graphite. Amorphous structure and behavior are not visible in samples without hydrothermal carbonization or lower temperature pyrolysis [101]. Findings suggest that hydrothermal carbonization or pyrolysis at lower temperatures is a crucial phase in the creation of graphite. When pre-carbonized material is utilized instead of raw biomass, it is also proposed that less energy is required during graphitization.

2.12.3.4. Effect of catalyst

Adding a catalyst to the graphitization process will improve the whole operation. The use of a catalyst during graphitization lowers the activation energy required for the conversion of amorphous to graphitic carbon. In general, this will aid in lowering the heat treatment temperature required to convert amorphous carbon to graphitic structure. The type of catalyst used has an impact on the final product. According to study in [102] they conclude that the catalyst is responsible for the formation of graphitic structures. The catalytic procedure allows both graphitizing and non-graphitizing carbon precursors to be converted into graphitic structure[99].Previous study has shown that iron has successfully stimulated the creation of graphitic structures and is the best metal for graphitization, and that the anion of metal salt influences the degree of graphitization.

Table 2.5 Different catalyst types for graphitization with their merits and demerits, if intended to apply for fluoride removal

Catalyst Type	Advantage	Disadvantage	Reference
Fe	Most active at lowest temperature (~ 750 °C). Fe may be there in graphite structure.	Porosity depend on amount of Fe used	[103]
FeCl2	Graphite produced Possessed a greater C=O and other surface functional group.	Competitive ion Cl- might be realized to the surface of graphite and compute for the active site	[104]
FeCl3	Carbonization step at lower temperature.	Graphite produced Possessed Low C=O. Competitive ion Cl- might be realized to the surface of graphite and compute for the active site	[95]

Ferrocene (C10H10Fe)	significantly Lower graphitization temperature (300 °C)	Availability.	[105]
K2FeO4	Used as both activating agent and a catalyst. Relatively low temperature for graphitization (800 °C). Possessed highly porous structure (micro porous structure).	Availability.	[96], [106]
Cu/Al2O3	Alumina support will remain as a support on graphitized carbon.	Further increase in the reaction temperature, decreasing in carbon yield observed. Before graphitization the catalyst activity may be stopped.	[107][13]

Table 3- 1: Process condition for graphitization of different biomass

Biomass	Heat treatment temperature	Catalyst	Additional information	Referance
Softwood sawdust	750°C	Ferum	Production of nanocarbon material, graphite obtains. Using tubular reactor for pyrolysis	[108]
Sawdust	900°C and 1000°C	Nickel (II) nitrate, Ferum (III) Nitrate	2.5 or 5 mmol/g sawdust	[99]
Sawdust	600°C to 800°C	Iron (III)chloride	Catalytic action of both Fe and Cl species is able to effectively catalyze the growth of carbon nanofibers on mesoporous carbon structure	[109]
Lignin	900°C	--	KOH or K_2CO_3 activation Lignin to activator ratio 1:1 Carbonized first at 250°C	[110]
Cellulose	800°C	Fe (III)NO_3 Fe (III)Cl Ammonium Iron (III) citrate	Anion of Iron salt effect the extent of graphitization.	[111]
Coconut she	900°C and 10°C 00°C	K_2CO_3, Fe (III)NO_3	Carbonization at 400°C Carbonized at 500°C	[112][113]
Bamboo	800°C	K_2FeO_4	Carbonization at 400°C Sample pre-treated with H_2SO_4	[106]
Microalgae	1000°C	Ferrous chloride	Without pre carbonization	[114]

CHAPTER THREE

3. MATERIALS AND METHODS

3.5. Materials and Equipment

Muffle furnace (model: SX-2.5-12) with an operating temperature around 1200°C, oven (model: NE9-56S), sieve (model: CEN-MKII-00-A), analytical balance (JA203H), beaker plastic bottles, Micro Processor pH-mV meter (SL-145), vacuum pump, filter paper, magnetic stirrer (XMTD-231), jar test (SW6), wood cutter machine, Grinder, glass paper, mortar and pestle,crucible (S-613F). Instruments such as an x-ray diffractometer (model: XRD700s) and a Fourier transform infrared (FTIR) were used (model: JASCOFTIR-6600typeA).

Table 3. 1List of chemical reagents

No	Reagents	Sources of product
1	Sodium Hydroxide (NaOH)	Apha chemicals
2	Potassium hydroxide (KOH)	Apha chemicals
3	Hydrochloric acid (HCl)	Alpha chemicals
4	Sodium fluoride (NaF)	Abron chemicals
5	Aluminium sulfate hexadecahydrate ($Al_2(SO_4)_3.16H_2O$	Central drug house (P) Ltd
6	Ferric chloride hexhydrate ($FeCl_3.6H_2O$)	Trust chemicals
7	Aluminum powder (Al)	Trust chemicals

3.6. Overall Flow Diagram or structural frame work

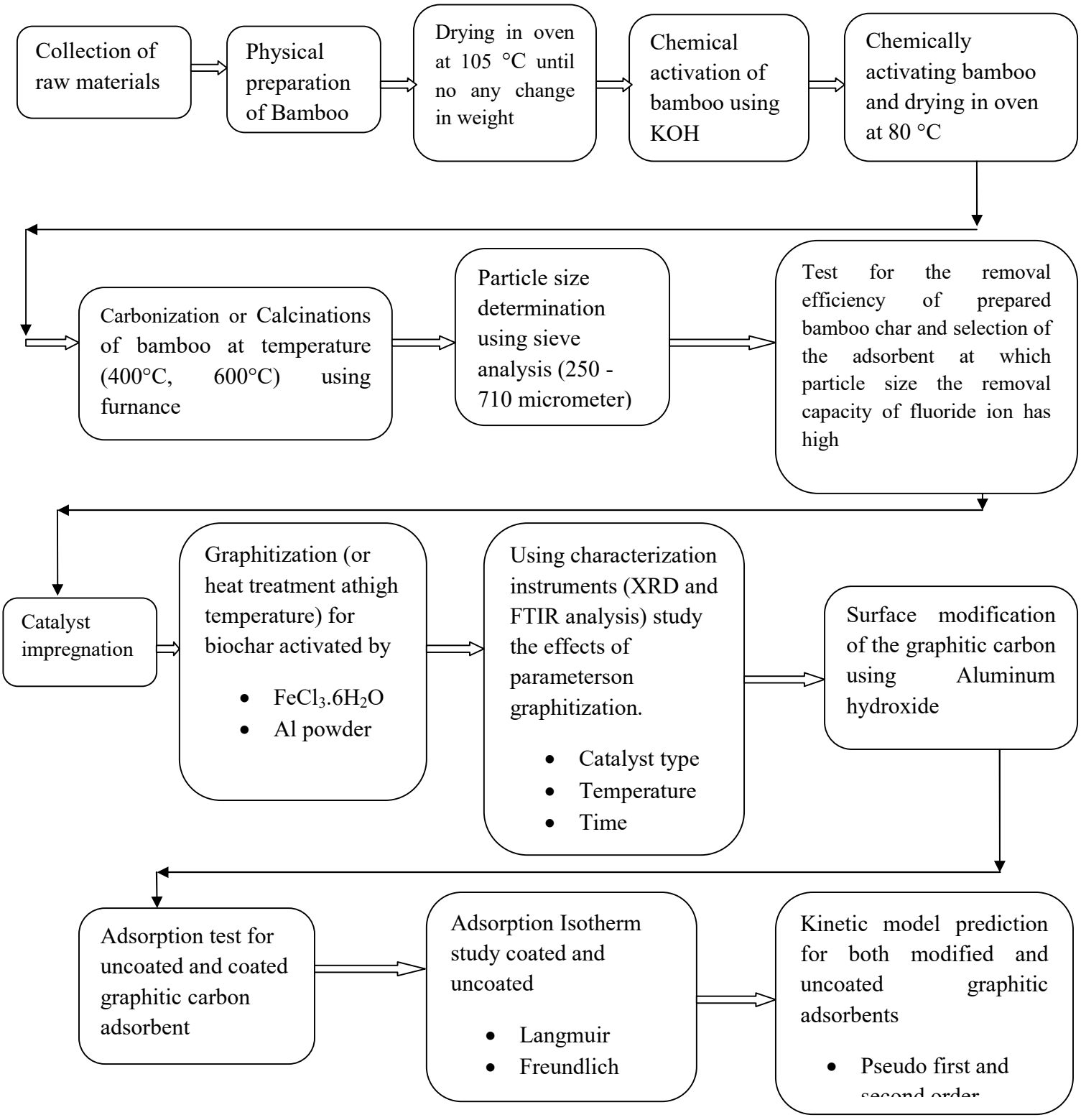

Figure 3. 1Structural frame work

3.7. Methods

3.7.1. Experimental procedure for preparation of bamboo char

3.7.1.1.Moisture content removal

The raw bamboo used in this study was collected from Shashemene area of Oromia regional state and it was cut into pieces of approximately 2x1.5cm in size and its thickness approximately 1 cm. Smaller particles with increased surface area and it also enabled more efficient chemical activation of the raw material. Then the bamboo was separated from the solution and dehydrated in an oven at 105^{o}C until its weight becomes constant. The moisture removal between 15 minutes was collected to obtain drying curve.

3.7.1.2. Chemical activation

Chemical activation of the bamboo was done using activating agents, named as potassium hydroxide (KOH) which was an effective activating agent as compared to NaOH and H3PO4 [17] [59]. The mixture then immersed 30% by volume for the chemical activation 1:4 bamboo precursors to activator was soaked for 24 hr and dehydrated in oven at 105°C for until its weight becomes constant.

3.7.1.3.Biochar yeiled

Biochar dried biomass samples were pyrolyzed in an electrical muffle furnace at different temperature (400 °C and 600 °C) for carbonization time 2h. The percentage of biochar yield was calculated using the equation described below

$$\text{Biochar yield} = \left(\frac{m\ \text{BC}}{m\ \text{RB}}\right) * 100\% \quad \ldots\ldots\ldots\ldots\ldots\ldots\ldots\ldots\ldots\ldots\ldots\ldots\ldots\ldots\ldots\ldots$$

Where $\text{Yield}_{\text{biochar}}$ = mass yield of biochar in %; m_{BC} = mass of biochar in g, m_{RB} = mass of raw bamboo in g.

Experimental procedure for raw material preparation

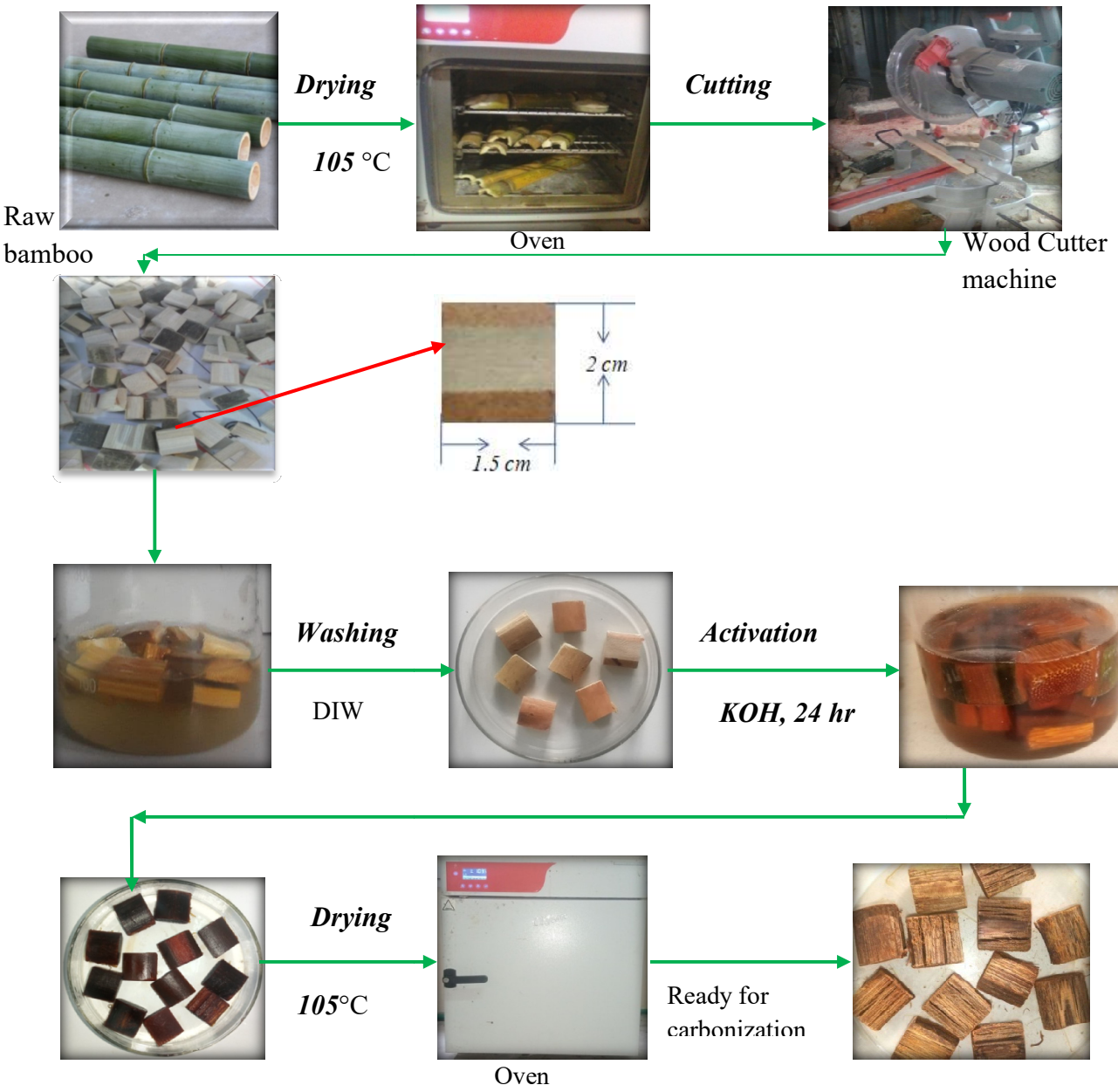

Figure 3. 2 Experimental procedure for raw material preparation

3.7.1.4. Carbonization

The impregnated dried sample was inserted into stainless steel reactor that have been designed then ordered and manufactured at ASTU mechanical engineering department welding & sheet metal workshop. Then after carbonized on box type resistance muffle furnace at different temperature of 400 °C and 600 °C and calcination time was for 2 hr as it was an optimal

calcination period [59]. After collecting the product, the charcoal was further crushed into smaller particles using mortar and pestle. To remove remaining impurities such as ash, the synthesized activated carbon, was washed with a hydrochloric acid (HCl) aqueous solution (5% by weight). Bamboo char was screened using sieve of 250-355, 355-500 and 500-710, μm size in order to obtain uniform particles division.

3.7.2. Experimental procedure for preparation of graphite

Bamboo char powder was dispersed in aqueous solution of 20w/w% catalyst ($FeCl_3.6H_2O$) which is 80 percent bamboo to 20 percent catalyst, with continuous stirring for 8 h, and it was dried at 105°C to obtain a solid mixtureThe mixture was then transferred a Crucibles then it was inserted in to muffle furnace and heated at 800°C, 900°C, and 1000°C for graphitization time 1.5 hr, 2.5 hr and 3.5 hr. Finally, the collected samples were washed repeatedly with diluted HCl (5% by weight) and deionized water to remove residual inorganic impurities, followed by drying at 80 °C. Those operating conditions were selected after detail study on related works as it was discussed on literature part of this study. The resultant samples were denoted as G-$FeCl_3.6H_2O$ $_{800°C.}$ Similarly for catalyst Al powder was prepared and denoted as G-$Al_{800°C}$.

3.7.3. Method of coating of aluminum hydroxide on bamboo driven graphite surface

Aluminum hydroxide was coated on bamboo driven graphite using a stirred tank reactor, then filtered and dried using a vacuum filter and drying oven. In a stirred tank reactor, a 2 gram graphite sample was combined with 30 ml of 1M aluminum sulfate solution as it was an optimal volume and concentration [59]. A magnetic stirrer was used to agitate the reactor at 80 rpm with a 1M sodium hydroxide solution. When sodium hydroxide interacts with aluminum sulfate, aluminum hydroxide is formed, which is then deposited on the graphite surface. The addition of sodium hydroxide is critical in this procedure, and it was monitored by measuring the pH of the mixture. The addition of sodium hydroxide was stopped after the pH of the reaction media reached the required value of 7. Finally, a mixture of sodium sulfate and aluminum hydroxide deposited to graphite surface. After that, the entire slurry was filtered and dried at 105°C until the appropriate adsorbent was obtained. However, in order to remove all sodium sulfate, the coated

graphite was carefully washed with deionized water and dried again in an oven at 105 degrees Celsius.

Experimental procedure for carbonization and graphitization

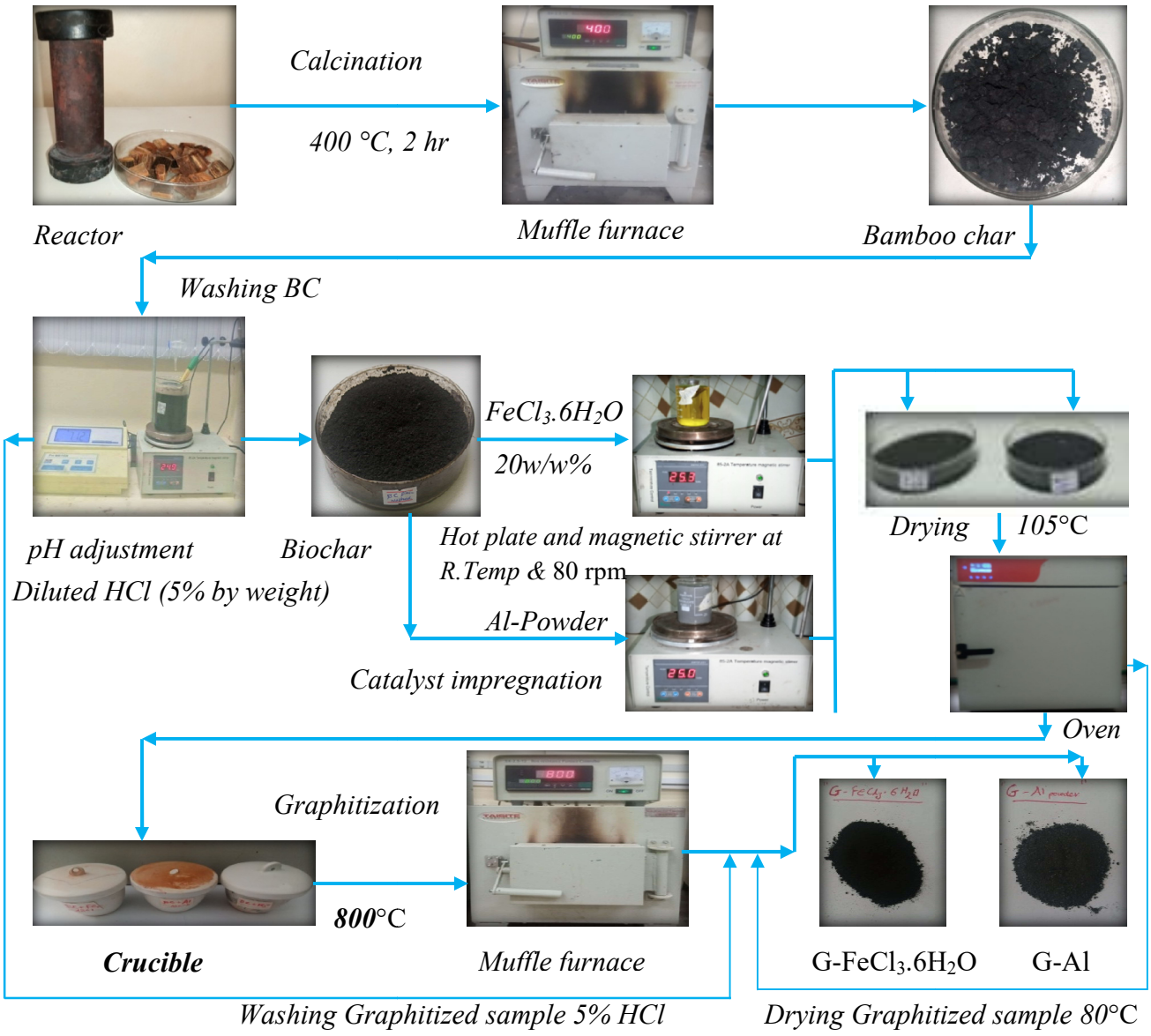

Figure 3. 3 Experimental procedure for carbonization and graphitization

3.7.4. Preparation of synthetic fluoride water

Standard Solutions and Reagents In a volumetric flask, 2.21 g of anhydrous sodium fluoride (99.0 percent NaF, Abron chemicals) was dissolved in 1000 ml deionized water to make a 1000 mg F-/L fluoride stock solution. By diluting the stock solution with deionized water, standards and samples solutions of fluoride at a necessary concentration range were created.

3.7.4.1. Instrumentation

For routine F - determination, F - ion selective electrodes were used. The pH was determined using apH/ion meter. The concentration of the liquid phase F - was determined as follows (according to the procedure outlined in the instrument's manual): The mixture was thoroughly swirled (uniformly at stirrer speed of level 80 rpm) using the magnetic stirrer after equal quantities (100 ml) of samples were placed in a 500 ml beaker.

$$Cf = (10 \,\hat{}\,(-\mathrm{Px})) * 19000 \quad \ldots\ldots\ldots\ldots\ldots\ldots\ldots\ldots\ldots\ldots (3.1)$$

Where C F^- is fluoride concentration, Px-is reading from the instrument the precision of the measured value was determined by measuring 5 replicate fluoride solutions of 10 mg/l with the pre-calibrated instrument.

All of the experiments were carried out in a jar for a predefined amount of time with an impeller spinning at 200 rpm and on atmospheric temperature.

3.7.5. Batch Adsorption Procedures

The effects of various adsorbent preparation and adsorption operation parameters on fluoride ion adsorption on bamboo char and bamboo driven graphite samples (G-$FeCL_3.6H_2O$ and G-Al) were evaluated in this study. Furthermore, an alternate modification of graphite was performed to improve its properties by coating graphite surface using aluminum hydroxide and testing its adsorption capacity. All of the experiments were carried out in a jar for a predefined amount of time with an impeller spinning at 200 rpm. Before fluoride analysis, a sample was taken out of the flask and filtered using Whatman filter paper at a predetermined contact time filtered through a 0.2 µm the filtrate was analyzed for residual fluoride content. The following equation [16] was

used to calculate the percent adsorption efficiency and defluoridation capacity of the selected adsorbents:

$$\% \text{ Adsorption} = \left(\frac{Co - Ct}{Co}\right) x\ 100 \quad \ldots\ldots\ldots\ldots\ldots\ldots\ldots\ldots\ldots\ldots(3.2)$$

$$\text{Defluoridation Capacity } \left(\frac{mg\ F-}{g}\right) = \frac{C0 - C}{m} \ldots\ldots\ldots\ldots\ldots\ldots\ldots\ldots(3.3)$$

Where, Co = initial F - concentration Ct = F - concentration at time t, m = dose of adsorbent in g/l. to ensure that F - does not adsorb on the inner walls of the adsorption vessels (glass baker), blank runs were performed. In this procedure a 10 mg F -/l solution was added to a glass vessel and the F - concentration measured after 1 h and again after 6 h. No significant reduction in F - concentration was found.

3.8. Factor Affecting Fluoride Removal Capacities

3.8.1. Effect of Adsorbent Dose and Contact Time

To investigate the effect of dose and contact time of coated, experimental investigations were carried out at different dosages by increasing by 0.5 intervals with contact time of 2 hr (0.5, 1, 1.5, and 2.0 g/l) of adsorbent with initial fluoride concentration of 11.72 mg/L. The dosage range was selected based on initial preliminary screening experiments and the initial F^- concentration was selected based on the average fluoride concentration around adama Ethiopia.

3.8.2. Effect of particle size

The effect of particle size of bamboo char was studied by considering the adsorbent size from 250-355, 355-500, 500- 710, µm to investigate the removal capacity.

Experimental procedures for Adsorption test and surface modification

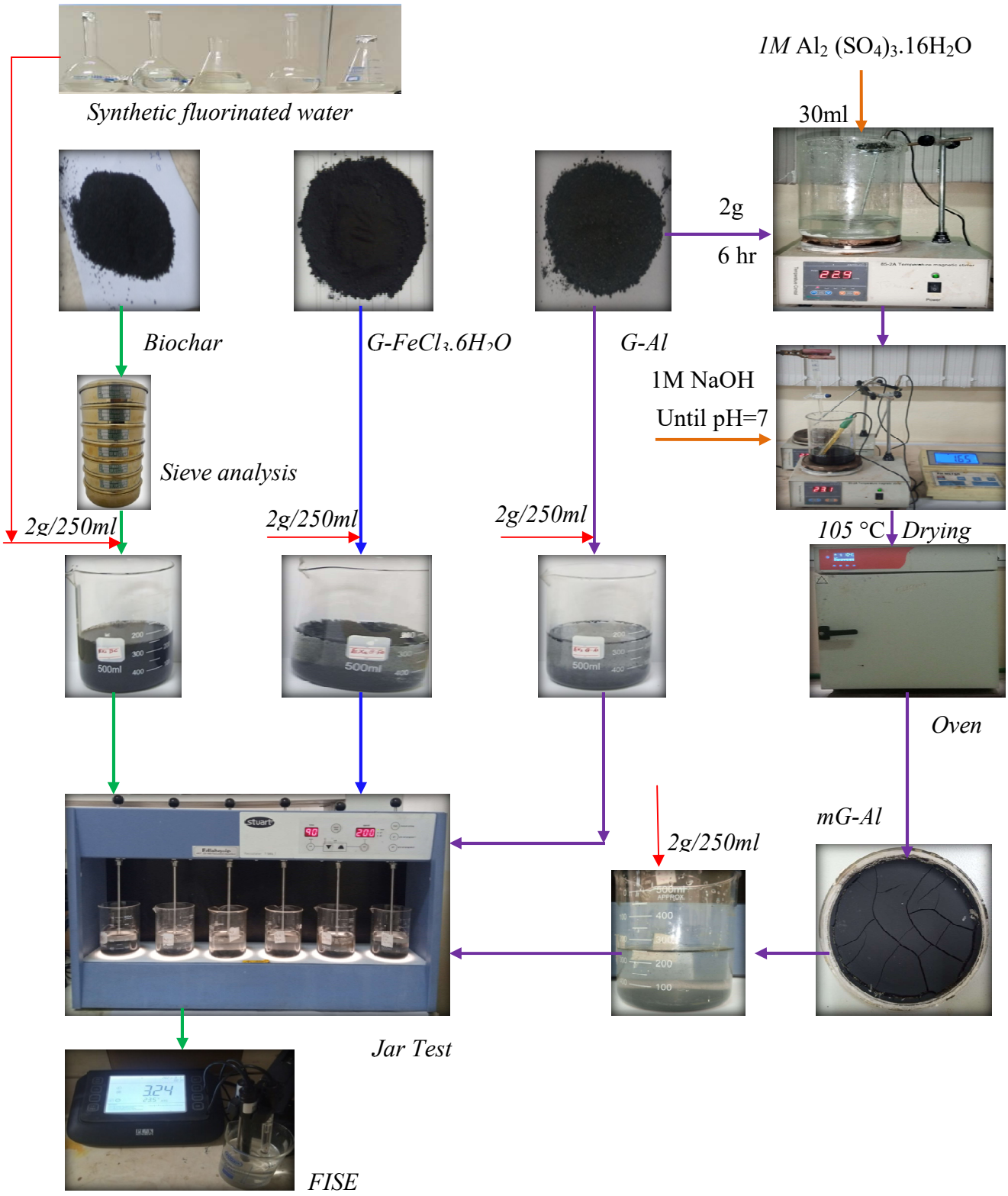

Figure 3. 4 Experimental procedures for Adsorption test and surface modification

3.9. Determination of Adsorption Isotherms

Adsorption at constant temperature, isotherm tests were carried out to investigate the link between the adsorbent's solid phase and solution phase concentrations. For both biochar and graphitic carbon adsorbents, data for plotting isotherms was acquired by mixing a constantadsorbent dose of 2 g/250ml with 5 series of rising in F^- concentration (3 mg/l, 5 mg/l, 7 mg/l, 9 mg/l and 11.72 mg/l). The adsorbent–liquid mixture was agitated until it reaches equilibrium. A residual fluoride in solution was determined and all the values necessary to plot an isotherm were generated and calculated from these determinations.

Langmuir adsorption isotherms

Langmuir sorption isotherm assumes the monolayer coverage on a structurally homogeneous surface of the adsorbent. The Langmuir isotherm model can be represented in the form

$$\frac{Ce}{qe} = \frac{Ce}{Qo} + \frac{1}{QoKl} \quad \text{.....(3.4)}$$

Where Ce is the equilibrium fluoride concentration (mg/L), qe the amount of fluoride adsorbed per unit mass of the adsorbent at equilibrium (mg/g), qo is the monolayer adsorption capacity of the adsorbent (G-Al) (mg/g), The values of Langmuir constants Kl and qo can be calculated from the slope and intercept of the linear plot of Ce/qe versus Ce.

Freundlich adsorption isotherms

The Freundlich isotherm is the earliest known connection defining non-ideal and reversible adsorption that is not limited to monolayer formation. This empirical model may be applied to multilayer adsorption with non-uniform adsorption heat and affinities distribution throughout the heterogeneous surface [22]. The Freundlich isotherm has fewer limitations than the Langmuir isotherm, in that it can cope with both homogeneous and heterogeneous surfaces, as well as physical and chemical adsorption. This model is particularly good at describing the adsorption behavior of organic molecules and reactive materials. The slope and intercept of the linear plot between log qe and log Ce can be used to compute these constants. Adsorption on heterogeneous surfaces is a need for the validity of a Freundlich type adsorption model [67]. The rise in

equilibrium fluoride removal capability seen with residual fluoride concentration can support the heterogeneous adsorption situation.

$$\log(qe) = \log(Kf) + \frac{1}{n}\log(Ce) \ldots\ldots\ldots\ldots\ldots\ldots \text{(3.5)}$$

Where, qe = the amount of fluoride adsorbed per unit weight of adsorbent (mg/g) at equilibrium Ce = the equilibrium fluoride concentration (mg/L) KF = the measurement of the adsorption capacity (mg/g) based on Freundlich isotherm 1/n = the adsorption intensity (the degree to which adsorption is a function of concentration).

3.10. Adsorption Kinetics model

The solute uptake rate is characterized by sorption kinetics, which determines the sorption reaction's and residence time. It is one of the most essential criteria in determining sorption efficiency. In order to investigate the controlling mechanism of adsorption processes such as mass transfer and chemical reaction, the pseudo-first-order and pseudo-second-order equations were used to model the kinetics of fluoride adsorption on both (G-Al) graphitic carbon and modified G-Al graphitic carbon adsorbents.

3.10.1. Pseudo-First Order Kinetic Model

This model, which assumes first-order adsorption kinetics, is also known as the Largergren model. Lagergren's first order rate equation is one of the most extensively used rate equations for describing adsorbate adsorption from the liquid phase. Most systems follow the pseudo-first-order rate equation when adsorption is preceded by diffusion via a boundary. Lagergren's pseudo first-order rate expression has the following linear form:

$$Ln(qe - qt) = Lnqe - k1t \ldots\ldots\ldots\ldots\ldots\ldots \text{(3.6)}$$

Where qe and q_t (mg/g) are the amounts of fluoride ions adsorbed at equilibrium or adsorption capacity at equilibrium and the adsorption at time t, respectively, and K_1 is the kinetic constant of pseudo-first-order adsorption (min^{-1}). For both (G-Al) graphitic carbon and modified G-Al graphitic carbon adsorbents. The plot of log ($q_e - q_t$) versus t was give a linear relationship from which k_1 and q_e can be determined from the slop and intercept of the plot, respectively.

3.10.2. Pseudo second order kinetic model

The pseudo second-order equation predicts behavior over the entire adsorption duration, with the adsorption (chemisorptions) process serving as the rate-controlling phase [20, 21, 23], involving valance forces via electron sharing or exchange (between adsorbate and adsorbent). The advantage of this model is that it may be used to predict adsorption capacity, pseudo-second order rate constant, and starting adsorption rate without knowing any parameters beforehand. The pseudo-second-order equation is expressed as follows:

$$\frac{t}{qt} = \frac{1}{k2qe^2} + \frac{t}{qe} \quad \text{.....(3.7)}$$

= Where q_t (mg/g) is the amount of fluoride ions adsorbed at time t, K_2 is the pseudo-second-order rate constant of adsorption (g/ (mg.min)), q_e is the adsorption capacity at equilibrium (mg/g) and t is the contact time (min). For both (G-Al) graphitic carbon and modified G-Al graphitic carbon adsorbents.The plot of t/qt against t of the preceding equation should produce a linear connection if the second order kinetic equation is appropriate. The slop and intercept of the plot t/qt against t, respectively, can be used to get the q_e and K_2. The significance of the pseudo second-order model will be determined by the correlation coefficients (>0.9) from the plot (t/qt) vs. t and the determination of the values q_e and k_2 from the slope and intercept of the related plot [22].

3.11. Characterization Instrument

3.11.1.X-ray diffraction (XRD)

X-ray scattering techniques are a group of non-destructive analytical techniques that reveal crystallographic structure information. X-ray crystallography is applied in two key areas: fingerprint characterization and structural identification of crystalline materials. When an X-ray beam contacts the crystal, it is elastically scattered in several different directions while maintaining its wavelength. From the various angles and intensities of these diffracted beams, a three-dimensional picture of the electron concentrations within the structure can be seen. Each crystalline solid has its own set of patterns that may be used to identify the material and deduce additional details such as the atoms' mean positions in the crystal structure, their bonding, and

disorder. In this study bamboo char and graphite synthesis on distinct parameter effects studied by comparing diffraction data to a database kept by the International Centre for Diffraction Data, powder diffraction and previous related research work is often used to identify components manliy graphite. It may also be used to characterize heterogeneous solid mixtures in order to estimate the relative abundance of crystalline components, and it can reveal structural information on unknown materials when combined with lattice refinement techniques like Rietveld refinement. Powder diffraction is another popular method for determining crystallinematerial stresses. Powder XRD (XRD 7000S) utilizing CuK radiation to discover a crystalline phase of samples.

3.11.2. Fourier Transform Infrared Spectroscopy (FTIR)

The FTIR method is particularly useful for identifying organic and inorganic compounds. It can be used to quantify some components of a combination that is unknown. FTIR is one of the most potent tools for determining chemical bond types (functional groups). In this study the functional group in raw bamboo, biochar, activated biochar, and graphitic carbon material at various graphitization parameters was investigated using fourier transform infrared spectroscopy (FTIR). This spectrum shows the wavelength of light absorbed, which is typical of the chemical bond. The chemical bonds in a molecule can be established by reading the infrared absorption spectrum.

3.11.3.Thermo gravimetric analysis or thermal gravimetric analysis (TGA)

TGA is a method of thermal analysis in which the mass of a sample is measured over time as the temperature changes. Thermo-gravimetric analysis (TGA) is conducted on an instrument referred to as a thermo-gravimetric analyzer. A thermo-gravimetricanalyzer continuously measures mass while the temperature of a sample is changed over time. Mass, temperature, and time are considered base measurements in thermo-gravimetric analysis while many additional measures may be derived from these three base measurements.TGA can be used to evaluate the thermal stability of a material. In a desired temperature range, if a species is thermally stable, there will be no observed mass change. Negligible mass loss corresponds to little or no slope in the TGA trace. TGA also gives the upper use temperature of a material. Beyond this temperature

the material will begin to degrade. For this sudy TGA was used to determine thermal stability of selected catalysts (Aluminum powder and Ferric chloride hexahydrate) for bamboo driven graphite preparation.

3.11.4.X'Pert HighScore Software

X'Pert High Score is a complete full powder pattern analysis tool. It unites phase identification, crystallographic analysis, cluster analysis, and calculations in one software package covering all common powder diffraction applications. X’pert High score Plus are software packages that incorporates the latest technologies and algorithms for X-ray powder diffraction data analysis. X’pert high score is a comprehensive phase identification program for powder diffraction data. For this study diffraction data was used on X’pert High score plus software for identification of graphite formation from bamboo driven graphite samples. Those results were confirmed graphite formation, X’pert High score plus software result was presented on Appendix A of this study.

CHAPTER FOUR

4. RESULT AND DISCUSSION

4.5. Carbonization at different temperature

4.5.1. Biochar yield

From those triplicate data for yield of biochar estimation at 400 °C and 600°Clisted on Table 4.1 the char yield at 400°C carbonization have maximum (45.05%) and minimum of (42.41%), taking the average weight after carbonization the biocharyieldat 400 °C is 43.62% . in similar manner calculating biochar yield at 600°C was 34.15% we can conclude that pre carbonization at relatively low temperature (400°C) have better biochar yield. from this correlation occurred between the pyrolysis temperature and the biochar yield, indicating a decrease in yield due to the increased pyrolysis temperature.

Table 4. 1 Biochar yield at different temperature

Exp. Code	Temperature	Time	Weight before carbonization	Weight After carbonization	Average	Bamboo chars Yield (%)	Error (%)
Ex1400	At 400 C	2 h	26.5 g	11.24g	11.56 g	42.41	2.438
Ex2400				11.52 g		43.47	
Ex3400				11.94 g		45.05	3.507
Ex1600	At 600 C	2 h		8.77 g	9.05 g	33.09	2.876
Ex2600		2 h		9.03 g		34.07	
Ex3600		2 h		9.37 g		35.36	3.648

4.6. Study of graphitization parameters using XRD Instrument

4.6.1. Graphitization of bamboo char

The XRD analysis showed the crystalline nature and revealed the structure of aromatic layers as indicated by the extremes at 2θ (20–30◦). XRD analyses show that the carbonized bamboo formed in an amorphous and crystalline state. Crystallites perpendicular to aromatic layers have small dimensions and broadening is the result of these small dimensions[115]. The activated carbon from bamboo has formed indicated by Peaks formed at 40.62°, and 58.60°. Relatively a small shoulder was observed at 2θ = 24.17°, and 31.27°. This result shows that carbonization of bamboo at 400°C has very small amorphous nature. Implies that transformed the cellulose to carbon but some high content of cellulose is not broken completely by KOH and heat treatment to form amorphous carbon. This suggests that the crystallinity of the bamboo activated carbon is relatively high. XRD pattern matches well to previously reported pattern for non graphitic carbon [116]. It can be conclude by simple pyrolysis process is not responsible to the formation of stack graphite. Pyrolysisprocess at lower temperature acts as step leading for the formation of graphite in two-step process.

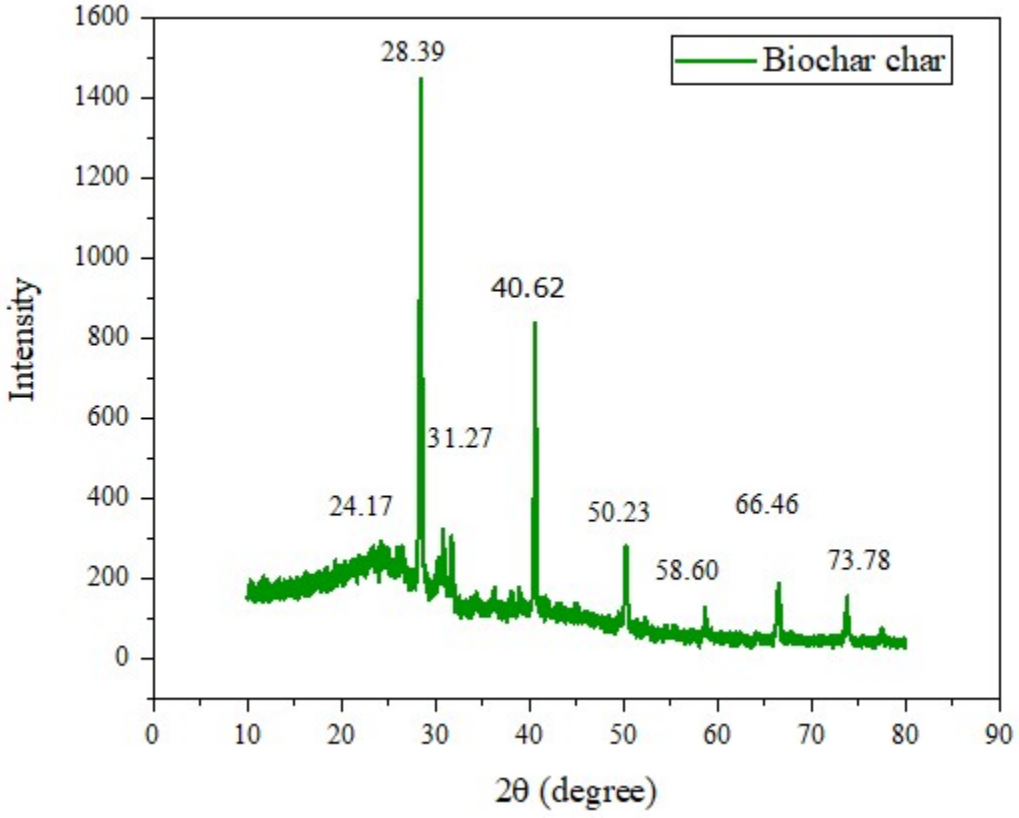

Figure 4. 1 X-ray diffraction pattern biochar at 400 °C

4.6.2. Effect of catalyst type

Two different catalysts (Aluminum powder (Al)and Ferrous chloride anhydrous ($FeCl_3.6H_2O$)), were studied to observe their effect on graphitization process of bamboo char at constant temperature 800 °C and 1.5 hr graphitization time.

4.6.2.1. XRD of graphitic sample using aluminum powder as a catalyst (G-Al 800 °C)

In figure 4.4 graphitic sample G-Al $_{800\ °C}$ new formation of broad amorphous peak between 20-30, this revealed that the structure of aromatic layers refer to the stacking structure of aromatic layers (graphite), are evolving to exist and the broadening has originated from the small dimensions of crystallites perpendicular to aromatic layers [117]. A typical graphite crystal structure was confirmed by the sharp peak appearing at approximately 2θ = 44.46° [118]. From XRD pattern a sharp more intense peak formed at 44.46 which was a graphitic reflection peak

that was not found in BC. The strong and dominant peak at 28.39° in BC becomes shortened have small intensities and a new dominant peak at 2θ = 38.35° was formed. 50.23°, 58.60° are eliminated in a graphitic sample G-Al $_{800\ °C.}$ Finally significant peaks more intense peak as compared to BC at 2θ = 77.99° was appeared.

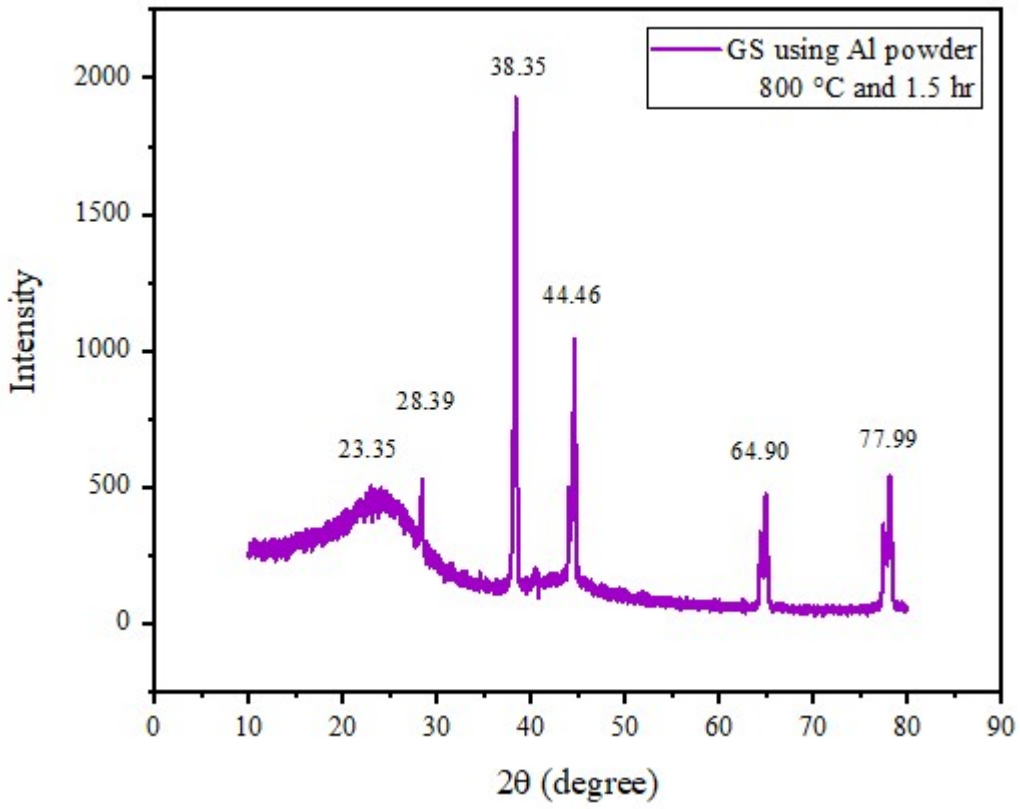

Figure 4. 2 X-ray diffraction pattern of G-Al at 800 °C

In Figure 3 graphitic sample using catalyst ($FeCl_3.6H_2O$) a typical amorphous graphite crystal structure, which was confirmed by the broad peaks appearing at approximately 2θ = 24° and sharp peak at 2θ = 44° [119]. In (G-$FeCl_3$.6(H_2O) The broadness of an amorphous graphite structure between 20 and 30 becomes decreasing relative to G-Al $_{800\ °C.}$ This indicates that it could be formation of graphitic reflection peak which favors using catalyst $FeCl_3.6H_2O$. Since little sharp peak at 2θ=26.84° appeared which is near to the obvious crystalline graphitic reflection peak which assigned to the planes of graphite [120]. An activated carbon reflection peak was formed at 2θ=43.07°.Finally the Sharp Peaks at 2θ=35.39° and small peaks at 29.97°, 62.44° was newly formed in graphitic sample G-$FeCl_3$.6 (H_2O). Notice that this comparison does

not necessarily determine which catalyst is better for graphitization because each type of catalyst behave different thermal behavior at 800 °C this comparison is only based on by searching an obvious graphite reflection peaks.

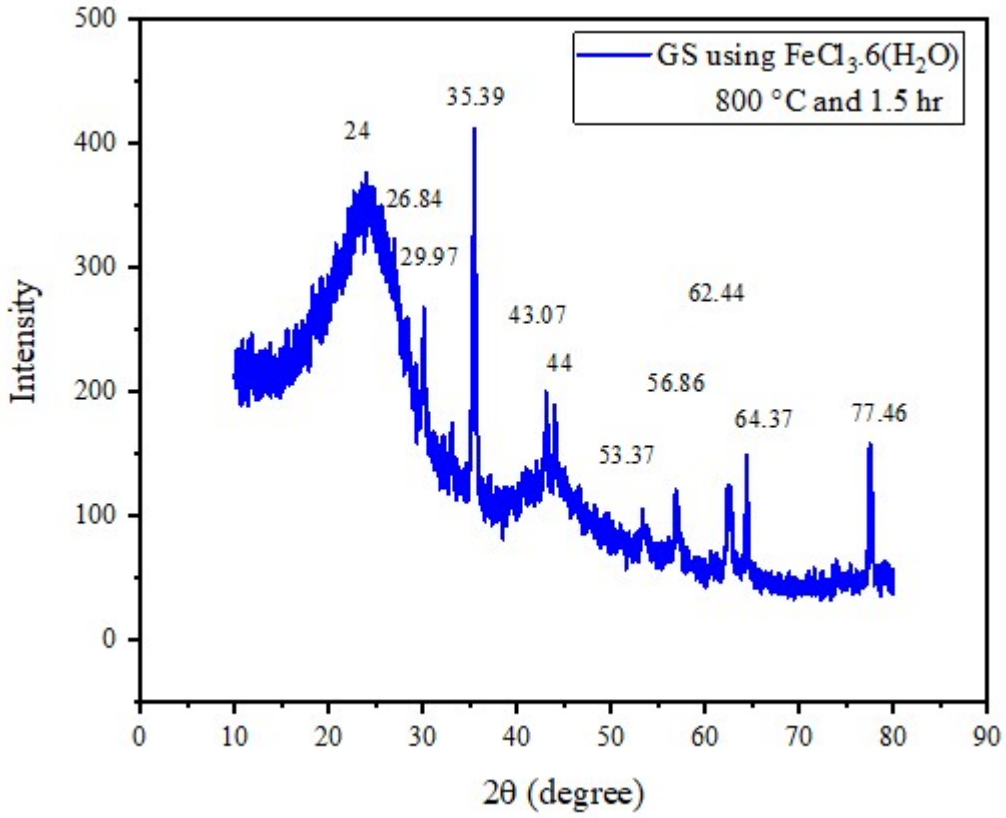

Figure 4. 3 X-ray diffraction pattern of G-$FeCl_3.6H_2O$ at 800 °C

4.6.2.2.D-spacing using Bragg's law

Periodically re-occurring distances of lattice planes (d-spacing) to the wavelength λ and the Bragg angle θ (n is an integer number).

$$n\lambda = 2\,d\sin\theta \quad \text{.....(3.8)}$$

Theoretically, ideal Bragg diffraction should yield infinitely sharp reflections (delta functions): a single exact wavelength diffracted at lattice planes with an exactly defined d-spacing would fulfill Bragg's law only for an exactly defined angle. However, neither the experimental setup nor

the investigated sample will ever be ideal. All imperfections of the experiment and the sample will contribute to some softening off Bragg's law, resulting in noticeable broadening of the observed peak profiles.There is a close relationship between the degree of graphitization and the interplanar spacing D002 of carbon materials. Dealing with a typical amorphous graphite crystal structure formation appeared near to 24° for both catalysts the graphitization degree can be discussed below by relating with their respective D-spacing.

In table 4.2 from the graphite samples using two catalyst (Al powder and$FeCl_3.6H_2O$) G-$FeCl_3.6H_2O$ have a low interlayer spacing relative to other graphite sample this implies that $FeCl_3.6H_2O$ have a tendency for better graphitization rather than Al powder. This is confirmed by [121] the smaller the value of carbon crystallites displacing (D002) is, the higher the degree of graphitization.

Table 4. 2 Inter layer spacing of bamboo driven graphite sample

Graphitic Sample	D-Spacing (A^0)
G-Al $_{800°C}$	3.696
G-$FeCl_3.6H_2O$ $_{800°C}$	3.599
Commercial Graphite	3.343

G-$FeCl_3.6H_2O$ have lower inter layer spacing-spacing than G-Al $_{800\ °C}$. But in G-$Al_{800°C.}$ Natural graphite has two peaks with the interplanar crystal spacing of 3.34A˚ and 1.67˚ A˚ corresponding to diffraction angles of 26.60˚and 54.8˚those are the characteristic spectrum of natural graphite [122]. Also in another study graphite peak corresponding to the (002) graphite plane composed of well ordered graphenes with an interlayer spacing of 3.35 A˚. Relatively high interplanar crystal spacing of (3.599, 3.696,) as compared to CG, it might be due to graphite formation was not detected yet or intercalation in graphene planes. Again from commercial graphite XRD pattern graphitic reflection peak at 26.65˚ with an interlayer spacing of 3.34 A˚. On XRD pattern of G-Al $_{800°C}$ sample,at 2θ = 44.46˚ the graphitic reflection peak was observed sharply. Further studying of other parameters my enhance formation of graphite. By this sense

graphitization using two catalyst types $FeCl_3.6H_2O$ and Al powder was studied further at different temperature.

4.6.3. Effect of graphitization temperature

4.6.3.1.Effect of graphitization temperature on graphitic sample (G-$FeCl_3.6H_2O$)

In Figure 4.7shows the XRD pattern of G-$FeCl_3$.6 H_2O at different temperature. Sample at 800 C° and 1.5hr the XRD pattern a relativelyvery small and sharp sample peak appeared at 26.84° which could be assigned near to graphite reflection peak. Increasing graphitization temperature to 900°C and 1000°C peaks observable and relatively intense and sharp peak was formed at 2θ= 26.60 and 26.65° which indicates the reflection of graphite plane. This confirmed by literature [123] Graphite shows very sharp diffraction peak at 2θ = 26.6° which corresponds to d-spacing of 0.34 nm, [117] Graphite has a strong and sharp diffraction peak at 2θ = 26.38°, corresponding to the highly organized graphene layer structure with an interlayer distance of 0.34 nm along the (002) orientation [120]. The graphite reflection peak at 26.65°in the sample at Temperature 1000 °C shows even sharp and strong peak as compared to 900 °C. Indicating higher degree of graphitization achieve at higher annealing temperature. This observation good agreement with observation from [124] and [125] that concluded as pyrolysis temperature increased degree of crystallinity also increased, more ordered carbon structure is formed.

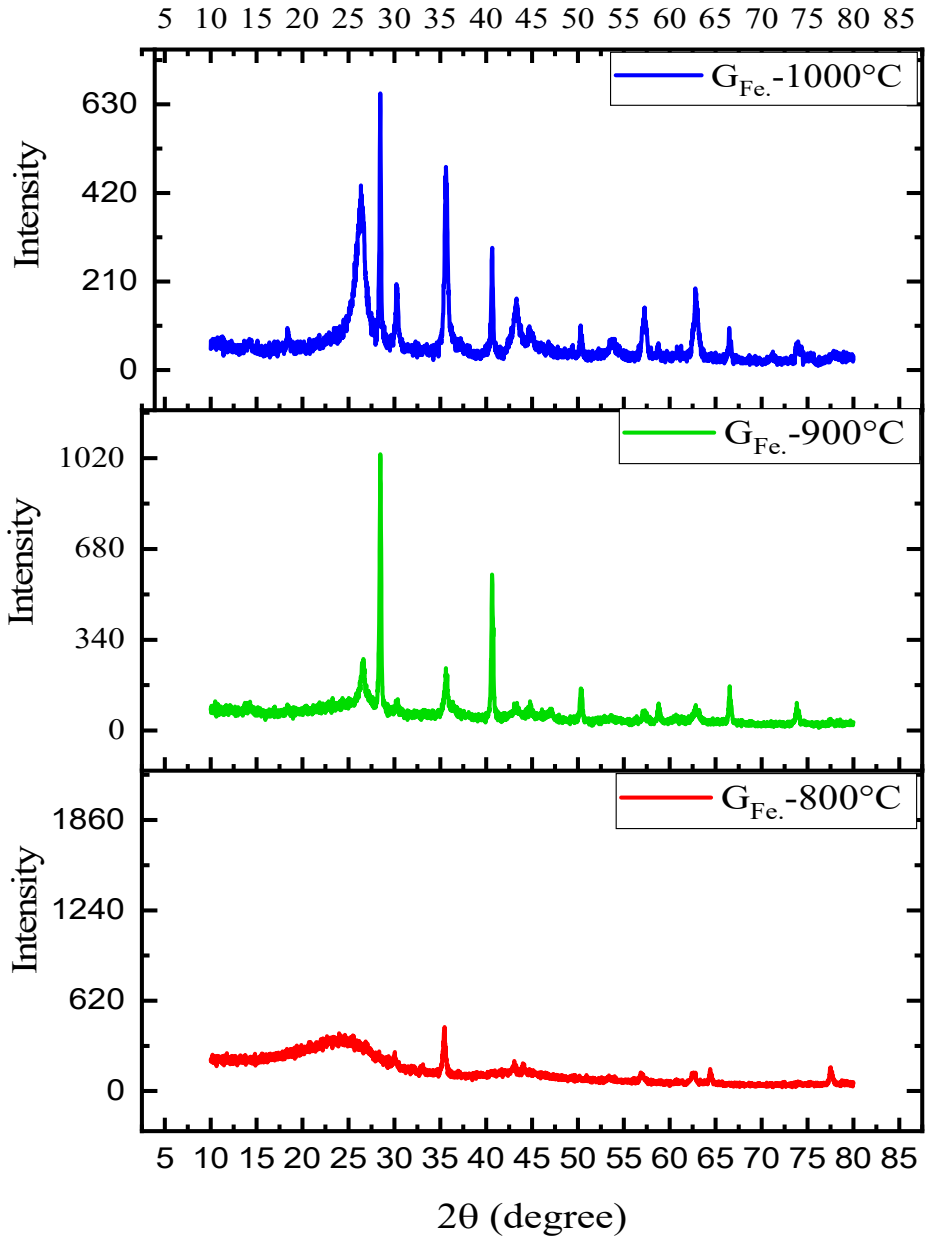

Figure 4. 4 Graphitization temperature effectson X-Ray diffraction patternof G-$FeCl_3$.6 H_2O.

From table 3 which shows D-spacing at graphite diffraction peak for each temperature, G-$FeCl_3$.6H_2O at 1000°C D-spacing = 3.347 A° which is near to the inter layer spacing of commercial graphite this also confirmed by previous works as discussed above.

The FWHM is colloquially also known as "half width" and describes the width of a peak at half of its height. Again using relative intensity parameter G-$FeCl_3$.6 (H_2O) 1000°C have I/I1 = 39

which mean is that graphite reflection peak is more intense at Temperature of 1000°C than 900°C and 800°C graphitization temperature.

Table 4.3 Inter layer spacing and other parameters of graphitic sample G-$FeCl_3$.6 (H_2O) at different temperature

Temperature (°C)	D-spacing (A˚)	I/I1	FWHM (deg)
900	3.350	15	0.1466
1000	3.347	39	0.4300
Commercial graphite	3.343	100	0.2344

4.6.3.2.Effect of graphitization temperature on graphitic sample (G-Al)

Graphitic sample from BC activated by Al powder shows another obvious graphite reflection peak at2θ≈ 44.46°. This confirmed by a typical graphite crystal structure, the sharp peaks appearing at approximately 2θ = 44° [126]. This peak was more intense than other graphitic sample due to this fact why graphitic sample (G-Al) further studied at different temperature to observe its XRD pattern and probable graphite reflection peak formation. A broad diffraction peak appears at 2θ ≈ 22.3° due to the short range order of stacked graphene sheets.In G-Al $_{900°C}$ becomes graphitic reflection peak was shifted to 44.65° and have comparable intensity with G-Al at 800 °C. The shoulder at 23.3° G-$Al_{800°C}$ becomes eliminated this might indicate that increasing graphitization temperature does not favor for better graphitization since the obvious graphitic reflection peak was not observed at 900°C. Graphitic reflection peak (002) peak disappears indicating that the graphene sheets are disordered [127]. Further increasing temperature to 1000°C many small diffraction peaks was observed in this case the graphite reflection peak at 2θ = 44.65° was disappeared or some shifts observed, becomes lower than at 900 and 800 °C of the same reflection peak with slight shift only. In all G-Al at 800, 900, and 1000 °C diffraction peak at 38.5°, 64.90°, and 77.99° are observed with slight shift.To sum up that increasing

graphitization temperature up to 1000°C the obvious graphite reflection peak at 2θ=26.65° is not observed. Graphitization increases with temperature is not necessarily true for bamboo driven graphite produced from bamboo char catalyzed by Al powder.

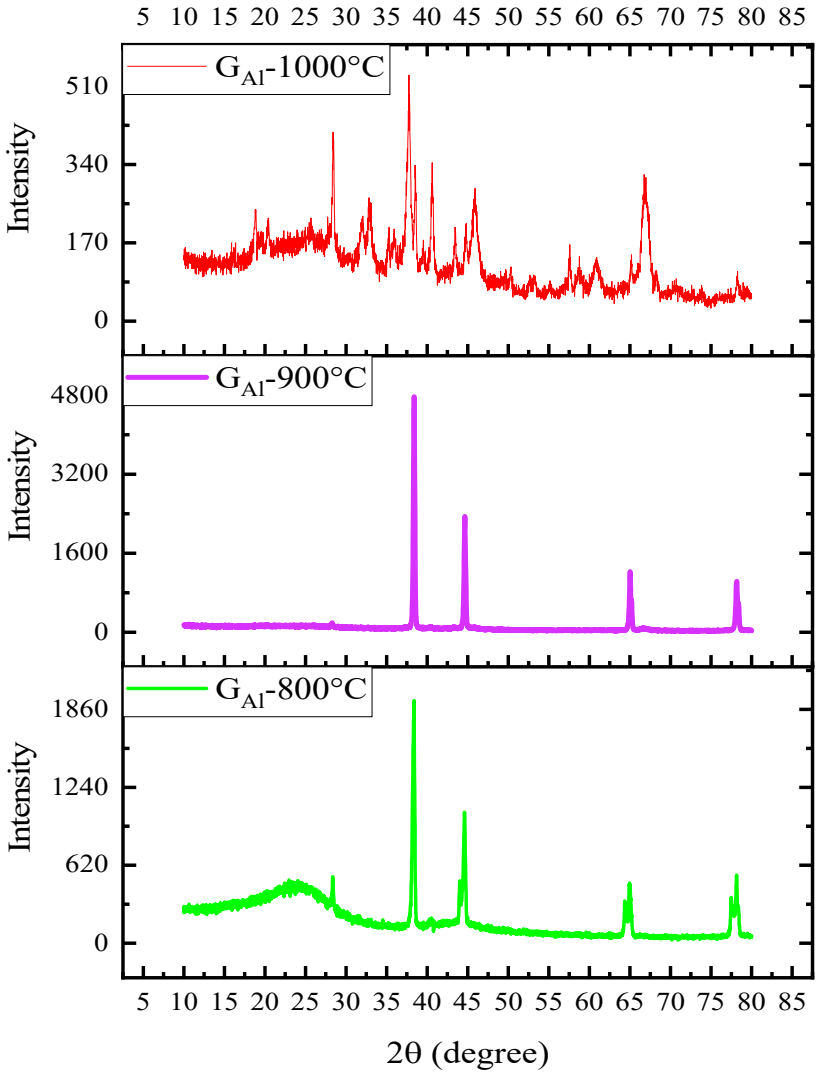

Figure 4. 5 Graphitization temperature effects on X-Ray diffraction pattern of G-Al.

4.6.4. Effect of graphitization time

Effect of time on graphitization effect was studied even though availability of data on time effect was limited. From XRD result, at time 1.5hr the graphite reflection peaks are detected well. Peak at 26.65 was confirmed by previous study as discussed above. But after increasing graphitization time to 2.5 hr still the graphite reflection peaks at 26.47 and 44.46 observed as compared to graphite at 1.5 hr there is a slight shift and the intensity significantly lower. Further increasing graphitization duration to 3.5 hr the two obvious graphite reflection peaks was disappeared. This suggested that graphitization with time increment at a fixed temperature and catalyst($FeCl_3.6H_2O$) composition my not have a positive factor for better graphitization. But from XRD graph it can been seen that increasing time for graphitization of some other peaks become strong and have high intensity. According to [123], when the intensity of graphite reflection peak becomes small mean is that the graphite is converted to graphene sheet. After high temperature heat treatment (002) peak disappears probably indicating that the graphene sheets are disordered [126].

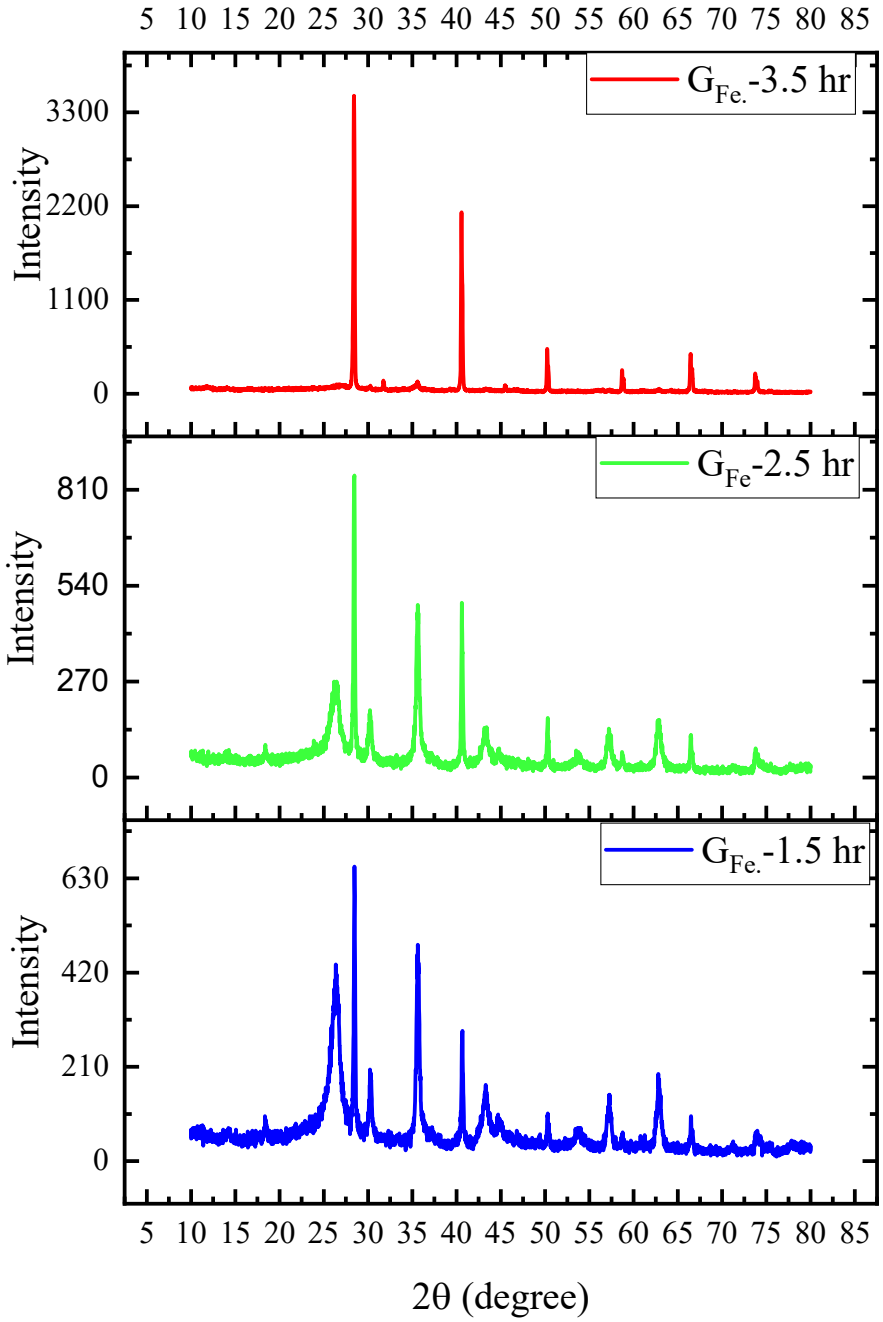

Figure 4. 6 Graphitization time effects on X-Ray diffraction pattern of G-$FeCl_3$.6 H_2O

4.7. TGA of selected catalyst for graphitization

4.7.1. TGA for Feric chloride hexhaydrate (Al)

Thermogravimetric curves of catalyst Al powder showed that, Al powder was thermally stable only weight loss of 6.34 % at 640°C. Although more studies are required to comment on the formation of final product, Al powder could be appeared on the final product.Aluminium powder sample show a Four-step degradation at 270-672°C, 672-748°C, 748-865°C, 865-1012°C.

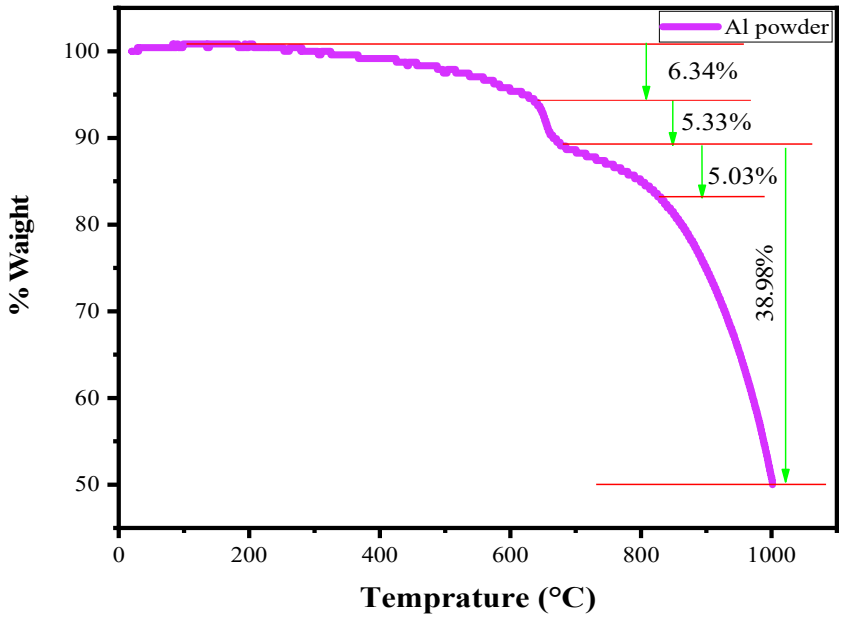

Figure 4. 7TGA curve of the catalyst Aluminum powder

4.7.2. TGA for Feric chloride hexhaydrate ($FeCl_3.6H_2O$)

Catalyst Feric chloride hexhaydrate ($FeCl_3.6H_2O$) samples were analysed by thermogravimetric analysis to observe its thermal stablity and to determine and understand possible incorporation of catalyst ions with final product which is bamboo driven graphite. Two distinct weight losses are observed. The first weight loss is about 39.87% in the temperature range of 30°C and 245°C the second lose between 245°C and 480°C. The initial weight loss is due to the presence of plenty of

water molecules in the sample. This behaviour was different than that of Aluminium powder. In fact, the conversion of bamboo to graphite through thermal methode using those catalyst have its owen chemical reaction that affects both the molecular structure and bonding energy of the graphite, thermal stablity of catalysts could be a major factor on final product as it was resulting different thermal behaviour of those catalyst (Al and $FeCl_3.6H_2O$).

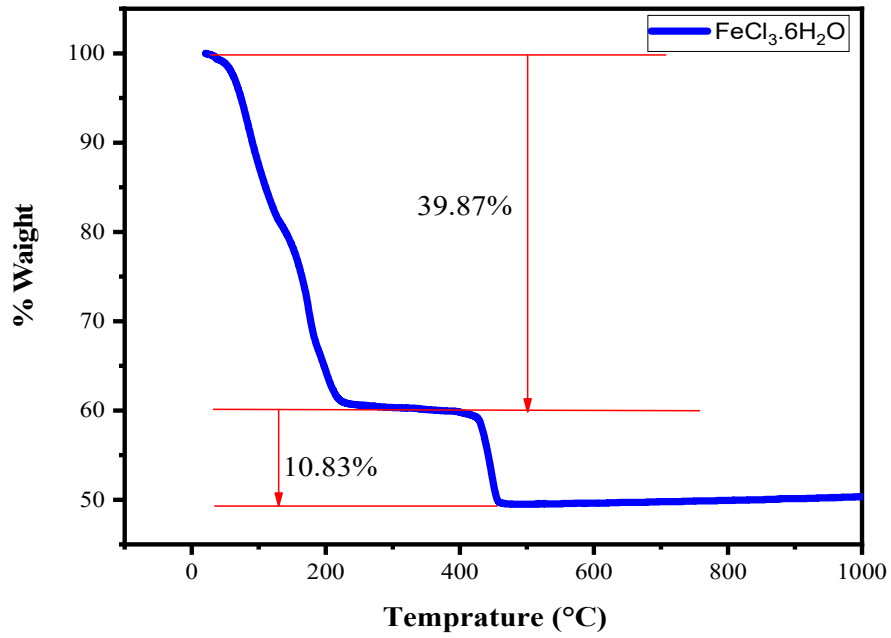

Figure 4. 8TGA curve of the catalyst Ferric chloride hexahaydrate

4.8. Fourier Transform Infrared Spectroscopy (FTIR)

4.8.1. FTIR spectra of raw bamboo and biochar char

The strong and broad band near 3408 cm^{-1} indicates the presence of hydroxyl groups of cellulose and lignin in raw bamboo powder and also in a biochar indicated peak at 3401 cm^{-1} indicates O-H stretching bond. Peaks obtained at 2926 cm^{-1} in both (RB and BC) and peak at 1450 and 1380 in BC represents C-H bending in class of alkane. Peak between 1648 cm^{-1} and 1760 cm^{-1} is the characteristic of aldehydes and ketones stretching vibration. The sharp and less intense peaks at

1732 cm^{-1} for row bamboo and 1743 cm^{-1} for biochar represents C=C stretching in aldehyde and ester group respectively. In biochar spectra relatively broad peak at 1580 also represents C=O stretching bond in cyclic alkene group also in row bamboo peak at 1250 cm^{-1} represents C-N stretching bond.

A peak at 608 cm^{-1} in row bamboo which represents C-Br which is a halo compound in RB also disappeared in BC spectra. Peak at 831 cm^{-1} in row bamboo represents C=C bending and on biochar peak at 874 cm-1 indicates C-H bending peak and peak at 1241 cm^{-1}in biochar also represents C-O stretching bond. The C-O-C functional group of the cellulose and lignin of raw bamboo have been proved by the strong band at 1041 cm^{-1}in a frequency range of (1050-1040 cm^{-1}). In a row bamboo another aromatic C=C peak appears at 1634 and 1606 in which frequency range between (1600-1650 cm^{-1}) and peak at (1250 and 1260 cm^{-1}) in a frequency range of (1000-1280 $cm^{-1)}$ stretching vibrations of epoxy and C-O groups. The peak showed alkoxy stretching vibrating between the peaks 1040-1170 cm^{-1} is appeared at (1160 cm^{-1}) in spectra of RB this peak also disappeared on biochar spectra. To sum up from FTIR analysis of RB and BC it is clearly observed that in a biochar spectra new functional groups that are not seen on RB and more observable peaks like C-H and C-O-C, and C=O, than RB was appeared while some functional groups initially on RB were disappeared.

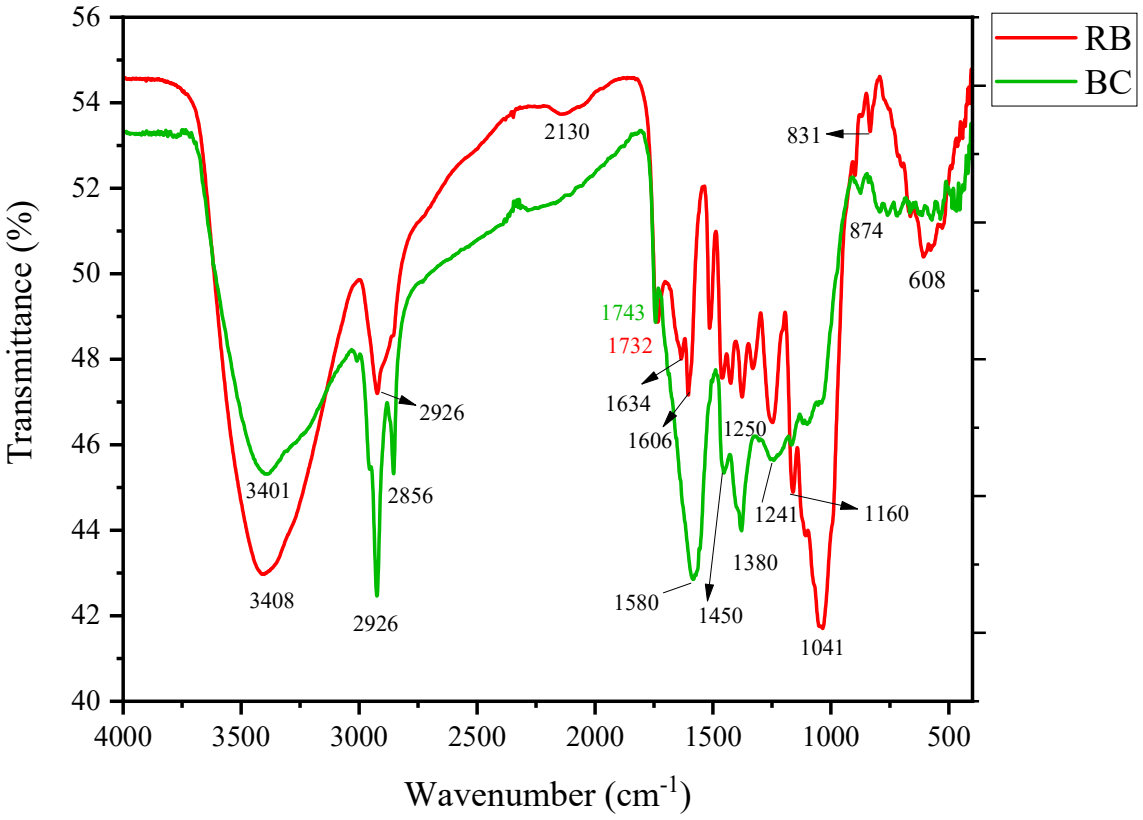

Figure 4. 9 FTIR spectra of raw bamboo (RB) and bamboo char (BC).

4.8.2. FTIR spectra of raw bamboo (RB) and activated bamboo char (ABC)

Spectrum showed the band at 3389 cm^{-1}, which corresponds to the stretching vibration of the hydroxyl groups (O–H). The O-H stretching bond in activated Biochar (ABC) becomes more broad this is due to the activating catalyst ($FeCl_3.6\ H_2O$) have a plenty of hydrogen and oxygen (6 mole of water molecules) injected to BC. Peak at 2926 cm^{-1} represents C-H stretching bond in class of alkane. And peak at 2856 cm-1 in biochar slightly shifted to 2859 in ABC. Also the peak 1580 was slightly shifted to high frequencies 1584 cm^{-1} after iron chloride in anhydrous form was impregnated or may be it indicates there is some interaction that affects the C-O stretching bond when the catalyst impregnated into a biochar. The peak obtained at 2926 cm^{-1} which is a C-H stretching bond in ABC becomes broad relative to same peak on biochar. The band at 2926

cm^{-1}corresponds to the vibration of the C–H bond that is in sp3 hybridization. The sharp and small peaks at 1743 cm^{-1} for RB, BC are a C=O stretching also appeared in ABC spectra. The broad distortion between 2856 cm^{-1} and 1580 cm^{-1} signifies that BC is highly affected due to catalyst impregnation. For ABC new bands are recorded at 667 cm^{-1} these bands characteristic of aromatic C-CI stretching and ring deformation can be assigned to the effects of intercalation.

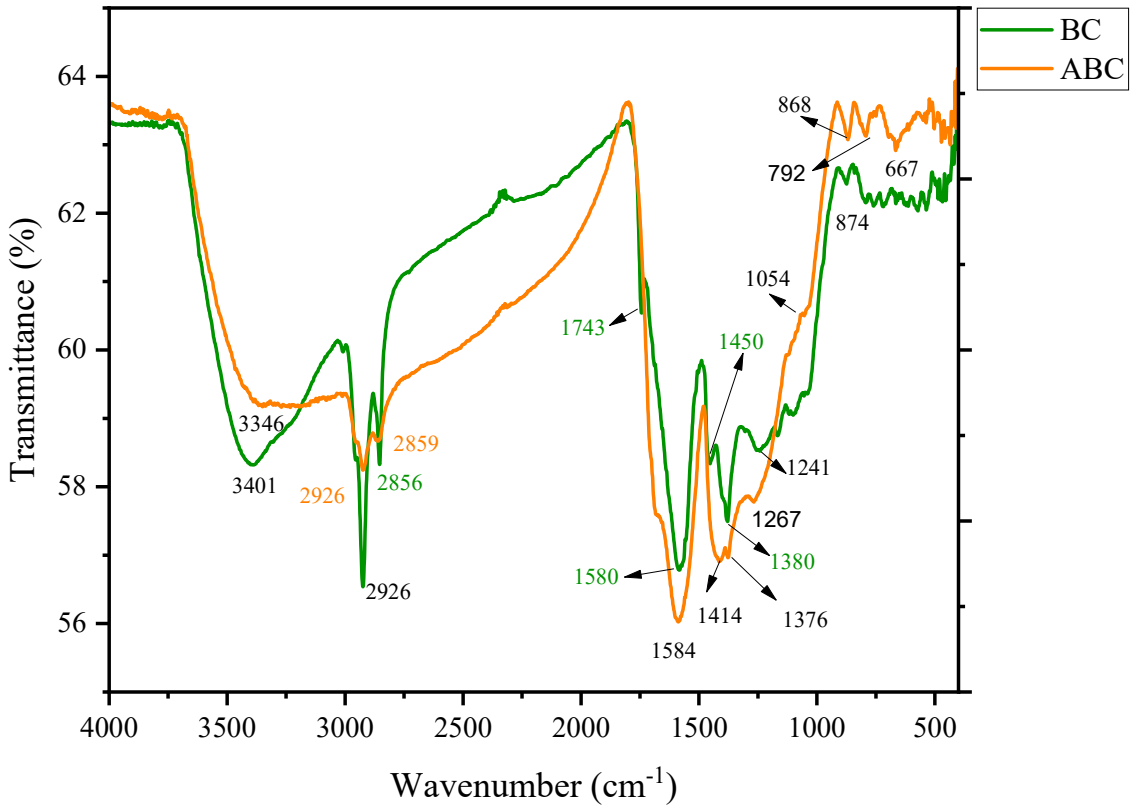

Figure 4. 10 FTIR spectra of raw bamboo (RB) and activated bamboo char (ABC).

4.8.3. FTIR spectra of graphitic sample at different temperature

The most intense and broad peak of both G 900°C and G 1000 °C spectra is located around 3606 cm^{-1} and 3556 respectively,which could be assigned to stretching vibrations of O-H bond (peaks between 3300 and 3600 cm^{-1}) which is due to presence of hydroxyl groups from ABC which is catalyst that had plenty of water molecule on its structure ($FeCl_3.6H_2O$) impregnated on BC again it can be related to adsorbed moisture of hydroxyl groups in initial RB and on process conditions. Another peak locating at wavenumber of 1643cm^{-1} arises from sp2 carbon atoms from C=C bonds in a graphitic sample (G 1000 °C) honeycomb lattice in which peak appeared in the range of frequency between (1600cm^{-1} and 650 cm^{-1})) which is in a class of alkenes. Peak locating at (1392 $cm^{-1}$for $G_{900°C}$ and 1398 cm^{-1} $G_{1000°C}$) represent C-O stretching vibration of ester group. Bands at 2989 and represent C-H stretch vibrations of bamboo driven graphite hear at this spectra observable and new peak 2895 was appeared mean is that C-H stretching formation favors higher temperature as it was appeared and more visible when graphitization temperature rises to 1000°C . Functionalized graphitic sample displays a peak at 1744 cm^{-1} for G 900 °C and G 1000°C which is characteristic band for C=O stretch of the COOH group. 1000-1280 cm^{-1} stretching vibrations of epoxy C-O groups.Characteristic peaks C=C of graphene materials in the range of 1340–1700 cm-1. The peak showed alkoxy stretching vibrating between the peaks at (1040-1170 cm^{-1}). Other peaks also detected it could be resulting from catalyst impregnation or raw bamboo or it accounts for impurities in initial biomass (RB). These results indicate that there are a large number of residues, including hydroxyl and carboxyl groups. They play important roles in the formation surface modified graphite for fluoride ion removal application.

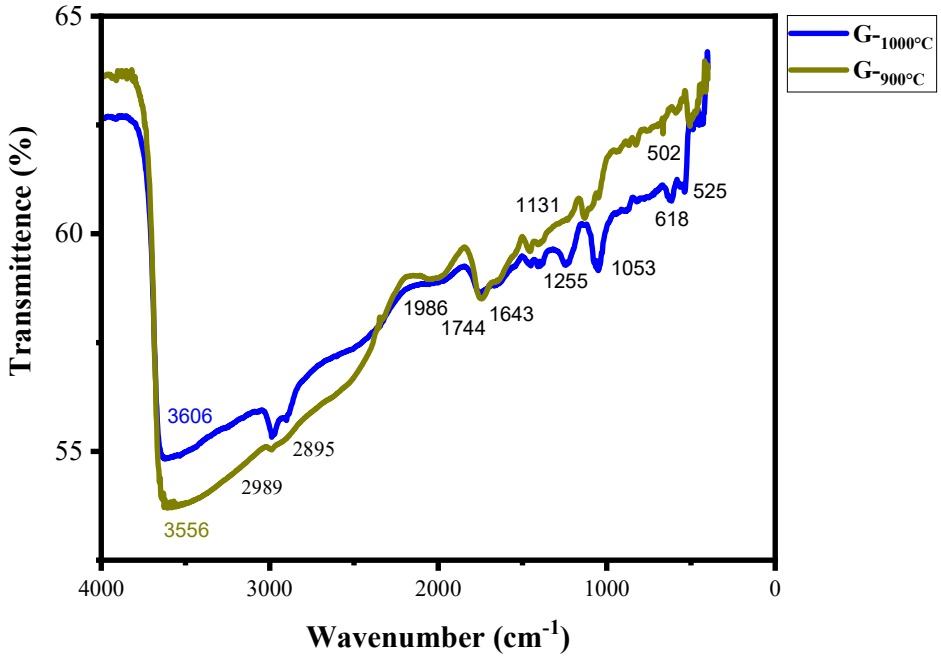

Figure 4. 11 FTIR spectra for graphitic sample at differenttemperature (G- $FeCl_3$.6 H_2O $_{900\ °C}$ and G- $FeCl_3$.6 H_2O $_{1000°C}$).

4.8.4. FTIR spectra of biochar and graphitic sample (G-Al 900°C)

The broad peak at 3401 shifted in to 3422 which is the hydrogen bonded O-H stretching vibration in G-Al $_{900°C}$ it indicates some interaction between Al powder and O-H group. Peaks obtained at 2926 cm-1 and which is C-H stretching bond shifted to 2921 cm-1 and becomes broad which implies number of C-H stretching bond increases and also C-H bending becomes increasing at 1460 cm-1 in graphitic sample G-$Al_{900°C}$.Also a sharp peak at 2556 cm-1 which is a C-H stretching bond exists on both BC and graphitic sample G-$Al_{900°C.}$ Small peak at 2722 cm^{-1}represents C-H stretching bond of aldehyde group. 2349 cm-1 O=C=O stretching. Week Peak at 1736 cm-1 C=O stretching which was an ester group. Strong in BC at a Peak of at 1580 becomes eliminated in graphitic sample G-$Al_{900°C}$ and Strong peak at 1639 cm-1 which represents C=C stretching of alkenes group in range of frequency (1626-1662 cm-1) was appeared. At peak of 1384 cm-1 which is O-H bending of phenol group appeared in spectra of G-$Al_{900°C.}$ A very small peak at 1254 cm-1which represents C-O stretching of aromatic ester group also appeared. Strong and broad peak at 995 cm-1 which is C=C bending of alkenes group.This may indicate formation

of carbon to carbon bonds which arethe skeleton of graphitic structure, thiswas confirmedby graphitic reflection on XRD at 2 Tehta = 44.65 degree.

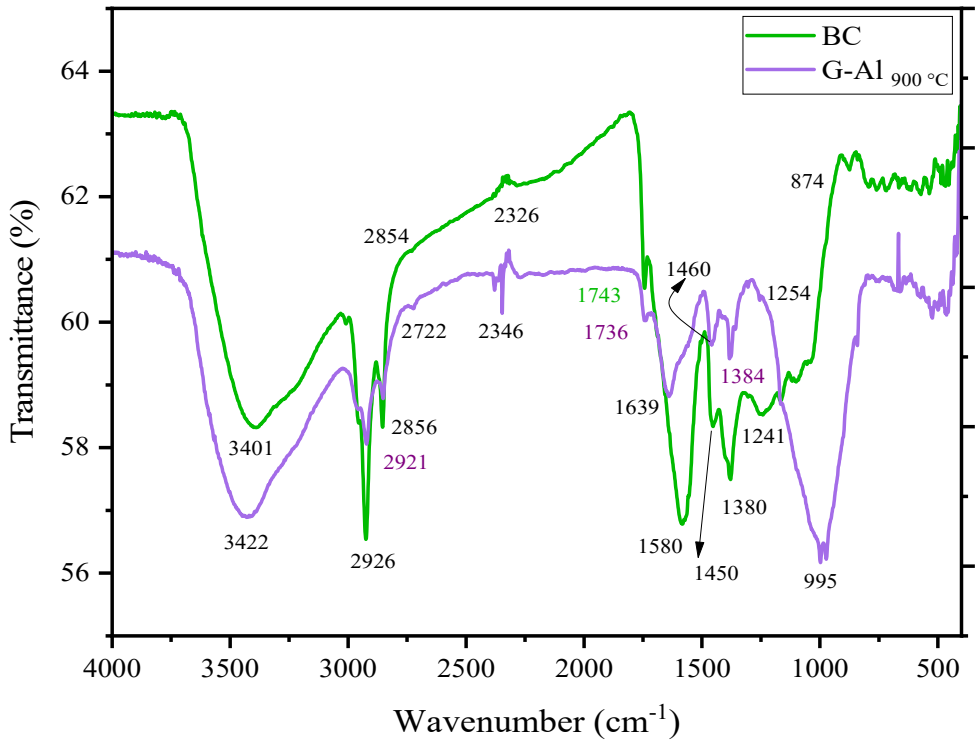

Figure 4. 12 FTIR spectra of biochar and graphitic sample (G-Al 900°C)

For comparison and to observe effects on functionality with parameters and process condition of each sample those all FTIR analysis was drown in single diagram shown below.

4.9. Batch Adsorption study

4.9.1. Effect of Contact Time

Effect of contact time for which the fluoride ion is in contact with the bamboo char was examined. The sorption effect of fluoride ion on biochar, given in Figure 4.13 illustrates that the percentage of fluoride removal by bamboo char increases linearly as a function of contact time in the time interval examined showing the possibility of relatively high removal as the time of contact increases. From the removal trained it can be seen that the mass transfer or adsorption rate to the surface of the active sites is slower for bamboo char.

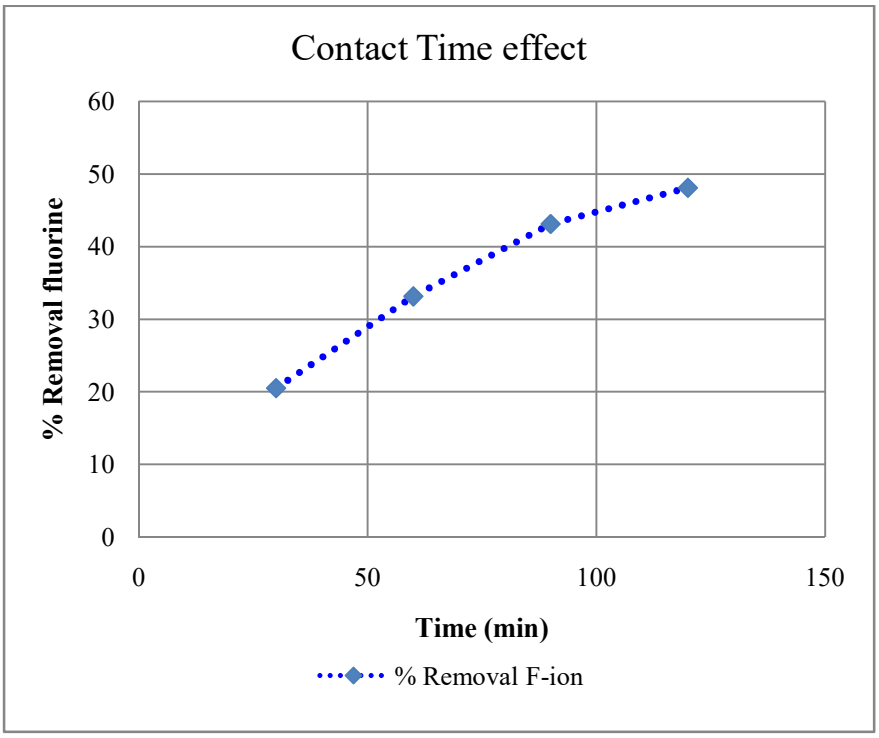

Figure 4. 13 Effect of contact time on fluoride removal of bamboo char.

4.9.2. Effect of Dose

Figure 4.12 displays the effect of amount of adsorbent on the uptake of fluoride ion was examined. The effect of the adsorbent dose on fluoride ion was tested at the agitation time of 120 min by varying the adsorbent dosage. The result showed that the removal of the fluoride ions increases with an increase in the amount of bamboo char dose. The increase of fluoride removal

capacity with increase of bamboo char dose can be attributed with an increasing number of active sites because of an increase in the adsorbent dose.

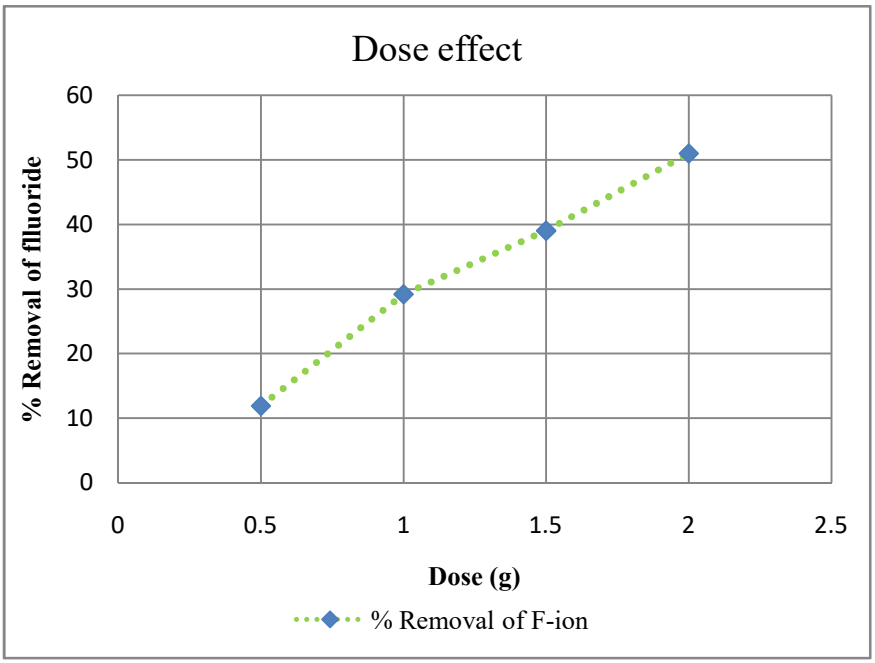

Figure 4. 14 Effect of dose on fluoride removal of bamboo char.

4.9.3. Effect of particle size

The effect of bamboo char particle size on residual fluoride concentration was presented in Figure 4.17. A decrease of bamboo char particle size resulted in an increase in fluoride adsorption. Because reducing the bamboo char particle size is believed to increases the effective surface area providing more active sites for fluoride removal. The examinations were made using different ranges of particle sizes. The fluoride removal percent increased from 23.25% to 30.01% and then to 48.7% after a contact time of 120 min for each sieve particle size ranges of500- 710, 355-500, 250-355 micrometer sizes respectively.

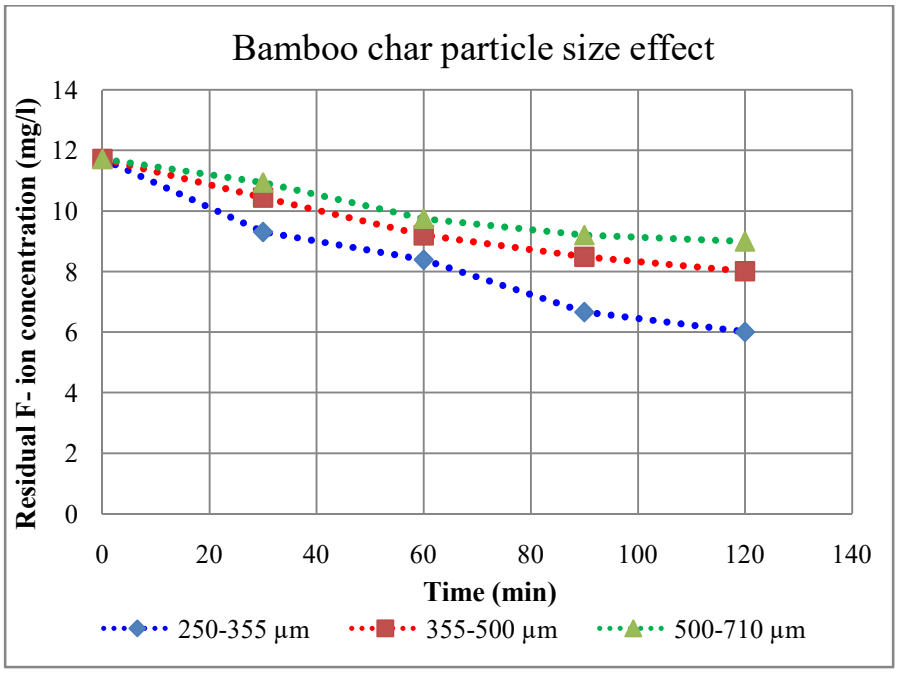

Figure 4. 15 Effect of particle sizes on fluoride removal of bamboo char.

4.9.4. Adsorption of fluoride ion using graphitic sample prepared by Al powder (G-Al) and G-$FeCl_3.6H_2O$

The effect of adsorbent G-Al on residual fluoride concentration was presented in Figure 4.14. The residual fluorine concentration after a contact time of 120 min reduced from initial fluoride concentration 11.72 mg/l to 5.055 mg/l. fluoride Removal of 56.84 % after agitation for 2 hrs. the adsorption was fast during the first hour this was due to initially the number of active sights in G-Al surface is high but as time increases further the adsorption rate become small and seems steady if further increasing in time this implies that all the active sights are becoming fully occupied by F-ion. The effect of adsorbent G-$FeCl_3.6H_2O$ at 1000°C on residual fluoride concentration was presented in Figure 4.14. The residual fluorine concentration after a contact time of 120 min reduced from initial fluoride concentration 11.72 mg/l to 7.65 mg/l. the fluoride removal percent of 34.65 % after agitation for 2 hrs.

Figure 4. 16 Adsorption of fluoride ion using graphitic sample G-$FeCl_3$.6 (H_2O) at 1000 °C

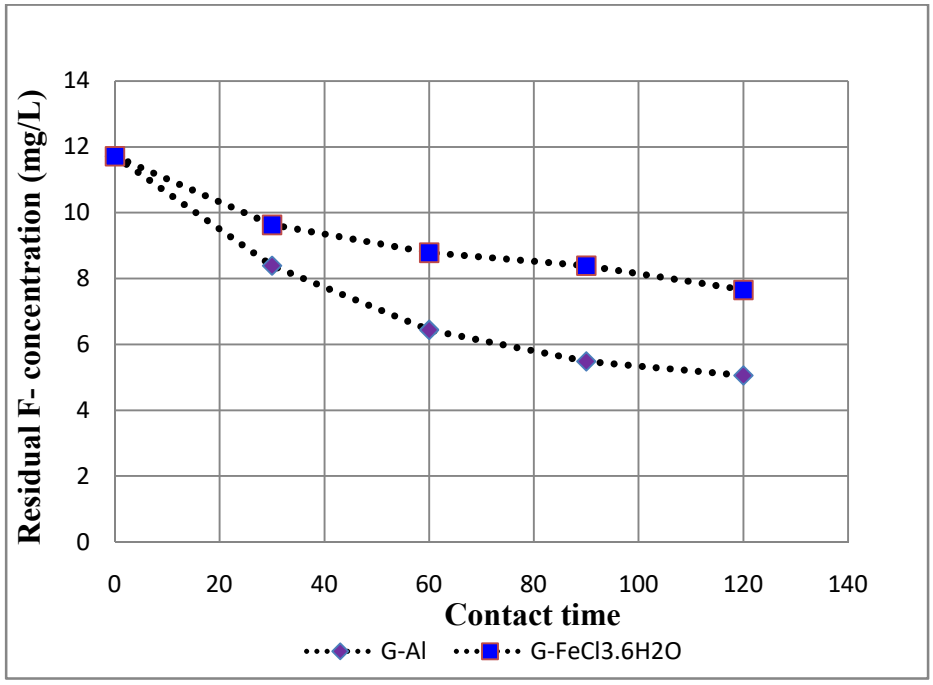

Figure 4. 17 Adsorption of fluoride ion using graphitic sample G-Al

4.9.5. Adsorption Isotherms Study

Adsorption isotherm was studied for both uncoated graphitic sample (G-Al) and modified graphitic sample (mG-Al), which shows the relationship between the bulk aqueous phase activity (concentration) of adsorbate and the amount adsorbed at constant temperature. In this study, the general purpose Langmuir and Fruendlich and adsorption isotherm models were used. The isotherm experiments were carried out at 5 different initial fluoride concentration of both G-Al and modified G-Aladsorbents in a range from 3mg/l to 11.72mg/L.

4.9.5.1.Adsorption Isotherms of G-Al

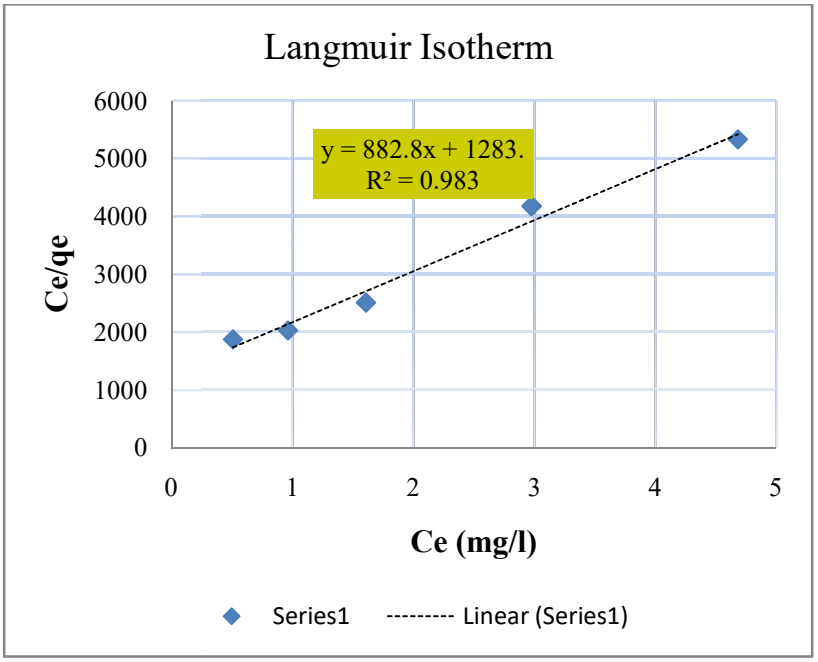

Figure 4. 18Langmuir plots for the sorption of fluoride ions using adsorbent (G-Al $_{900\ ^{\circ}C}$)

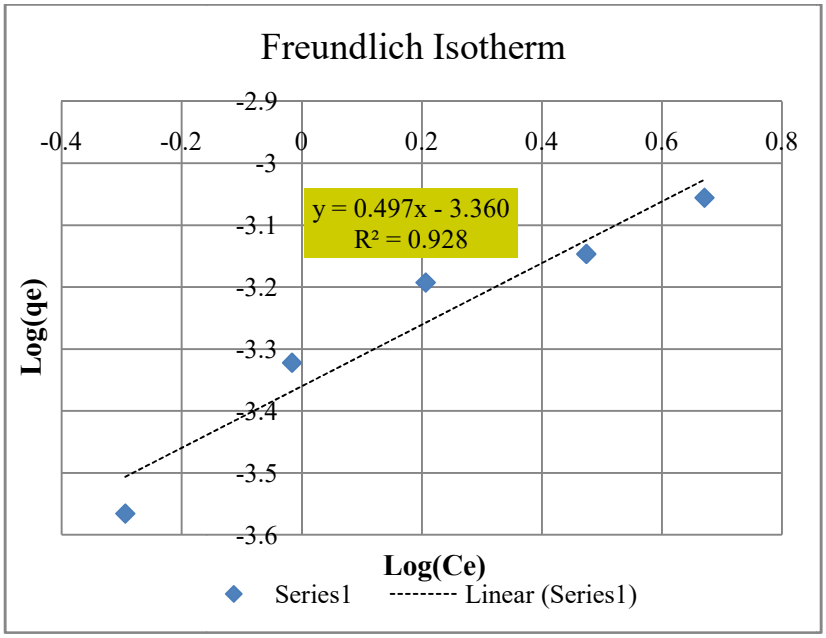

Figure 4. 19 Freundlich plots for the sorption of fluoride ions using adsorbent (G-Al $_{900\ ^{\circ}C}$)

Table 4. 4 Linear isotherm equations and parameters on sorption of fluoride ion G-Al $_{900\ ^{\circ}C}$

Isotherm	Linear		
Langmuir	Parameters		
	Qo (mg/g)	Kl (l/mg)	R^2
	0.001133	0.68875	0.983
Freundrich	Parameters		
	KF (mg/g)	n	R2
	0.000437	2.012072	0.928

As can be seen from the table above, the correlation coefficient value for the linear version of Langmuir is greater (R2 = 0.983) than the values for Freundlich (0.928). The Langmuir isotherm model was shown to be the best representation of fluoride adsorption by graphitic sample based on correlation coefficient values (G-Al). The experimental fluoride adsorption data was found to be well suited to the Langmuir isotherm, with correlation values of 0.983. The Langmuir parameters and correlation coefficients for G-Al adsorbent were determined. Fixed number of vacant or adsorption sites are available on the surface of G-Al. As Langmuir assumes all the vacant sites have equal size and shape on the surface of adsorbent each site of graphite surface (G-Al) can hold maximum of one fluoride ion.

4.9.5.2.Adsorption Isotherms for modified Graphite-Al (mG-Al)

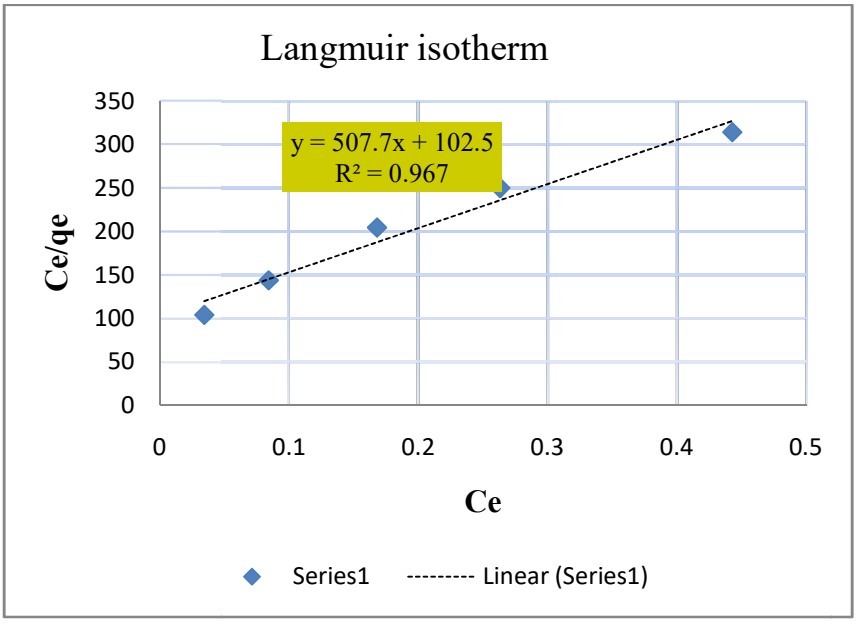

Figure 4. 20 Langmuir plots for the sorption of fluoride ions using modified G-Al $_{900\ ^{\circ}C}$.

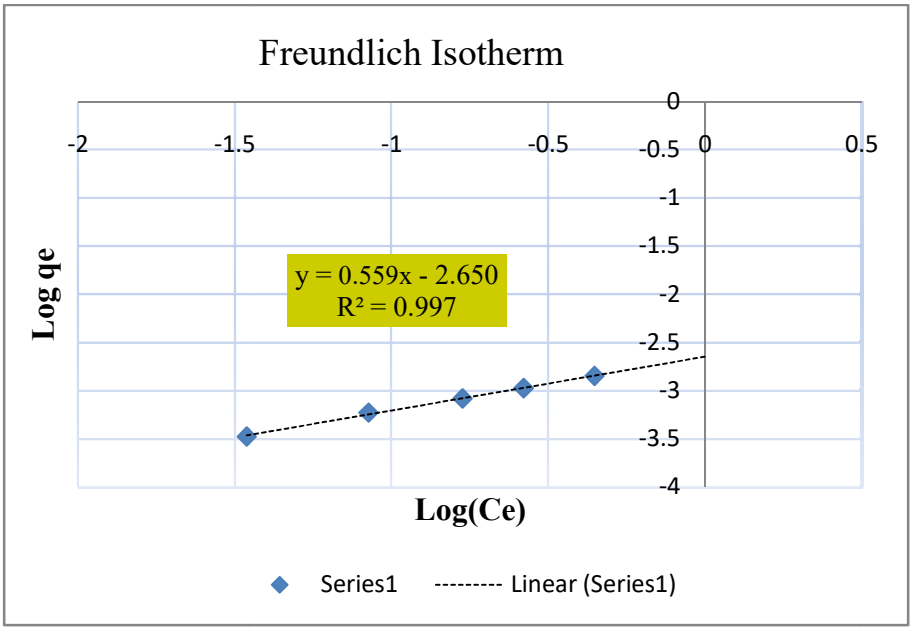

Figure 4. 21Freundlich plots for the sorption of fluoride ions using modified G-Al $_{900\ ^{\circ}C}$

Table 4. 5 Linear isotherm equations and parameters on sorption of fluoride ion using modified G-Al $_{900\ °C}$.

Isotherm	Linear		
Langmuir	Parameters		
	Qo (mg/g)	KL (L/mg)	R2
	0.00197	4.953171	0.967
Freundrich	Parameters		
	KF (mg/g)	n	R2
	0.000437	0.558999	0.997

As seen in the table above, the correlation coefficient value for the linear version of Freundlich is stronger (0.997) than the Langmuir (R^2 = 0.967). Based on correlation coefficient values, the Freundlich isotherm model was shown to be the best description of fluoride adsorption by coated graphitic sample (G-Al). The heterogeneous surface may have different types of adsorption sites, according to the Freundlich isotherm model, and their affinities on the graphitic sample (G-Al) are heterogeneous.

4.9.6. Adsorption Kinetics model Prediction

Two types of adsorption processes: physical (physisorption) and chemical (adsorption) (chemisorption). Physical adsorption is caused by weak forces of attraction (van der Waals), whereas chemisorption is caused by the development of a strong bond between the solute and the adsorbent, resulting in electron transfer. Pseudo-first and pseudo-second order kinetic models are the two types of kinetic models. Using data from fluoride removal on G-Al and coated G-Al at various time intervals, two fluoride removal kinetic models, pseudo-first-order and pseudo-second-order models, were investigated. Both the pseudo-first-order kinetic model equation and the pseudo-second-order kinetic model equation were used to apply the experimental data: The initial rapid fluoride removal is likely due to fluoride ions immediately utilizing the most readily

available active sites on the outer surface of G-Al or mG-Al, while slower adsorption at a later stage could be due to fluoride ions gradually diffusing into the porous adsorbent's interior surface for adherence. The kinetics of sorbate absorption at the solid-solution interface defines the solute uptake rate, which regulates the sorbate uptake residence time.

4.9.6.1. Kinetic models for fluoride removal (G-Al) and modifiedGraphitic sample (mG-Al)

The second order kinetic model (R^2= 0.996) exhibited a better fit than the first order kinetic model (R^2 = 0.983), as seen in Figures 4.27 and 4.28. As a result, the adsorption of fluoride onto a graphitic sample (G-Al) followed pseudo-second-order kinetics. The pseudo-second-order kinetic model is the governing adsorption kinetic model for fluoride adsorption onto Graphitic material (G-Al). Because the fluoride adsorption onto the graphitic sample (G-Al) followed pseudo second-order kinetics, pseudo second-order kinetics was chosen as the better model to fit the experimental results in this study. Figures 4.27 and 4.28 show that the second order kinetic model (R^2= 0.999) had a better fit than the first order kinetic model (R^2 = 0.963). Fluoride adsorption onto a coated graphitic sample (G-Al) followed pseudo-second-order kinetics as a result. The governing adsorption kinetic model for fluoride adsorption onto a coated Graphitic material is the pseudo-second-order kinetic model (G-Al). Since the adsorption of fluoride onto Graphitic sample (G-Al) followed pseudo second-order kinetics, pseudo second-order kinetics was chosen as the better model to fit the experimental results in this study.

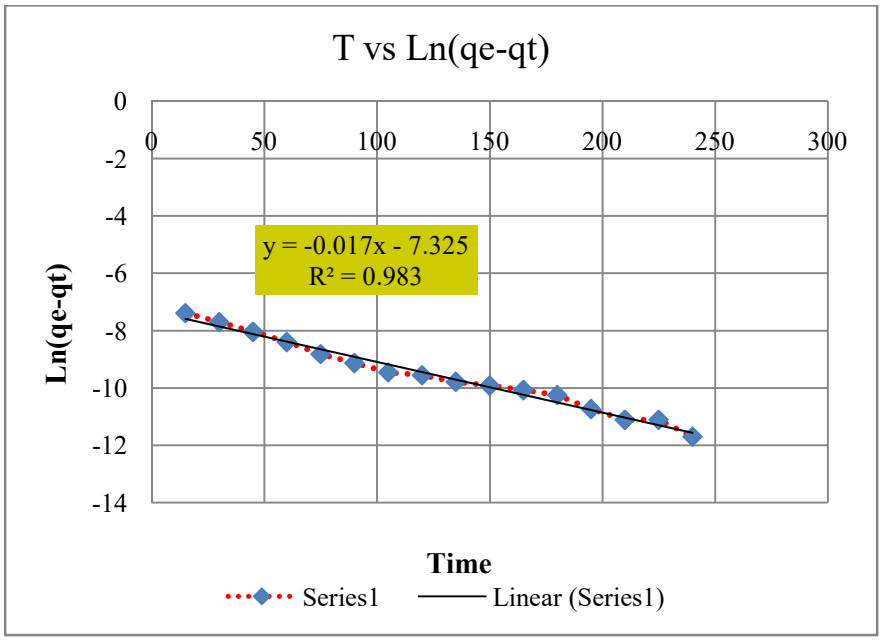

Figure 4. 22 Pseudo first order kinetics models for fluoride adsorption usingG-Al $_{900\ ^{\circ}C}$.

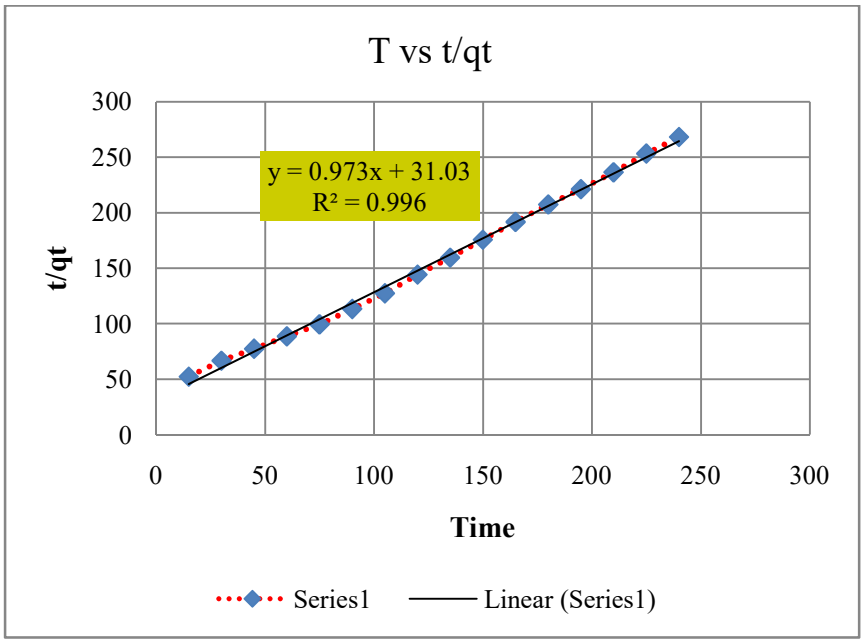

Figure 4. 23 Pseudo second order kinetics models for fluoride adsorption usingG-Al $_{900\ ^{\circ}C}$

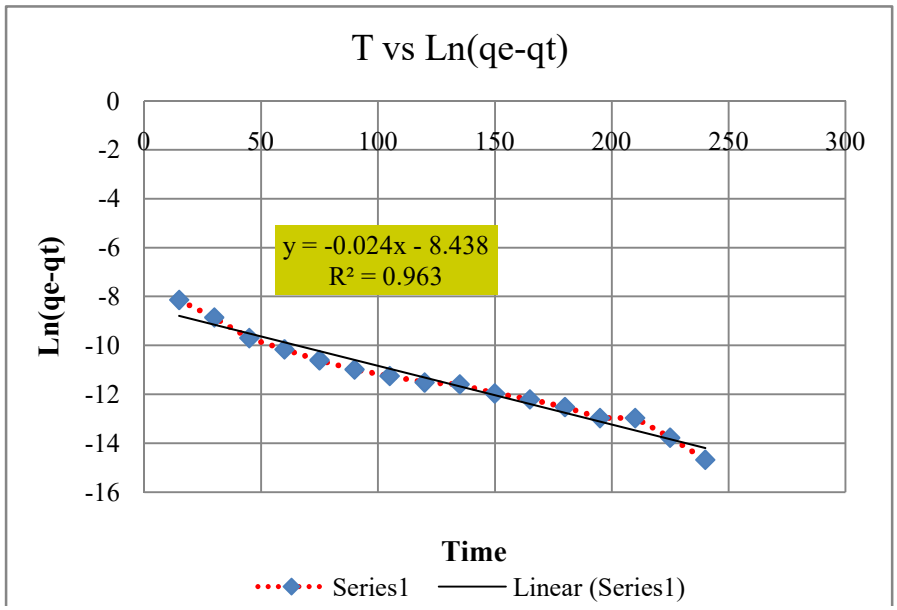

Figure 4. 24 Pseudo first order kinetics models for fluoride adsorption on modified G-Al $_{900\ ^{\circ}C}$.

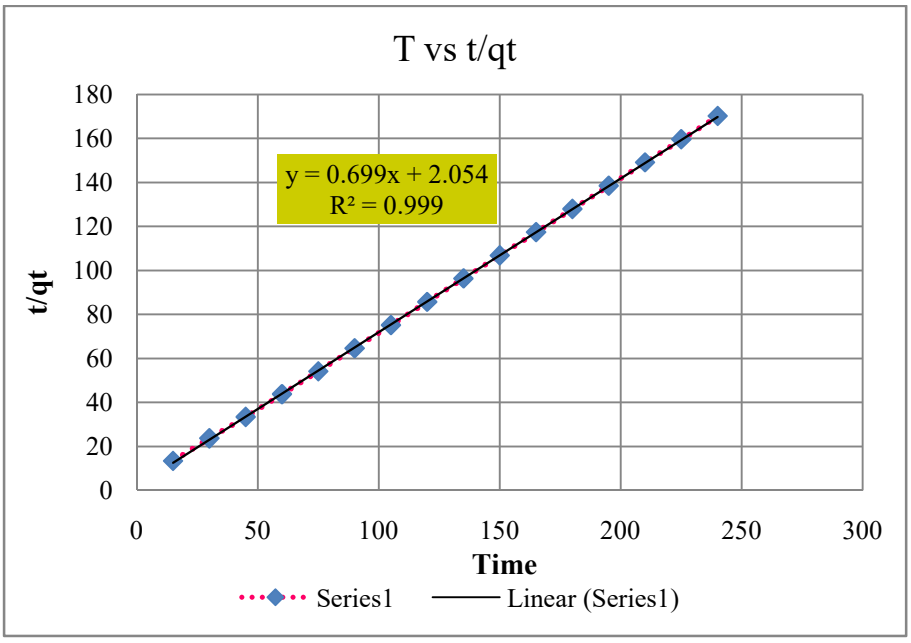

Figure 4. 25 Pseudo second order kinetics models for fluoride adsorption on modified G-Al $_{900\ ^{\circ}C}$

CHAPTER FIVE

5. CONCLUSIONS AND RECOMMENDATIONS

5.1. Conclusions

Excess amount of fluoride in drinking water is a public health concern globally and especially in the Rift Valley part of Ethiopia. Under this study, as a low-cost adsorbent for water treatment, fluoride removal from drinking water was assessed using locally available adsorbents,bamboo char and graphitized the biochar which was surface modified by using locally available chemical, aluminum sulphate. Availability of bamboo in Ethiopia from different area can be good supply for graphite synthesis in addition to fluoride removal. Since carbonization was used for step leading process it was selected based on amount of yield at different temperature. The results show that the calcinationstemperature varies significantly in changing the yield of biochars, as biochar yield was decreased from 43.62% to 34.15% at carbonization temperature 400°C and 600°C respectively. Then after the main parameter to select fluoride removal capacity like contact time, dosage and particle size was determined. For a given initial (11.72 mg/l) fluoride concentration, the removal efficiency of the adsorbent (biochar) increased with increasing adsorbent dose.Fluoride removal reaches 51.00% using 2 gram adsorbent dose. Fluoride removal percent increased from 23.25% to 30.01% and then to 48.7% after a contact time of 120 min for each sieve particle size ranges of 500-710, 355-500, 250-355 micrometer sizes respectively.

In this study the effects of different parameters were studied during graphitic sample preparation including, catalyst type, graphitization temperature, graphitization time. Generally, carbon rich material like bamboo was a good candidate for graphite synthesis as a precursor. Based on the observation it can be deduces higher heat treatment temperature more graphitic carbon is produce.A noticeable graphitic reflection peak was detected around 26.60°as temperature increases to 900°C. As temperature increased more to 1000°C the sample shows sharp and more intense peakwas detected. Those investigations indicating higher degree of graphitization achieve at higher annealing temperature. At higher temperature upon heating process catalyst particle will quickly grew into particle with considerable size, good crystallinity, and good dispersion that can facilitate formation of graphitic structure. it can be deduce that the usage of

Iron salt has been successfully catalyzed the graphitic structure formation, even though it was expected that anion of metal salt influenced degree of graphitization.From XRD pattern Sample (G-Al) at different temperature it can be conclude that graphitization increases with temperature is not necessarily true for graphitic sample produced using Al powder as a catalyst. Since graphitic reflection peak was not becoming intense and strong rather become small and eliminated with increment in temperature, this probably shows that Graphitic reflection peak (002) peak disappears indicating that the graphene sheets are disordered.

After graphitic sample was prepared adsorbent preparation fluoride removal efficiency was cheeked using adsorbents (G-$FeCl_3.6H_2O$, G-Al and mG-Al). Based on fluoride removal efficiency G-Al 900(fluoride Removal of 56.84 % after agitation for 2 hrs) was selected and studied and surface modified to see the effect on adsorption. This thesis work also confirmed that preparation of the adsorbent that enhance fluoride removal efficiency (fluoride Removal of 95.63% after agitation for 2 hrs) when surface modification of graphitic sample was done on G-Al using aluminum hydroxide. For both bamboo driven graphite G-Al and mG-Al,the adsorption kinetics was also determined and the kinetic results obtained from those studies fitted well with the pseudo second order kinetic model for both adsorbents. The equilibrium data obtained in this study was closely fitted with the Langmuir isotherm, which indicated that the monolayer adsorption was involved in the process of fluoride removal for graphitic carbon (G-Al_{900C}). Freundlich isotherm model was shown to be the best description of fluoride adsorption by modified graphitic sample (mG-Al_{900C}). From those results generally, carbon rich material like bamboo will be selected as precursor and have a good potential for graphite synthesis from biomass, it can be seen that beside other enormous application of graphite modified graphitic carbon can have considerable potential for the removal of excess fluoride from aqueoussolution.

5.2. Recommendations

Based on the finding of present investigation and to put practice for further studies the following points should be considered: the removal of fluoride using modified graphitic carbon in continuous mode has to be practice and the methods has to be optimize for further study and cheek regeneration capability of adsorbent. Determination of specific surface area, pore volume and pore diameter of biochar and graphitic samples. Other adsorption capacity determinant factors such as pH of fluorinated water should be studied. For better understanding Analysis morphology of raw bamboo, biocharand graphitic samples and also surface modified graphitic sample before and after treatment should be done using a scanning electron microscope (SEM). Strongly recommended that graphite preparation from biomass have to be encouraged and studied more and more since it can alleviate many problems related to graphite such as supply risk and environmentally impacts as well. This study can give some information that lignocellulostic biomass such as bamboo is good candidate for graphite preparation using those results as bench mark recommended that optimizing parameters and study detail on possible impurities and removal mechanism.

REFFERANCE

[1] J. C. Crittenden, R. R. Trussell, D. W. Hand, K. Howe, and G. Tchobanoglous, *MWH's water treatment: principles and design*. John Wiley & Sons, 2012.

[2] D. Hinrichsen and H. Tacio, "The coming freshwater crisis is already here," *linkages between Popul. water. Washington, DC Woodrow Wilson Int. Cent. Sch.*, pp. 1–26, 2002.

[3] L. Birnhack, N. Voutchkov, and O. Lahav, "Fundamental chemistry and engineering aspects of post-treatment processes for desalinated water—a review," *Desalination*, vol. 273, no. 1, pp. 6–22, 2011.

[4] K. E. Heller, S. A. Eklund, and B. A. Burt, "Dental caries and dental fluorosis at varying water fluoride concentrations," *J. Public Health Dent.*, vol. 57, no. 3, pp. 136–143, 1997.

[5] J. A. Lalumandier and R. G. Rozier, "The prevalence and risk factors of fluorosis among patients in a pediatric dental practice," *Pediatr. Dent.*, vol. 17, p. 19, 1995.

[6] J. E. Williams and J. D. Zwemer, "Community water fluoride levels, preschool dietary patterns, and the occurrence of fluoride enamel opacities," *J. Public Health Dent.*, vol. 50, no. 4, pp. 276–281, 1990.

[7] R. W. Premathilaka and N. D. Liyanagedera, "Fluoride in drinking water and nanotechnological approaches for eliminating excess fluoride," *J. Nanotechnol.*, vol. 2019, 2019.

[8] A. V Jamode, V. S. Sapkal, and V. S. Jamode, "Defluoridation of water using inexpensive adsorbents," *J. Indian Inst. Sci.*, vol. 84, no. 5, p. 163, 2004.

[9] R. T. Haimanot, A. Fekadu, and B. Bushra, "Endemic fluorosis in the Ethiopian Rift Valley.," *Trop. Geogr. Med.*, vol. 39, no. 3, pp. 209–217, 1987.

[10] P. D. Nemade, A. Vasudeva Rao, and B. J. Alappat, "Removal of fluorides from water using low cost adsorbents," *Water Sci. Technol. Water Supply*, vol. 2, no. 1, pp. 311–317, 2002.

[11] P. Adler and W. H. Organization, *Fluorides and human health*. World Health Organization, 1970.

[12] C. Reimann, K. Bjorvatn, B. Frengstad, Z. Melaku, R. Tekle-Haimanot, and U. Siewers, "Drinking water quality in the Ethiopian section of the East African Rift Valley I—data and health aspects," *Sci. Total Environ.*, vol. 311, no. 1–3, pp. 65–80, 2003.

[13] J. Hoekstra, A. M. Beale, F. Soulimani, M. Versluijs-Helder, J. W. Geus, and L. W. Jenneskens, "Base metal catalyzed graphitization of cellulose: A combined Raman spectroscopy, temperature-dependent X-ray diffraction and high-resolution transmission electron microscopy study," *J. Phys. Chem. C*, vol. 119, no. 19, pp. 10653–10661, 2015.

[14] K. Tekin, S. Karagöz, and S. Bektaş, "A review of hydrothermal biomass processing,"

Renew. Sustain. Energy Rev., vol. 40, pp. 673–687, 2014.

[15] D. Mohan, R. Sharma, V. K. Singh, P. Steele, and C. U. Pittman Jr, "Fluoride removal from water using bio-char, a green waste, low-cost adsorbent: equilibrium uptake and sorption dynamics modeling," *Ind. Eng. Chem. Res.*, vol. 51, no. 2, pp. 900–914, 2012.

[16] Y. T. TH, "Relationship between natural water quality and health," *United Nations Educ. Sci. Cult. Organ. Paris*, 1983.

[17] I. V Veksler, A. M. Dorfman, M. Kamenetsky, P. Dulski, and D. B. Dingwell, "Partitioning of lanthanides and Y between immiscible silicate and fluoride melts, fluorite and cryolite and the origin of the lanthanide tetrad effect in igneous rocks," *Geochim. Cosmochim. Acta*, vol. 69, no. 11, pp. 2847–2860, 2005.

[18] S. Naseem, T. Rafique, E. Bashir, M. I. Bhanger, A. Laghari, and T. H. Usmani, "Lithological influences on occurrence of high-fluoride groundwater in Nagar Parkar area, Thar Desert, Pakistan," *Chemosphere*, vol. 78, no. 11, pp. 1313–1321, 2010.

[19] M. T. Shah and S. Danishwar, "Potential fluoride contamination in the drinking water of Naranji area, northwest frontier province, Pakistan," *Environ. Geochem. Health*, vol. 25, no. 4, pp. 475–481, 2003.

[20] V. Sivasankar, A. Darchen, K. Omine, and R. Sakthivel, "Fluoride: A world ubiquitous compound, its chemistry, and ways of contamination," in *Surface modified carbons as scavengers for fluoride from water*, Springer, 2016, pp. 5–32.

[21] D. C. Adriano, "Other trace elements," in *Trace Elements in the Terrestrial Environment*, Springer, 1986, pp. 470–501.

[22] R. B. Symonds, W. I. Rose, and M. H. Reed, "Contribution of C1-and F-bearing gases to the atmosphere by volcanoes," *Nature*, vol. 334, no. 6181, pp. 415–418, 1988.

[23] A. Siddique, M. Mumtaz, S. Saied, Z. Karim, and N. A. Zaigham, "Fluoride concentration in drinking water of Karachi City (Pakistan)," *Environ. Monit. Assess.*, vol. 120, no. 1, pp. 177–185, 2006.

[24] A. Farooqi, H. Masuda, M. Kusakabe, M. Naseem, and N. Firdous, "Distribution of highly arsenic and fluoride contaminated groundwater from east Punjab, Pakistan, and the controlling role of anthropogenic pollutants in the natural hydrological cycle," *Geochem. J.*, vol. 41, no. 4, pp. 213–234, 2007.

[25] G. Singh, B. Kumari, G. Sinam, N. Kumar, and S. Mallick, "Fluoride distribution and contamination in the water, soil and plants continuum and its remedial technologies, an Indian perspective–a review," *Environ. Pollut.*, vol. 239, pp. 95–108, 2018.

[26] W. H. O. Repor, "Fluoride and fluorides: Environmental health criteria," *World Heal. Organ.*, 1984.

[27] W.-T. Tsai, "The decomposition products of sulfur hexafluoride (SF6): Reviews of environmental and health risk analysis," *J. Fluor. Chem.*, vol. 128, no. 11, pp. 1345–1352,

2007.

[28] V. Saxena and S. Ahmed, “Dissolution of fluoride in groundwater: a water-rock interaction study,” *Environ. Geol.*, vol. 40, no. 9, pp. 1084–1087, 2001.

[29] K. Biswas, S. K. Saha, and U. C. Ghosh, “Adsorption of fluoride from aqueous solution by a synthetic iron (III)− aluminum (III) mixed oxide,” *Ind. Eng. Chem. Res.*, vol. 46, no. 16, pp. 5346–5356, 2007.

[30] W. R. Dolbier Jr, *Guide to fluorine NMR for organic chemists*. John Wiley & Sons, 2016.

[31] J. Fawell, K. Bailey, J. Chilton, E. Dahi, and Y. Magara, *Fluoride in drinking-water*. IWA publishing, 2006.

[32] F. Edition, “Guidelines for drinking-water quality,” *WHO Chron.*, vol. 38, no. 4, pp. 104–108, 2011.

[33] K. Biswas, K. Gupta, A. Goswami, and U. C. Ghosh, “Fluoride removal efficiency from aqueous solution by synthetic iron (III)–aluminum (III)–chromium (III) ternary mixed oxide,” *Desalination*, vol. 255, no. 1–3, pp. 44–51, 2010.

[34] B. Shimelis, F. Zewge, and B. S. Chandravanshi, “Removal of excess fluoride from water by aluminum hydroxide,” *Bull. Chem. Soc. Ethiop.*, vol. 20, no. 1, pp. 17–34, 2006.

[35] R. Ellepola, “Fluoride levels in the ground water of some selected districts of Sri Lanka,” 1988.

[36] W. Fernando, N. Nanayakkara, L. Gunarathne, and R. Chandrajith, “Serum and urine fluoride levels in populations of high environmental fluoride exposure with endemic CKDu: a case–control study from Sri Lanka,” *Environ. Geochem. Health*, vol. 42, no. 5, pp. 1497–1504, 2020.

[37] G. Golgire, S. Shetti, A. Patil, M. Khairnar, A. Varekar, and V. Doijad, “Estimation of fluoride level in drinking water and prevalence of dental fluorosis in Vairag village of Solapur district, Maharashtra, India: A cross sectional study,” *Epidemiol.*, vol. 6, no. 275, pp. 1165–2161, 2016.

[38] H. T. Dean, “Classification of mottled enamel diagnosis,” *J. Am. Dent. Assoc.*, vol. 21, no. 8, pp. 1421–1426, 1934.

[39] W. J. Muller, R. G. M. Heath, and M. H. Villet, “Finding the optimum: Fluoridation of potable water in South Africa,” *WATER SA-PRETORIA-*, vol. 24, pp. 21–28, 1998.

[40] G. Notcutt and F. Davies, “Biomonitoring of volcanogenic fluoride, Furnas Caldera, Sao Miguel, Azores,” *J. Volcanol. Geotherm. Res.*, vol. 92, no. 1–2, pp. 209–214, 1999.

[41] A. Nicolay, P. Bertocchio, E. Bargas, F. Coudore, G. Al Chahin, and J.-P. Reynier, “Hyperkalemia risks in hemodialysed patients consuming fluoride-rich water,” *Clin. Chim. acta*, vol. 281, no. 1–2, pp. 29–36, 1999.

[42] S. K. Jha, V. K. Mishra, D. K. Sharma, and T. Damodaran, “Fluoride in the environment

and its metabolism in humans," *Rev. Environ. Contam. Toxicol. Vol. 211*, pp. 121–142, 2011.

[43] E. Michel-Crosato, M. G. H. Biazevic, and E. Crosato, "Relationship between dental fluorosis and quality of life: a population based study," *Braz. Oral Res.*, vol. 19, no. 2, pp. 150–155, 2005.

[44] L. Valenzuela-Vasquez, J. Ramirez-Hernandez, J. Reyes-Lopez, A. Sol-Uribe, and O. Lazaro-Mancilla, "The origin of fluoride in groundwater supply to Hermosillo City, Sonora, Mexico," *Environ. Geol.*, vol. 51, no. 1, pp. 17–27, 2006.

[45] N. Das, P. Pattanaik, and R. Das, "Defluoridation of drinking water using activated titanium rich bauxite," *J. Colloid Interface Sci.*, vol. 292, no. 1, pp. 1–10, 2005.

[46] K. A. Alfredo, D. F. Lawler, and L. E. Katz, "Fluoride contamination in the Bongo District of Ghana, West Africa: geogenic contamination and cultural complexities," *Water Int.*, vol. 39, no. 4, pp. 486–503, 2014.

[47] P. S. Kumar *et al.*, "Treatment of fluoride-contaminated water. A review," *Environ. Chem. Lett.*, vol. 17, no. 4, pp. 1707–1726, 2019.

[48] T. K. Rao, I. V Kasiviswanath, and Y. L. N. Murthy, "Defluoridation of water by nanotechnology," *Water Sci. Technol. Water Supply*, vol. 9, no. 5, pp. 485–492, 2009.

[49] B. S. Feleke, "Fluoride removal from water by locally produced aluminum hydroxide." Addis Ababa University, 2005.

[50] D. L. Ozsvath, "Fluoride and environmental health: a review," *Rev. Environ. Sci. Bio/Technology*, vol. 8, no. 1, pp. 59–79, 2009.

[51] H. Zuo *et al.*, "Toxic effects of fluoride on organisms," *Life Sci.*, vol. 198, pp. 18–24, 2018.

[52] E. Kalisinska *et al.*, "Fluoride concentrations in the pineal gland, brain and bone of goosander (Mergus merganser) and its prey in Odra River estuary in Poland," *Environ. Geochem. Health*, vol. 36, no. 6, pp. 1063–1077, 2014.

[53] A. K. Gupta and S. Ayoob, *Fluoride in drinking water: status, issues, and solutions*. CRC Press, 2016.

[54] E. Y. Wong and M. K. Stenstrom, "Onsite defluoridation system for drinking water treatment using calcium carbonate," *J. Environ. Manage.*, vol. 216, pp. 270–274, 2018.

[55] G. Howard, J. Bartram, S. Pedley, O. Schmoll, I. Chorus, and P. Berger, "Groundwater and public health," *Prot. Groundw. Heal. Manag. Qual. Drink. sources. London, Int. Water Assoc. Publ.*, pp. 3–19, 2006.

[56] H. Kloos and R. T. Haimanot, "Distribution of fluoride and fluorosis in Ethiopia and prospects for control," *Trop. Med. Int. Heal.*, vol. 4, no. 5, pp. 355–364, 1999.

[57] R. Tekle-Haimanot *et al.*, "The geographic distribution of fluoride in surface and

groundwater in Ethiopia with an emphasis on the Rift Valley," *Sci. Total Environ.*, vol. 367, no. 1, pp. 182–190, 2006.

[58] Z. Feleke, "Investigation leading to the defluoridation of water in Ethiopia," *Rep. Submitt. to Ethiop. Sci. Technol ogy Comm. Addis Ababa, Ethiop.*, 2001.

[59] R. Bundi, "Enhancement of Defluoridation Efficiency of Bone Char using Surface Modification and Sequential application with Bamboo Char." ASTU, 2020.

[60] H. Demelash, A. Beyene, Z. Abebe, and A. Melese, "Fluoride concentration in ground water and prevalence of dental fluorosis in Ethiopian Rift Valley: systematic review and meta-analysis," *BMC Public Health*, vol. 19, no. 1, pp. 1–9, 2019.

[61] A. K. Chaturvedi, K. P. Yadava, K. C. Pathak, and V. N. Singh, "Defluoridation of water by adsorption on fly ash," *Water. Air. Soil Pollut.*, vol. 49, no. 1, pp. 51–61, 1990.

[62] C. N. Sawyer, P. L. McCarty, and G. F. Parkin, *Chemistry for environmental engineering and science*, vol. 5. McGraw-Hill New York, 2003.

[63] G. Moges, F. Zewge, and M. Socher, "Preliminary investigations on the defluoridation of water using fired clay chips," *J. African Earth Sci.*, vol. 22, no. 4, pp. 479–482, 1996.

[64] Y. Xiuru, S. Kuanxiu, W. Jianping, H. Liuchang, and Y. Zhaohui, "Preparation of CeO2-TiO2/SiO2 and its removal properties for fluoride ion," *J. Rare Earths*, vol. 16, no. 4, pp. 279–280, 1998.

[65] K. Biswas, K. Gupta, and U. C. Ghosh, "Adsorption of fluoride by hydrous iron (III)–tin (IV) bimetal mixed oxide from the aqueous solutions," *Chem. Eng. J.*, vol. 149, no. 1–3, pp. 196–206, 2009.

[66] X. Wu, Y. Zhang, X. Dou, and M. Yang, "Fluoride removal performance of a novel Fe–Al–Ce trimetal oxide adsorbent," *Chemosphere*, vol. 69, no. 11, pp. 1758–1764, 2007.

[67] M. S. Onyango, Y. Kojima, O. Aoyi, E. C. Bernardo, and H. Matsuda, "Adsorption equilibrium modeling and solution chemistry dependence of fluoride removal from water by trivalent-cation-exchanged zeolite F-9," *J. Colloid Interface Sci.*, vol. 279, no. 2, pp. 341–350, 2004.

[68] S. A. Wasay, S. Tokunaga, and S.-W. Park, "Removal of Hazardous Anions from Aqueous Solutions by La (lll)-and Y (lll)-lmpregnated Alumina," *Sep. Sci. Technol.*, vol. 31, no. 10, pp. 1501–1514, 1996.

[69] H. S. Parmar, J. B. Patel, P. Sudhakar, and V. J. Koshy, "Removal of fluoride from water with powdered corn cobs," *J. Environ. Sci. Eng.*, vol. 48, no. 2, pp. 135–138, 2006.

[70] D. Mohan, K. P. Singh, and V. K. Singh, "Wastewater treatment using low cost activated carbons derived from agricultural byproducts—a case study," *J. Hazard. Mater.*, vol. 152, no. 3, pp. 1045–1053, 2008.

[71] R. S. Sathish, S. Sairam, V. G. Raja, G. N. Rao, and C. Janardhana, "Defluoridation of

water using zirconium impregnated coconut fiber carbon," *Sep. Sci. Technol.*, vol. 43, no. 14, pp. 3676–3694, 2008.

[72] G. Alagumuthu and M. Rajan, "Equilibrium and kinetics of adsorption of fluoride onto zirconium impregnated cashew nut shell carbon," *Chem. Eng. J.*, vol. 158, no. 3, pp. 451–457, 2010.

[73] W. Nigussie, F. Zewge, and B. S. Chandravanshi, "Removal of excess fluoride from water using waste residue from alum manufacturing process," *J. Hazard. Mater.*, vol. 147, no. 3, pp. 954–963, 2007.

[74] A. Mohammad-Khah and R. Ansari, "Activated charcoal: preparation, characterization and applications: a review article," *Int J Chem Tech Res*, vol. 1, no. 4, pp. 859–864, 2009.

[75] T. Srinivasan, "Removal of fluorides from water by alkali impregnated alum impregnated paddy husk carbon," *Cent. Pub. Heal. Eng. Res. Inst. Bull*, vol. 1, p. 30, 1959.

[76] K. R. Bulusu, B. KR, S. BB, and N. WG, "Fluorides in water, defluoridation methods and their limitations," 1979.

[77] S. H. Sheshmani, F. M. ARAB, and R. Amini, "Iron (iii) hydroxide/graphene oxide nano composite and investigation of lead adsorption," 2013.

[78] N. H. Jabarullah, A. S. Kamal, and R. Othman, "A Modification of Palm Waste Lignocellulosic Materials into Biographite Using Iron and Nickel Catalyst," *Processes*, vol. 9, no. 6, p. 1079, 2021.

[79] D. D. L. CHUNG, "graphite," *J. Mater. Sci.*, vol. 37, no. 8, pp. 1475–1489, 2002.

[80] J. Deng, M. Li, and Y. Wang, "Biomass-derived carbon: synthesis and applications in energy storage and conversion," *Green Chem.*, vol. 18, no. 18, pp. 4824–4854, 2016.

[81] J. C. Serrano-Ruiz, R. M. West, and J. A. Dumesic, "Catalytic conversion of renewable biomass resources to fuels and chemicals," *Annu. Rev. Chem. Biomol. Eng.*, vol. 1, pp. 79–100, 2010.

[82] A. S. Kamal, R. Othman, and N. H. Jabarullah, "Preparation and synthesis of synthetic graphite from biomass waste: A review," *Syst. Rev. Pharm.*, vol. 11, no. 2, pp. 881–894, 2020.

[83] Y. Liu *et al.*, "Cascade utilization of lignocellulosic biomass to high-value products," *Green Chem.*, vol. 21, no. 13, pp. 3499–3535, 2019.

[84] Z. Melese, "Socio Economic Contribution of Lowland Bamboo (Oxythenanthera Abyssinica) in Pawe District, Ethiopia," 2020.

[85] K. Embaye, *Ecological aspects and resource management of bamboo forests in Ethiopia*, vol. 273, no. 273. 2003.

[86] S. Gebrekidan, L. Tiki, and Y. Mulatu, "Indigenous knowledge on highland bamboo (Yushania alpina) management and utilization practices in Kokosa Woreda, South East

Ethiopia," *Sci. Res. Essays*, vol. 13, no. 11, pp. 111–122, 2018.

[87] K. L. Cockle and J. I. Areta, "Specialization on bamboo by Neotropical birds," *Condor*, vol. 115, no. 2, pp. 217–220, 2013.

[88] A. Nigatu, M. Wondie, A. Alemu, D. Gebeyehu, and H. Workagegnehu, "Productivity of highland bamboo (Yushania alpina) across different plantation niches in West Amhara, Ethiopia," *Forest Sci. Technol.*, vol. 16, no. 3, pp. 116–122, 2020.

[89] A. Tolessa, B. Woldeyes, and S. Feleke, "Chemical composition of lowland bamboo (Oxytenanthera abyssinica) grown around Asossa Town, Ethiopia," *World Sci. News*, no. 74, pp. 141–151, 2017.

[90] M. Hassena, R. Ensermu, W. M. Mwangi, and H. Verkuijl, *A comparative assessment of combine harvesting vis-a-vis conventional harvesting and threshing in Arsi Region, Ethiopia*. CIMMYT, 2000.

[91] J. Hammond, S. Shackley, S. Sohi, and P. Brownsort, "Prospective life cycle carbon abatement for pyrolysis biochar systems in the UK," *Energy Policy*, vol. 39, no. 5, pp. 2646–2655, 2011.

[92] S. Pang, "Advances in thermochemical conversion of woody biomass to energy, fuels and chemicals," *Biotechnol. Adv.*, vol. 37, no. 4, pp. 589–597, 2019.

[93] Y. Lin *et al.*, "Combustion, pyrolysis and char CO2-gasification characteristics of hydrothermal carbonization solid fuel from municipal solid wastes," *Fuel*, vol. 181, pp. 905–915, 2016.

[94] M. T. Johnson and K. T. Faber, "Catalytic graphitization of three-dimensional wood-derived porous scaffolds," *J. Mater. Res.*, vol. 26, no. 1, pp. 18–25, 2011.

[95] A. Gutiérrez-Pardo, J. Ramírez-Rico, R. Cabezas-Rodríguez, and J. Martínez-Fernández, "Effect of catalytic graphitization on the electrochemical behavior of wood derived carbons for use in supercapacitors," *J. Power Sources*, vol. 278, pp. 18–26, 2015.

[96] L. Hou *et al.*, "Hierarchically porous and heteroatom self-doped graphitic biomass carbon for supercapacitors," *J. Colloid Interface Sci.*, vol. 540, pp. 88–96, 2019.

[97] L. I. Nasibulina *et al.*, "Direct synthesis of carbon nanofibers on the surface of copper powder," *Carbon N. Y.*, vol. 48, no. 15, pp. 4559–4562, 2010.

[98] S. Wang *et al.*, "Correlation in structure and properties of highly-porous graphene monoliths studied with a thermal treatment method," *Carbon N. Y.*, vol. 96, pp. 174–183, 2016.

[99] M. Sevilla, C. Sanchis, T. Valdés-Solís, E. Morallón, and A. B. Fuertes, "Synthesis of graphitic carbon nanostructures from sawdust and their application as electrocatalyst supports," *J. Phys. Chem. C*, vol. 111, no. 27, pp. 9749–9756, 2007.

[100] M. Sevilla, C. S. Martinez-de Lecea, T. Valdés-Solís, E. Morallón, and A. B. Fuertes,

"Solid-phase synthesis of graphitic carbon nanostructures from iron and cobalt gluconates and their utilization as electrocatalyst supports," *Phys. Chem. Chem. Phys.*, vol. 10, no. 10, pp. 1433–1442, 2008.

[101] G. B. Barin, I. de Fátima Gimenez, L. P. da Costa, A. G. Souza Filho, and L. S. Barreto, "Influence of hydrothermal carbonization on formation of curved graphite structures obtained from a lignocellulosic precursor," *Carbon N. Y.*, vol. 78, pp. 609–612, 2014.

[102] E. Thompson, A. E. Danks, L. Bourgeois, and Z. Schnepp, "Iron-catalyzed graphitization of biomass," *Green Chem.*, vol. 17, no. 1, pp. 551–556, 2015.

[103] Z. Pan, Y. Zheng, F. Guo, P. Niu, and X. Wang, "Decorating CoP and Pt nanoparticles on graphitic carbon nitride nanosheets to promote overall water splitting by conjugated polymers," *ChemSusChem*, vol. 10, no. 1, pp. 87–90, 2017.

[104] O. Fromm *et al.*, "Carbons from biomass precursors as anode materials for lithium ion batteries: New insights into carbonization and graphitization behavior and into their correlation to electrochemical performance," *Carbon N. Y.*, vol. 128, pp. 147–163, 2018.

[105] K. Mugadza, P. G. Ndungu, A. Stark, and V. O. Nyamori, "Conversion of residue biomass into value added carbon materials: utilisation of sugarcane bagasse and ionic liquids," *J. Mater. Sci.*, vol. 54, no. 19, pp. 12476–12487, 2019.

[106] Y. Gong, D. Li, C. Luo, Q. Fu, and C. Pan, "Highly porous graphitic biomass carbon as advanced electrode materials for supercapacitors," *Green Chem.*, vol. 19, no. 17, pp. 4132–4140, 2017.

[107] J. Almirón, H. Alcazar, R. Churata, F. Roudet, K. Ziouche, and D. Chicot, "Effect of impregnation solutions on the synthesis of Ni-Cu/Al2O3 catalyst to obtain carbon nanofibers," *Mater. Res. Express*, vol. 5, no. 12, p. 125010, 2018.

[108] M. G. S. Bernd, S. R. Bragança, N. Heck, and L. C. P. da Silva Filho, "Synthesis of carbon nanostructures by the pyrolysis of wood sawdust in a tubular reactor," *J. Mater. Res. Technol.*, vol. 6, no. 2, pp. 171–177, 2017.

[109] W.-J. Liu, K. Tian, Y.-R. He, H. Jiang, and H.-Q. Yu, "High-yield harvest of nanofibers/mesoporous carbon composite by pyrolysis of waste biomass and its application for high durability electrochemical energy storage," *Environ. Sci. Technol.*, vol. 48, no. 23, pp. 13951–13959, 2014.

[110] M. Li *et al.*, "A SiOx/Sn/C hybrid anode for lithium-ion batteries with high volumetric capacity and long cyclability," *J. Alloys Compd.*, vol. 809, p. 151659, 2019.

[111] J. Hoekstra *et al.*, "The effect of iron catalyzed graphitization on the textural properties of carbonized cellulose: Magnetically separable graphitic carbon bodies for catalysis and remediation," *Carbon N. Y.*, vol. 107, pp. 248–260, 2016.

[112] J. Xia, N. Zhang, S. Chong, Y. Chen, and C. Sun, "Three-dimensional porous graphene-like sheets synthesized from biocarbon via low-temperature graphitization for a supercapacitor," *Green Chem.*, vol. 20, no. 3, pp. 694–700, 2018.

[113] Q. Liu, J. Gu, W. Zhang, Y. Miyamoto, Z. Chen, and D. Zhang, "Biomorphic porous graphitic carbon for electromagnetic interference shielding," *J. Mater. Chem.*, vol. 22, no. 39, pp. 21183–21188, 2012.

[114] X. Wu, K. Chen, Z. Lin, Y. Zhang, and H. Meng, "Nitrogen doped graphitic carbon from biomass as non noble metal catalyst for oxygen reduction reaction," *Mater. Today Energy*, vol. 13, pp. 100–108, 2019.

[115] M. A. Naeem *et al.*, "Batch and column scale removal of cadmium from water using raw and acid activated wheat straw biochar," *Water*, vol. 11, no. 7, p. 1438, 2019.

[116] B. Constant-Mandiola, H. Aguilar-Bolados, J. Geshev, and R. Quíjada, "Study of the Influence of Magnetite Nanoparticles Supported on Thermally Reduced Graphene Oxide as Filler on the Mechanical and Magnetic Properties of Polypropylene and Polylactic Acid Nanocomposites," *Polymers (Basel).*, vol. 13, no. 10, p. 1635, 2021.

[117] Y. Liu, X. Zhao, J. Li, D. Ma, and R. Han, "Characterization of bio-char from pyrolysis of wheat straw and its evaluation on methylene blue adsorption," *Desalin. Water Treat.*, vol. 46, no. 1–3, pp. 115–123, 2012.

[118] S. S. M. Isa, M. M. Ramli, D. S. C. Halin, N. A. M. Anhar, and N. Hambali, "Different carbonization process of bamboo charcoal using Gigantochloa Albociliata," in *AIP Conference Proceedings*, 2017, vol. 1885, no. 1, p. 20226.

[119] J.-C. Yoon, J.-S. Lee, S.-I. Kim, K.-H. Kim, and J.-H. Jang, "Three-dimensional graphene nano-networks with high quality and mass production capability via precursor-assisted chemical vapor deposition," *Sci. Rep.*, vol. 3, no. 1, pp. 1–8, 2013.

[120] Z. Xie, W. Guan, F. Ji, Z. Song, and Y. Zhao, "Production of biologically activated carbon from orange peel and landfill leachate subsequent treatment technology," *J. Chem.*, vol. 2014, 2014.

[121] S. J. Goldie, S. Jiang, and K. S. Coleman, "Cobalt nanoparticle catalysed graphitization and the effect of metal precursor decomposition temperature," *Mater. Adv.*, vol. 2, no. 10, pp. 3353–3361, 2021.

[122] Y. Wang, J. E. Panzik, B. Kiefer, and K. K. M. Lee, "Crystal structure of graphite under room-temperature compression and decompression," *Sci. Rep.*, vol. 2, no. 1, pp. 1–7, 2012.

[123] A. Sayah *et al.*, "Electrochemical synthesis of polyaniline-exfoliated graphene composite films and their capacitance properties," *J. Electroanal. Chem.*, vol. 818, pp. 26–34, 2018.

[124] M. Zakeri, E. Abouzari-lotf, M. Miyake, S. Mehdipour-Ataei, and K. Shameli, "Phosphoric acid functionalized graphene oxide: a highly dispersible carbon-based nanocatalyst for the green synthesis of bio-active pyrazoles," *Arab. J. Chem.*, vol. 12, no. 2, pp. 188–197, 2019.

[125] W. N. R. W. Isahak, M. W. M. Hisham, and M. A. Yarmo, "Highly porous carbon materials from biomass by chemical and carbonization method: a comparison study," *J.*

Chem., vol. 2013, 2013.

[126] X. Wang and L. Zhang, "Green and facile production of high-quality graphene from graphite by the combination of hydroxyl radicals and electrical exfoliation in different electrolyte systems," *Rsc Adv.*, vol. 9, no. 7, pp. 3693–3703, 2019.

[127] Y. Cuixia, X. Yingming, W. Lin, L. Xuefeng, S. Yuebing, and J. Hongtao, "Effect of different pyrolysis temperatures on physico-chemical characteristics and lead (ii) removal of biochar derived from chicken manure," *RSC Adv.*, vol. 10, no. 7, pp. 3667–3674, 2020.

APPENDICES

Appendix A

X-pert software data for bamboo driven graphite formation

Graphite using $FeCl_3.6H_2O_{1000°C}$

Name and formula

Reference code:	00-012-0212
Mineral name:	Graphite
PDF index name:	Carbon
Empirical formula:	C
Chemical formula:	C

Crystallographic parameters

Crystal system:	Hexagonal
Space group:	P63/mmc
Space group number:	194
a (Å):	2.4640
b (Å):	2.4640
c (Å):	6.7360
Alpha (°):	90.0000
Beta (°):	90.0000
Gamma (°):	120.0000

Peak list

No.	h	k	l	d [A]	2Theta[deg]	I [%]
1	0	0	2	3.34700	26.651	100.0
2	1	0	0	2.13200	42.361	2.0
3	1	0	1	2.03600	44.462	3.0
4	1	0	2	1.80000	50.674	1.0
5	0	0	4	1.68200	54.512	8.0
6	1	0	3	1.54100	59.983	2.0
7	1	1	0	1.23200	77.400	6.0
8	1	1	2	1.15500	83.661	6.0
9	0	0	6	1.12000	86.907	2.0
10	2	0	1	1.05000	94.381	2.0
11	1	1	4	0.99400	101.601	4.0
12	0	0	8	0.84200	132.368	1.0

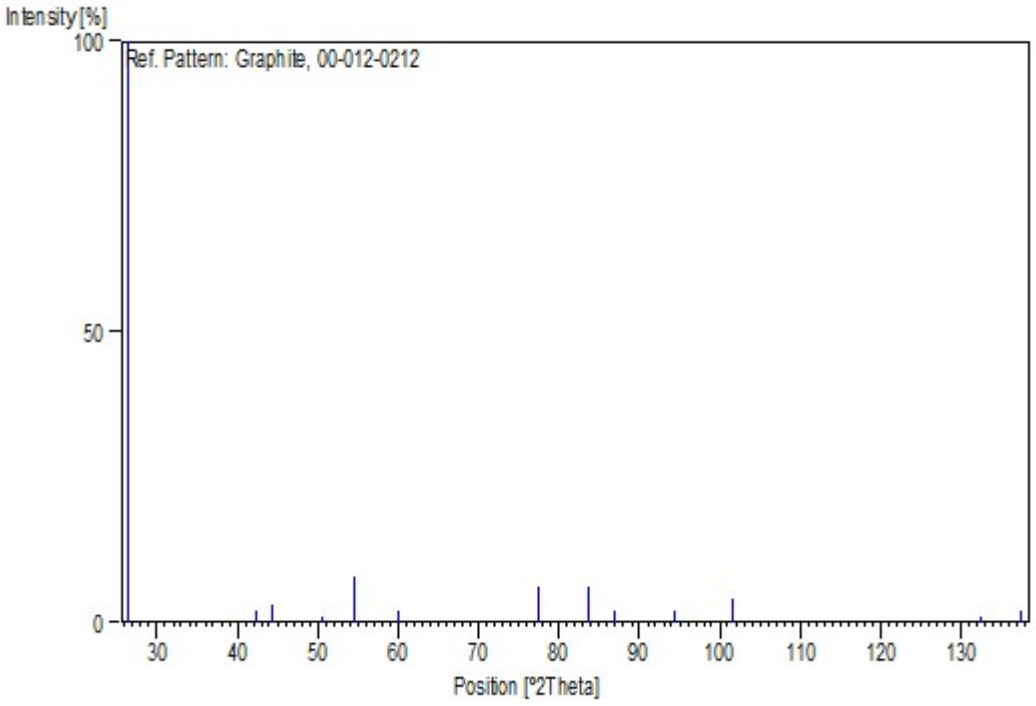

Graphite $FeCl_3.6H_2O_{900°C}$

Name and formula

Reference code:	00-025-0284
Mineral name:	Graphite, syn
PDF index name:	Carbon
Empirical formula:	C
Chemical formula:	C

Crystallographic parameters

Crystal system:	Hexagonal
Space group:	P63/mmc
Space group number:	194
a (Å):	2.4560
b (Å):	2.4560
c (Å):	6.6960
Alpha (°):	90.0000
Beta (°):	90.0000
Gamma (°):	120.0000

Status, subfiles and quality

Status:	Marked as deleted by ICDD
Subfiles:	Inorganic
	Mineral
	Alloy, metal or intermetalic
	Forensic

Peak list

No.	h	k	l	d [A]	2Theta[deg]	I [%]
1	0	0	2	3.35000	26.603	100.0
2	1	0	0	2.12700	42.465	3.0
3	1	0	1	2.02700	44.670	15.0
4	1	0	2	1.79500	50.826	3.0
5	0	0	4	1.67400	54.794	6.0
6	1	0	3	1.53980	60.034	4.0
7	1	0	4	1.31540	71.691	1.0
8	1	1	0	1.22800	77.699	4.0
9	1	1	2	1.15290	83.848	6.0
10	1	0	5	1.13330	85.640	1.0
11	0	0	6	1.11600	87.297	1.0
12	2	0	1	1.05030	94.346	1.0
13	1	1	4	0.99020	102.142	4.0
14	2	0	3	0.96010	106.703	1.0
15	1	0	7	0.87240	124.005	1.0
16	0	0	8	0.83700	133.943	1.0
17	2	0	5	0.83280	135.322	1.0
18	1	1	6	0.82590	137.713	4.0
19	2	1	1	0.79820	149.613	2.0

Stick Pattern

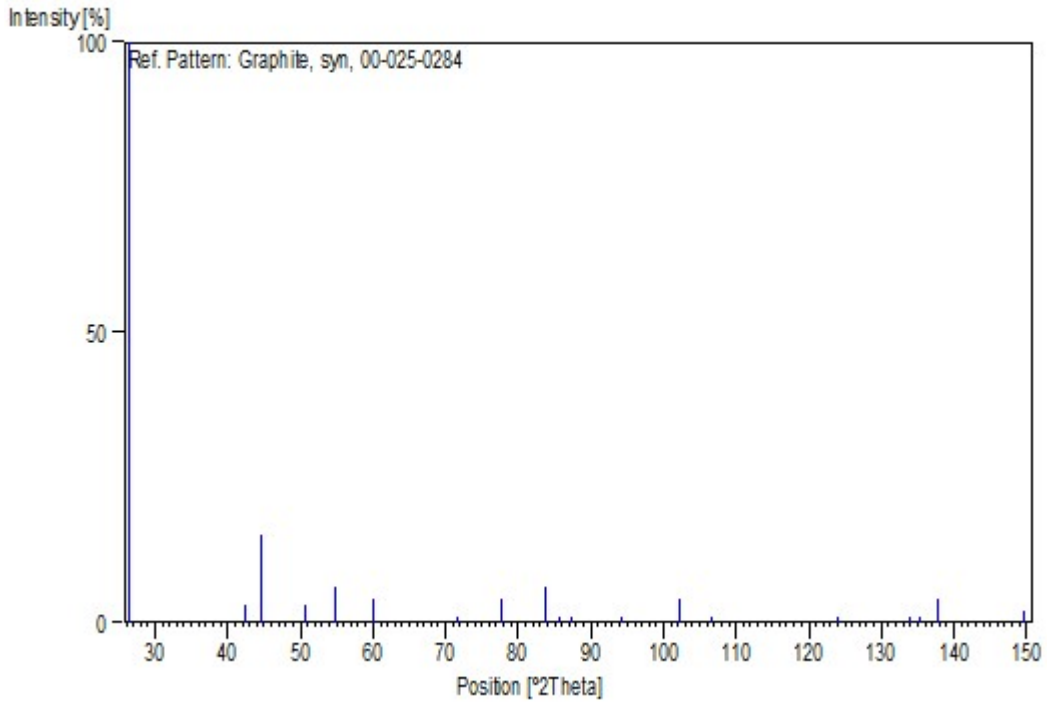

Graphite using-Al powder

Name and formula

Reference code:	01-074-2328
Mineral name:	Graphite, syn
PDF index name:	Carbon
Empirical formula:	C
Chemical formula:	C

Crystallographic parameters

Crystal system:	Rhombohedral
Space group:	R-3m
Space group number:	166
a (Å):	2.4600
b (Å):	2.4600
c (Å):	33.4500

Alpha (°):	90.0000
Beta (°):	90.0000
Gamma (°):	120.0000

Status, subfiles and quality

Status:	
Subfiles:	Inorganic
	Mineral
	Alloy, metal or intermetalic
	Modelled additional pattern

Peak list

No.	h	k	l	d [A]	2Theta[deg]	I [%]
1	0	0	3	11.15000	7.923	100.0
2	0	0	6	5.57500	15.884	5.0
3	0	0	9	3.71667	23.923	13.1
4	0	0	12	2.78750	32.084	3.2
5	0	0	15	2.23000	40.416	0.1
6	1	0	1	2.12611	42.484	0.7
7	1	0	4	2.06448	43.816	1.0
8	0	1	8	2.0998	46.601	0.7
9	1	0	7	1.94580	46.642	0.1
10	0	1	8	1.89823	47.882	0.6
11	0	0	18	1.85833	48.977	0.1
12	1	0	10	1.79692	50.767	0.1
13	0	1	11	1.74483	52.396	0.1
14	1	0	13	1.64096	55.993	0.4
15	0	0	21	1.592011	57.841	0.4
16	0	1	14	1.49217	57.951	0.3
17	1	0	16	1.44546	62.159	0.1
18	0	1	17	1.39375	64.405	0.2
19	2	1	1	1.31554	67.102	0.1
20	1	0	19	1.35711	69.167	0.1

Stick Pattern

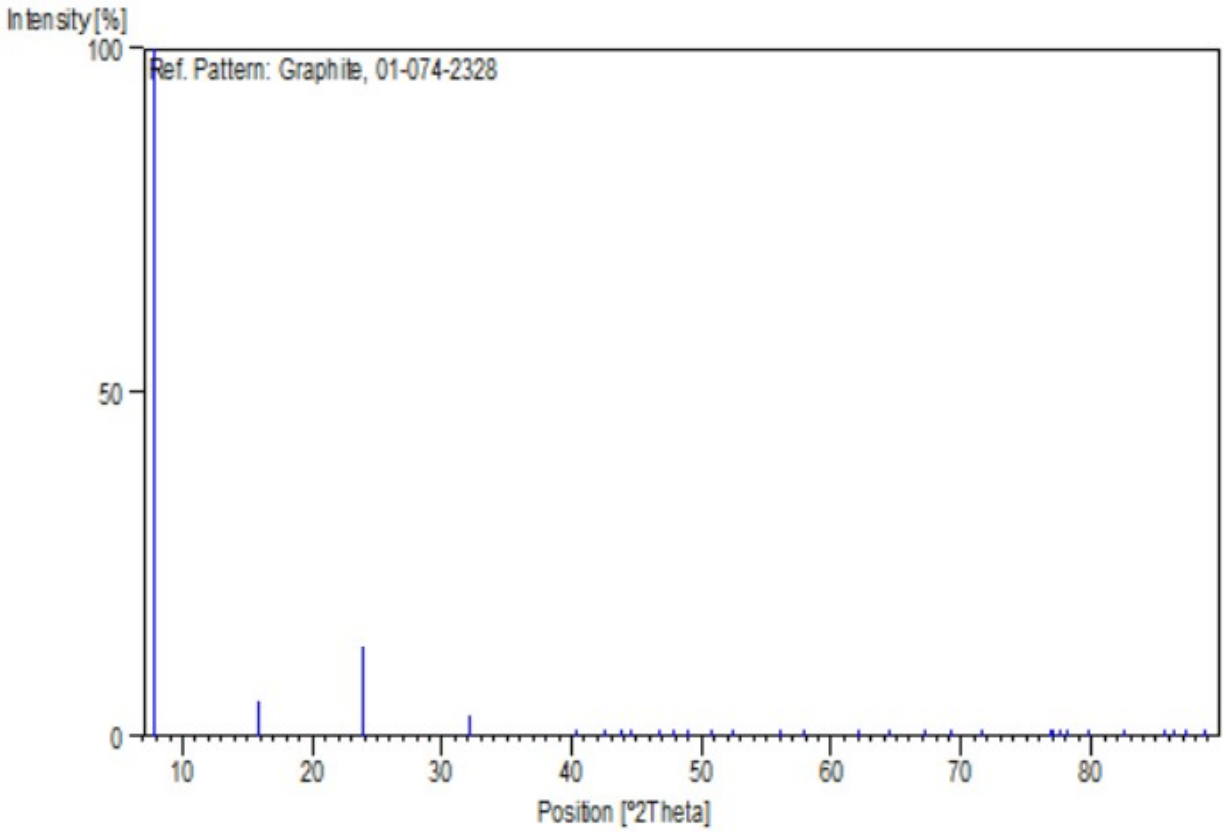

Appendix B

Adsorption data, conversion and plots

Adsorption Isotherm Graphite using Al

B1.1. Data

time	Co(px)	Co(mg/lit)	Cf1(px)	Cf1(mg/lit)	Cf2(px)	Cf2(mg/lit)	Average (mg/lit)	Co/Cf	Cf/Co
0	3.21	11.71531	3.21	11.71531	3.21	11.71531	11.71531	1	1
30			3.36	8.293801	3.37	8.105011	8.199406	1.4288	0.699888
60			3.48	6.291491	3.48	6.291491	6.291491	1.862088	0.537032
90			3.55	5.354928	3.55	5.354928	5.354928	2.187763	0.457088
120			3.57	5.113916	3.58	4.997509	5.055713	2.317242	0.431547
150			3.57	5.113916	3.6	4.772584	4.94325	2.369961	0.421948
180			3.59	4.883752	3.61	4.663947	4.773849	2.454059	0.407488
210			3.6	4.772584	3.61	4.663947	4.718266	2.48297	0.402744
240			3.62	4.557783	3.62	4.557783	4.557783	2.570397	0.389045

B1.2. Data

time	Co(px)	Co(mg/lit)	Cf1(px)	Cf1(mg/lit)	Cf2(px)	Cf2(mg/lit)	Average (mg/lit)	Co/Cf	Cf/Co
0	3.34	8.684676	3.34	8.684676	3.34	8.684676	8.684676	1	1
30			3.52	5.737908	3.52	5.737908	5.737908	1.513561	0.660694
60			3.61	4.663947	3.6	4.772584	4.718266	1.84065	0.543286
90			3.69	3.879302	3.68	3.969663	3.924482	2.212948	0.451886
120			3.73	3.537966	3.74	3.457432	3.497699	2.482968	0.402744
150			3.77	3.226663	3.76	3.301822	3.264242	2.660548	0.375862
180			3.79	3.081439	3.78	3.153215	3.117327	2.785936	0.358946
210			3.81	2.942752	3.8	3.011297	2.977024	2.917233	0.342791
240			3.82	2.875766	3.79	3.081439	2.978603	2.915687	0.342972

B1.3. Data

time	Co(px)	Co(mg/lit)	Cf1(px)	Cf1(mg/lit)	Cf2(px)	Cf2(mg/lit)	Average (mg/lit)	Co/Cf	Cf/Co
0	3.45	6.741454	3.45	6.741454	3.45	6.741454	5.355559	1.258777	0.794422
30			3.67	4.062128	3.68	3.969663	3.357999	2.007581	0.498112
60			3.84	2.746336	3.84	2.746336	2.414822	2.791698	0.358205
90			3.94	2.181492	3.96	2.083309	2.013783	3.347657	0.298716
120			3.98	1.989544	3.99	1.944257	1.85872	3.626934	0.275715
150			4.03	1.773183	4.03	1.773183	1.773183	3.801894	0.263027
180			4.04	1.732821	4.03	1.773183	1.714007	3.933154	0.254249
210			4.07	1.617162	4.06	1.654831	1.617591	4.167589	0.239947
240			4.07	1.617162	4.08	1.580351	1.598757	4.216685	0.237153

B1.4. Data

time	Co(px)	Co(mg/lit)	Cf1(px)	Cf1(mg/lit)	Cf2(px)	Cf2(mg/lit)	Average (mg/lit)	Co/Cf	Cf/Co
0	3.6	4.772584	3.6	4.772584	3.6	4.772584	4.772584	1	1
30			3.83	2.810306	3.85	2.683821	2.747064	1.73734	0.575593
60			3.99	1.944257	4.01	1.856751	1.900504	2.511221	0.398213
90			4.12	1.441297	4.13	1.408489	1.424893	3.349432	0.298558
120			4.19	1.226743	4.18	1.255318	1.24103	3.845663	0.260033
150			4.26	1.044128	4.26	1.044128	1.044128	4.570882	0.218776
180			4.29	0.974437	4.28	0.997134	0.985785	4.841403	0.206552
210			4.29	0.974437	4.29	0.974437	0.974437	4.897788	0.204174
240			4.31	0.93058	4.31	0.93058	0.93058	5.128614	0.194984

B1.5. Data

time	Co(px)	Co(mg/lit)	Cf1(px)	Cf1(mg/lit)	Cf2(px)	Cf2(mg/lit)	Average (mg/lit)	Co/Cf	Cf/Co
0	3.85	2.683821	3.85	2.683821	3.85	2.683821	2.683821	1	1
30			4.05	1.693377	4.06	1.654831	1.674104	1.603139	0.623776
60			4.22	1.144863	4.22	1.144863	1.144863	2.344229	0.42658
90			4.37	0.810501	4.38	0.792052	0.801276	3.349432	0.298558
120			4.46	0.6588	4.48	0.629149	0.643975	4.167588	0.239947
150			4.51	0.587156	4.51	0.587156	0.587156	4.570881	0.218776
180			4.54	0.547966	4.53	0.56073	0.554348	4.841402	0.206552
210			4.57	0.511392	4.57	0.511392	0.511392	5.248074	0.190546
240			4.57	0.511392	4.58	0.499751	0.505571	5.308492	0.188377

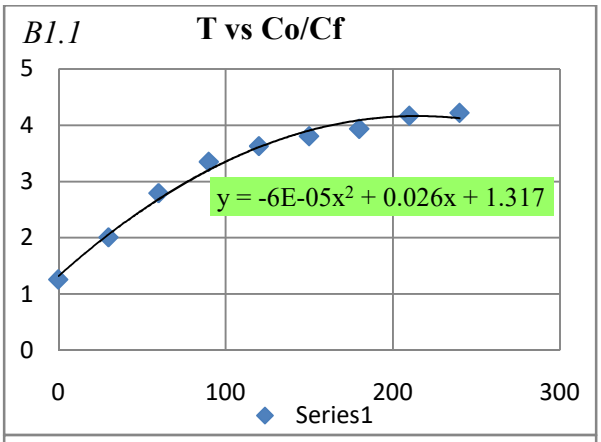
B1.1
T vs Co/Cf
y = -6E-05x² + 0.026x + 1.317
Series1

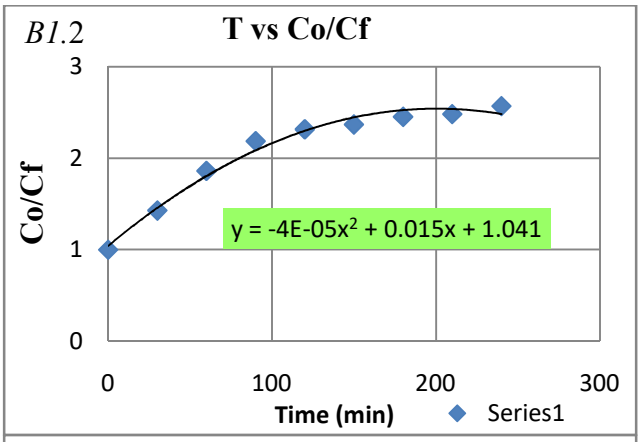
B1.2
T vs Co/Cf
Co/Cf
y = -4E-05x² + 0.015x + 1.041
Time (min)
Series1

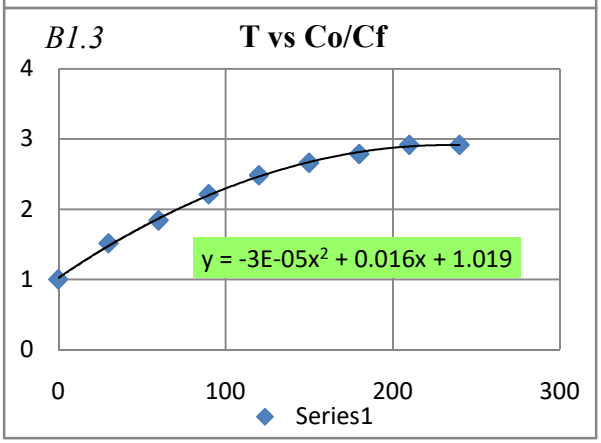
B1.3
T vs Co/Cf
y = -3E-05x² + 0.016x + 1.019
Series1

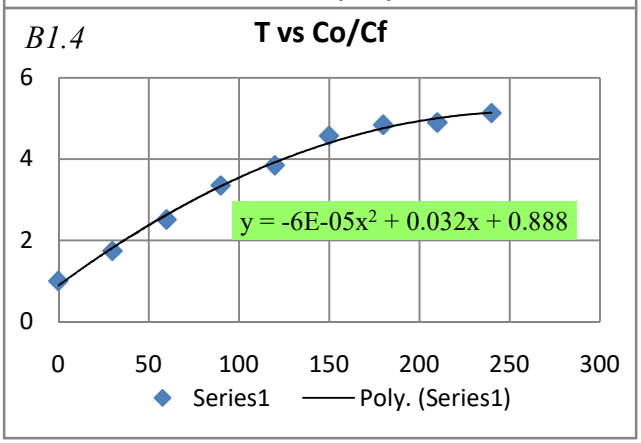
B1.4
T vs Co/Cf
y = -6E-05x² + 0.032x + 0.888
Series1
Poly. (Series1)

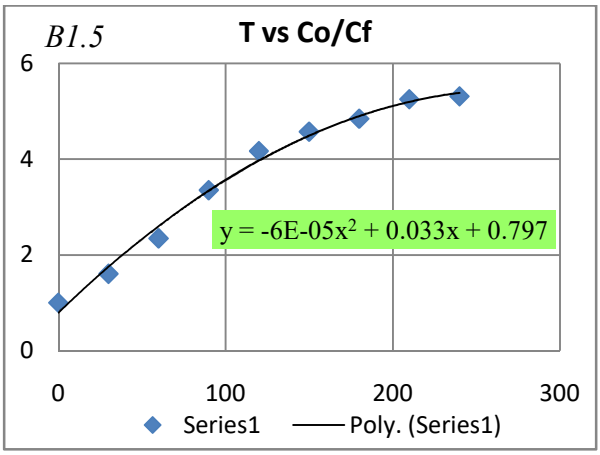
B1.5
T vs Co/Cf
y = -6E-05x² + 0.033x + 0.797
Series1
Poly. (Series1)

Modified Graphite-Aluminum powder (G-Al)

B2.1 Data

Time	Co(px)	Co(mg/lit)	Cf1(px)	Cf1(mg/lit)	Cf2(px)	Cf2(mg/lit)	Average (mg/lit)	Co/Cf	Cf/Co
0	3.21	11.71531	3.21	11.71531	3.21	11.71531	11.71531	1	1
30			4.08	1.580351	4.07	1.617162	1.598757	7.327763	0.136467
60			4.41	0.739186	4.41	0.739186	0.739186	15.84894	0.063096
90			4.52	0.573791	4.54	0.547966	0.560878	20.88743	0.047876
120			4.57	0.511392	4.58	0.499751	0.505571	23.17242	0.043155
150			4.59	0.488375	4.6	0.477258	0.482817	24.2645	0.041212
180			4.61	0.466395	4.61	0.466395	0.466395	25.11887	0.039811
210			4.64	0.435265	4.62	0.455778	0.445522	26.29572	0.038029
240			4.64	0.435265	4.63	0.445403	0.440334	26.6055	0.037586

B2.2

time	Co(px)	Co(mg/lit)	Cf1(px)	Cf1(mg/lit)	Cf2(px)	Cf2(mg/lit)	Average (mg/lit)	Co/Cf	Cf/Co
0	3.34	8.684676	3.34	8.684676	3.34	8.684676	8.684676	1	1
30			4.26	1.044128	4.27	1.02036	1.032244	8.413394	0.118858
60			4.63	0.445403	4.64	0.435265	0.440334	19.72292	0.050702
90			4.76	0.330182	4.77	0.322666	0.326424	26.60549	0.037586
120			4.81	0.294275	4.82	0.287577	0.290926	29.85185	0.033499
150			4.83	0.281031	4.83	0.281031	0.281031	30.90296	0.032359
180			4.86	0.262273	4.84	0.274634	0.268453	32.35079	0.030911
210			4.85	0.268382	4.86	0.262273	0.265328	32.7319	0.030551
240			4.87	0.256303	4.87	0.256303	0.256303	33.88442	0.029512

B2.3

time	Co(px)	Co(mg/lit)	Cf1(px)	Cf1(mg/lit)	Cf2(px)	Cf2(mg/lit)	Average (mg/lit)	Co/Cf	Cf/Co
0	3.45	6.741454	3.45	6.741454	3.45	6.741454	6.741454	0.999999	1.000001
30			4.41	0.739186	4.42	0.72236	0.730773	9.229325	0.10835
60			4.79	0.308144	4.81	0.294275	0.30121	22.39152	0.04466
90			4.94	0.218149	4.95	0.213184	0.215666	31.27303	0.031976
120			5.01	0.185675	5.02	0.181449	0.183562	36.74261	0.027216
150			5.05	0.169338	5.02	0.181449	0.175393	38.45384	0.026005
180			5.05	0.169338	5.04	0.173282	0.17131	39.37041	0.0254
210			5.06	0.165483	5.05	0.169338	0.16741	40.28747	0.024822
240			5.06	0.165483	5.06	0.165483	0.165483	40.75667	0.024536

B2.4

time	Co(px)	Co(mg/lit)	Cf1(px)	Cf1(mg/lit)	Cf2(px)	Cf2(mg/lit)	Average (mg/lit)	Co/Cf	Cf/Co
0	3.85	2.683821	3.85	2.683821	3.85	2.683821	2.683821	1	1
30			4.87	0.256303	4.88	0.250469	0.253386	10.59183	0.094412
60			5.33	0.08887	5.34	0.086847	0.087858	30.54718	0.032736
90			5.55	0.053549	5.54	0.054797	0.054173	49.54173	0.020185
120			5.67	0.040621	5.68	0.039697	0.040159	66.82995	0.014963
150			5.72	0.036204	5.71	0.037047	0.036625	73.27759	0.013647
180			5.73	0.03538	5.72	0.036204	0.035792	74.98444	0.013336
210			5.75	0.033787	5.74	0.034574	0.034181	78.51835	0.012736
240			5.76	0.033018	5.75	0.033787	0.033403	80.34728	0.012446

B2.5

time	Co(px)	Co(mg/lit)	Cf1(px)	Cf1(mg/lit)	Cf2(px)	Cf2(mg/lit)	Average (mg/lit)	Co/Cf	Cf/Co
0	3.6	4.772584	3.6	4.772584	3.6	4.772584	4.772584	1	1
30			4.61	0.466395	4.61	0.466395	0.466395	10.23293	0.097724
60			5.03	0.177318	5.04	0.173282	0.1753	27.22521	0.036731
90			5.21	0.117153	5.23	0.11188	0.114517	41.67589	0.023995
120			5.29	0.097444	5.31	0.093058	0.095251	50.10544	0.019958
150			5.33	0.08887	5.33	0.08887	0.08887	53.70318	0.018621
180			5.34	0.086847	5.34	0.086847	0.086847	54.95408	0.018197
210			5.35	0.08487	5.35	0.08487	0.08487	56.23413	0.017783
240			5.37	0.08105	5.37	0.08105	0.08105	58.88436	0.016982

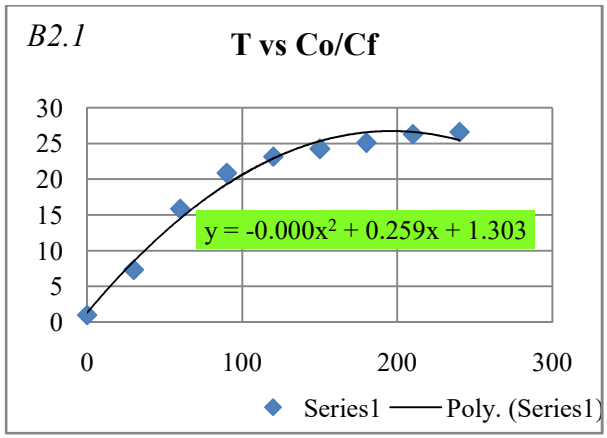
B2.1
T vs Co/Cf
y = -0.000x² + 0.259x + 1.303
Series1
Poly. (Series1)

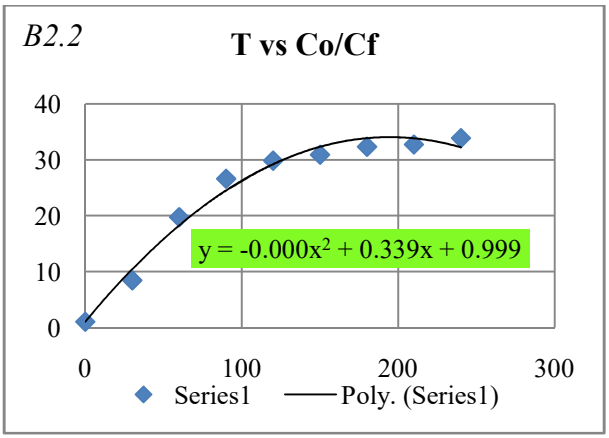
B2.2
T vs Co/Cf
y = -0.000x² + 0.339x + 0.999
Series1
Poly. (Series1)

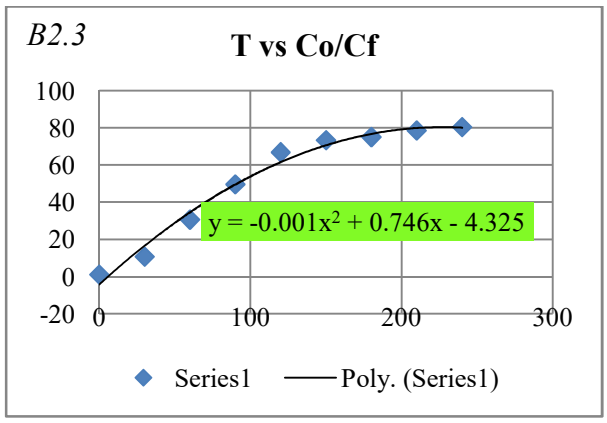
B2.3
T vs Co/Cf
y = -0.001x² + 0.746x - 4.325
Series1
Poly. (Series1)

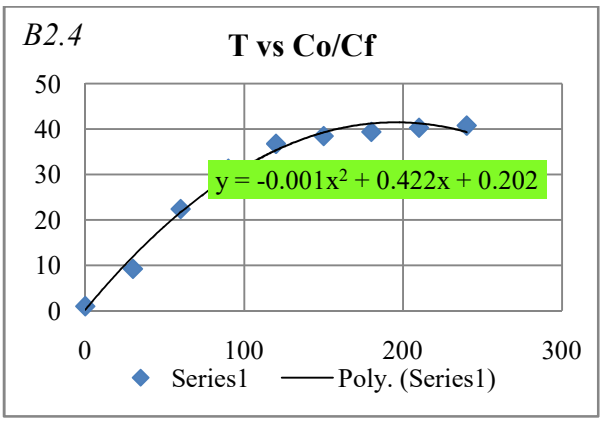
B2.4
T vs Co/Cf
y = -0.001x² + 0.422x + 0.202
Series1
Poly. (Series1)

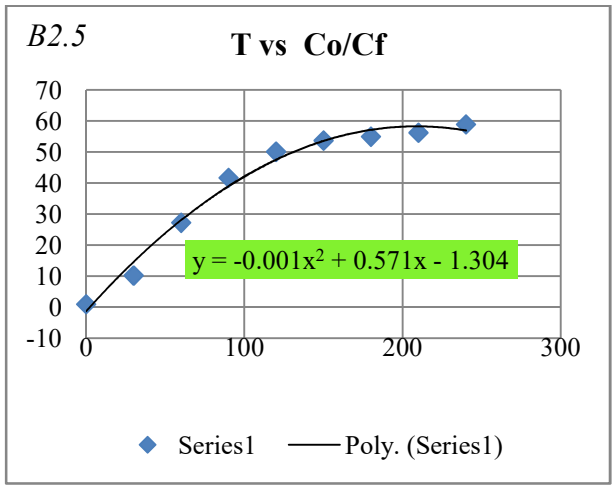
B2.5
T vs Co/Cf
y = -0.001x² + 0.571x - 1.304
Series1
Poly. (Series1)